QATAR UNIVERSITY

COLLEGE OF ENGINEERING

SUSTAINABLE CONCRETE USING SEAWATER, RECYCLED AGGREGATES, AND NON-CORROSIVE REINFORCEMENT

BY

ADEL YOUNIS

A Dissertation Submitted to

the College of Engineering

in Partial Fulfillment of the Requirements for the Degree of

Doctorate of Philosophy in Civil Engineering

January 2020

© 2020 Adel Younis. All Rights Reserved.

COMMITTEE PAGE

The members of the Committee approve the Dissertation of
Adel Younis defended on 26/11/2019.

Prof. Usama Ebead
Thesis/Dissertation Supervisor

Prof. Ashraf Ashour
Committee Member

Dr. Wael Alnahhal
Committee Member

Dr. Mohammad Irshidat
Committee Member

Approved:

Khalid Naji, Dean, College of Engineering

ABSTRACT

YOUNIS, ADEL S., Doctorate : January : 2020,

Doctorate of Philosophy in Civil Engineering

Title: Sustainable Concrete Using Seawater, Recycled Aggregates, and Non-Corrosive Reinforcement

Supervisor of Dissertation: Usama A. Ebead.

Using seawater and recycled concrete aggregate (RCA) in a concrete mix is potentially advantageous from a sustainability perspective. However, the high chloride levels expected in such a concrete mix demands the use of non-corrosive reinforcement in lieu of normal black steel to avoid corrosion problems. Glass fiber reinforced polymer (GFRP) is considered promising as an alternative reinforcement owing to its corrosion resistance and acceptable mechanical properties that minimize maintenance and repairs and extend service life. Yet, the relatively high initial cost of GFRP bars may mitigate its potential use. In view of that, the current thesis is aimed at verifying the safe and economic utilization of seawater, recycled concrete aggregate, and GFRP reinforcement to produce sustainable and efficient concrete structures.

The main body of the thesis consists of five key studies. In the first study, an extensive experimental program was conducted to compare the fresh and hardened properties of freshwater- and seawater-mixed concretes. In the second study, the performance of concrete mixed with seawater and recycled coarse aggregates (at 100% replacement level) was experimentally investigated. The third study was carried out to experimentally examine the flexural performance of seawater-mixed recycled-aggregate GFRP-reinforced concrete beams. In the fourth study, a life cycle cost analysis (LCCA) was performed (considering 100-year analysis period) to verify the

cost performance of structural concrete combining seawater, RCA, and GFRP reinforcement for high-rise buildings as compared to the traditional reinforced concrete (i.e., with freshwater, natural aggregates, and black steel reinforcement). The fifth study evaluates the cost effectiveness of different reinforcement alternatives in a concrete water chlorination tank using LCCA: a comparison was established between four concrete reinforcing materials, namely, black steel, epoxy-coated steel, stainless steel, and GFRP through a 100-year analysis period. The results of these five studies suggest the potential use of the proposed combination (seawater + RCA + GFRP reinforcement) to produce safe and economic concrete structures.

DEDICATION

To my parents.

ACKNOWLEDGMENTS

The work described in this dissertation was carried out at the Department of Civil and Architectural Engineering at Qatar University between October 2015 and October 2019. First, I would like to express my sincere gratitude to my advisor, Prof. Usama Ebead, for his continuous support during my Ph.D. research, for his patience, motivation, and guidance. He has been helping me at every step of conducting this research and writing my thesis.

I am very grateful to my publications' coauthors: Dr. Prannoy Suraneni, Prof. Antonio Nanni, and Prof. Simon Judd for giving me the opportunity to work under their direction and vision. Their advice and support have been critical to the success of this work.

I would also like to thank my committee members, Dr. Ashraf Ashour, Dr. Wael Alnahhal, and Dr. Mohammad Irshidat for their time and valuable feedback.

I would like to acknowledge the financial support provided by Qatar National Research Fund, QNRF (a member of Qatar Foundation) via the National Priorities Research Program (NPRP), under Project Number: NPRP 9-110-2-052.

Special thanks are due to Readymix Qatar (as a part of LafargeHolcim) for providing the expertise that greatly assists me in this research.

I would like also to acknowledge ATP Construction Composites for donating the GFRP bars used in the present research.

I would like to express my sincere gratitude to the rest of Prof. Ebead's research team members: Eng. HossamEldin El-Sherif, Eng. Tadesse G Wakjira, and Eng. Mohamed Ibrahim for their immense support and encouragement.

I am indebted to my friends Osama Abdeljaber, Atif Hafiz, and Lutfi Samara, who made these years of research an enjoyable experience.

Finally, these acknowledgments would not be complete without expressing my sincere gratitude to my parents Soliman Younis and Rodaina Nazmi; my sisters Diana and Hanan; and my brothers Mahmoud, Mo'ataz, and Ahmed. Without their infinite support, it would have been impossible to reach such level of education.

TABLE OF CONTENTS

DEDICATION v

ACKNOWLEDGMENTS vi

LIST OF TABLES xiv

LIST OF FIGURES xv

CHAPTER 1: INTRODUCTION 1

1.1 Background 1

1.2 Literature Appraisal 4

1.2.1 Seawater in plain concrete 4

1.2.2 Combining seawater and RCA in plain concrete 7

1.2.3 Flexural performance of RC beams 9

1.2.4 Life cycle cost analysis 10

1.3 Research Objectives and Significance 11

1.4 Thesis Outline 14

CHAPTER 2: CONCRETE CHARACTERIZATION METHODOLOGY 17

2.1 Concrete Mixtures 17

2.2 Material Characterization of Concrete Constituents 18

2.2.1 Water 18

2.2.2 Aggregates 19

2.2.3 Cementitious materials 22

2.3 Concrete mixture proportions.....24

2.4 Test and Observation Methods for Concrete.....25

2.4.1 Characterization of fresh concrete.....25

2.4.2 Mechanical characterization of hardened concrete 25

2.4.3 Permeability performance of hardened concrete.....27

2.4.4 Isothermal calorimetry.....29

2.4.5 Microstructure investigation.....30

CHAPTER 3: FRESH AND HARDENED PROPERTIES OF SEAWATER-MIXED CONCRETE 32

3.1 Fresh Concrete Properties 32

3.2 Mechanical Characteristics of Hardened Concrete 34

3.3 Permeability Performance of Hardened Concrete.....38

3.4 Isothermal Calorimetry 39

3.5 SEM Results.....42

3.5.1 Cement paste.....42

3.5.2 Mature, hardened concrete 45

3.6 Remedial Measures 48

3.7 Summary and Conclusions.....50

CHAPTER 4: PERFORMANCE OF SEAWATER-MIXED RECYCLED-AGGREGATE CONCRETE.....52

4.1 Fresh Concrete.....52

4.1.1 Density.....52

4.1.2 Air content.....52

4.1.3 Workability and setting.....53

4.2 Hardened Concrete.....55

4.2.1 Strength.....55

4.2.2 Microstructure.....58

4.2.3 Permeability.....61

4.2.4 Shrinkage.....62

4.3 Improving Performance of Concrete with Seawater and RCA.....64

4.4 Summary and Conclusions.....66

CHAPTER 5: FLEXURAL PERFORMANCE OF SEAWATER-MIXED RECYCLED AGGREGATE GFRP-REINFORCED CONCRETE BEAMS.....68

5.1 Experimental Program.....68

5.1.1 Concrete mixtures.....68

5.1.2 RC beam specimens.....71

5.1.3 Test setup.....72

5.2 Experimental Results.....74

5.2.1 Modes of failure.....74

5.2.2 Load-carrying capacity.....77

5.2.3 Deformational characteristics 77

5.2.4 Strain characteristics 80

5.2.5 Energy absorption 84

5.2.6 Ductility index 84

5.2.7 Cracking behavior 86

5.3 Theoretical Formulation 89

5.3.1 Cracking and ultimate Loads 89

5.3.2 Crack width 92

5.3.3 Deflection 93

5.4 Summary and Conclusion 97

CHAPTER 6: LIFE CYCLE COST ANALYSIS OF STRUCTURAL CONCRETE USING SEAWATER, RECYCLED CONCRETE AGGREGATES, AND GFRP REINFORCEMENT 98

6.1 Materials and Methods 98

6.1.1 Design alternatives 98

6.1.2 Reinforced concrete design 99

6.1.3 Concrete mix design 101

6.1.4 Life cycle cost model 102

6.2 Results and Discussion 109

6.2.1 Influence of concrete mixture cost 109

6.2.2 LCCA results 109

6.2.3 Sensitivity analysis 111

6.3 Summary and Conclusions 114

CHAPTER 7: COST EFFECTIVENESS OF REINFORCEMENT ALTERNATIVES FOR A CONCRETE WATER CHLORINATION TANK 116

7.1 Introduction 116

7.2 Research Significance 118

7.3 Materials and Design 120

7.4 Cost Modeling 123

7.4.1 Material cost 124

7.4.2 Construction cost 126

7.4.3 Repair/maintenance cost 127

7.4.4 End-of-life cost 130

7.4.5 Net present cost 131

7.5 Results and Discussion 132

7.5.1 LCCA results 132

7.5.2 Sensitivity analysis 136

7.6 Conclusions 145

CHAPTER 8: SUMMARY AND FUTURE OUTLOOK 147

8.1 Summary 147

8.2 Future Outlook 150

REFERENCES 151

APPENDIX 185

LIST OF TABLES

Table 2.1. Concrete mixtures. 17

Table 2.2. Chemical characterization of the two types of mixing water. 19

Table 2.3. Physical and chemical characterization of aggregates. 21

Table 2.4. Chemical characterization of the cement and slag. 23

Table 2.5. Concrete mixture proportions. 24

Table 3.1. Summary of permeability performance test results for Mixes A and B 39

Table 4.1. Summary of permeability performance test results for Mixes A and C. 61

Table 5.1. Concrete mixtures adopted in Study 3. 70

Table 5.2. Test matrix for the RC beams. 72

Table 5.3. Summary of the test results. 76

Table 5.4. Comparison of experimental and theoretical predictions. 91

Table 6.1. Design alternatives considered in Study 4. 98

Table 6.2. Summary of the design of conventional steel-reinforced concrete for tall buildings with different heights and gross floor areas [190]. 101

Table 6.3. Unit costs considered in the LCCA of Study 4 (as of 2017 prices). 104

Table 6.4. Summary of LCCA results. 110

Table 7.1. Maximum limits of water-soluble chloride content in concrete mixture according to different standards 117

Table 7.2. Reinforcement design for the RC water tank. 121

Table 7.3. Unit costs considered in Study 5 (as of 2019 prices). 125

LIST OF FIGURES

Figure 1.1. The waste produced and mineral resource depletion per 1 m^3 of natural aggregate and recycled-aggregate concretes [14]. 2

Figure 1.2. Positive and negative responses regarding seawater-mixed concrete, collected from previous research (adapted, with modifications, from [16]). 6

Figure 1.3. Relationship between compressive strength and cement content for natural-aggregate concrete (NAC) and recycled aggregate concrete (RAC) [14]. 8

Figure 1.4. Components of the life-cycle cost model for an RC structure. 11

Figure 1.5. A perspective towards sustainable concrete structures (NA stands for natural aggregates; C&D for construction and demolition; LCCA for life cycle cost analysis; and LCA for life cycle assessment). 13

Figure 1.6. Outline of the thesis body. 14

Figure 2.1. Particle size distributions for the aggregates used. 20

Figure 2.2. Concrete shrinkage test—measurement of (a) reference bar length and (b) specimen's length. 26

Figure 2.3. Rapid chloride permeability test. 28

Figure 2.4. Chloride migration test. 29

Figure 3.1. Slump flow for Mixes A and B as a function of time. 33

Figure 3.2. Initial setting time measurements for Mix A and Mix B. 34

Figure 3.3. Compressive strength test results for Mix A and Mix B concretes. 35

Figure 3.4. Tensile strength test results for Mix A and Mix B concretes. 36

Figure 3.5. Shrinkage test results for Mix A and Mix B concretes. 38

Figure 3.6. (a) Heat flow and (b) Cumulative heat release of the paste samples. 41

Figure 3.7. BSE images taken for the (a) 3-day freshwater paste and (b) 3-day seawater

paste. 43

Figure 3.8. SE images taken for the (a) 3-day freshwater paste and (b) 3-day seawater paste. 44

Figure 3.9. Typical microstructure for seawater- and freshwater-mixed 28-day cement pastes. 44

Figure 3.10. BSE images taken after 56 days for concrete of (a) Mix A and (b) Mix B (refer to Figure 3.11 for the ‘x’ mark). 45

Figure 3.11. Typical EDX microanalysis for the hydrated cement (‘x’ sign location in Figure 3.10) in the 56-day concrete of (a) Mix A and (b) Mix B. 46

Figure 3.12. Observation of salt impurities in the SE image of the 56-day seawater concrete. 47

Figure 3.13. (a) Slump flow and (b) compressive strength results for seawater concrete after remedial actions. 49

Figure 4.1. Slump flow as a function of time for Mix A and Mix C concretes. 54

Figure 4.2. Setting time test results for Mix A and Mix C concretes. 54

Figure 4.3. Compression test results for Mix A and Mix C concretes.....57

Figure 4.4. Splitting tensile test results for Mix A and Mix C concretes. 58

Figure 4.5. BSE images taken after 56 days for concrete of (a) Mix A and (b) Mix C. 59

Figure 4.6. SE images of the 56-day-aged concrete for (a) Mix A and (b) Mix C. 59

Figure 4.7. Pictorial representation of RCA micro cracks and dual ITZ [15]. 60

Figure 4.8. Shrinkage test results for Mix A and Mix C concretes. 63

Figure 4.9. Slump flow after changes in mixture design for Mix C. 64

Figure 4.10. Compressive strength results for Mix C concrete after applying mixture

design improvements, considering standard curing conditions. 65

Figure 5.1. Schematic drawing for a typical RC beam used in this study. 72

Figure 5.2. Test setup and instrumentation for RC beams.....73

Figure 5.3. Concrete crushing in Specimen B-S-2. 75

Figure 5.4. GFRP tensile rupture in Specimen B-F-2.....75

Figure 5.5. Load vs. deflection diagrams for (a) steel and (b) GFRP reinforced concrete beams. 78

Figure 5.6. Idealization of load-deflection diagrams for (a) steel and (b) GFRP reinforced concrete beams. 79

Figure 5.7. Load vs. rebar strain diagrams for (a) steel and (b) GFRP reinforced concrete beams. 82

Figure 5.8. Load Vs. concrete compressive strain diagrams for (a) steel and (b) GFRP reinforced concrete beams. 83

Figure 5.9. Schematic description of ductility index for RC beams based on energy concept [183]. 85

Figure 5.10. Crack pattern for Specimens (a) C-S-2 and (b) C-F-2; (c) idealization of the crack pattern in the RC beams tested. 87

Figure 5.11. Load vs. crack-width diagrams for samples of (a) steel and (b) GFRP reinforced concrete beams. 88

Figure 5.12. Equilibrium forces for a typical RC beam under flexure. 90

Figure 5.13. Predicted vs. experimental load-deflection diagrams (taking fc'=60 MPa) for (a) steel-RC and (b) GFRP-RC beams. 96

Figure 6.1. Components of the life cycle cost model of Study 4.....103

Figure 6.2. Cash flow diagrams for the design alternatives (future costs are not

discounted). 110

Figure 6.3. Life cycle cost results (considering the baseline scenario where r= 0.7%). 111

Figure 6.4. Sensitivity of LCC results to the discount rate. 112

Figure 6.5. Variation of the concrete cost with different RCA-to-NA price ratios. .. 113

Figure 6.6. Variation of LCCA results with respect to different RCA-to-NA price ratios. 113

Figure 7.1. Reinforcement details for the main vertical cross-section of the water tank (adapted, with modifications, from [258]). 120

Figure 7.2. Summary of LCCA results (100-year study period). 133

Figure 7.3. Cumulative NPC results for the reinforcement design alternatives. 135

Figure 7.4. Sensitivity of NPC to the assumed discount rate (C is fixed at 1.5M and CGFRP = 0.8C). 136

Figure 7.5. Sensitivity of NPC to the assumed construction cost (r is fixed at 0.6% and CGFRP = 0.8C). 137

Figure 7.6. NPC plots of (a) black vs. epoxy coated steel (b) black vs. stainless steel and (c) black steel vs. GFRP reinforced concrete as a function of discount rate and C/M ratio. 139

Figure 7.7. Sensitivity of (a) NPC and (b) breakeven year of GFRP reinforced concrete to the assumption of CGFRP (r is fixed at 0.6% and C=1.5M). 140

Figure 7.8. Effect of concrete strength on life cycle performance of (a) black steel and (b) epoxy coated steel reinforced concrete (considering the baseline scenario where r = 0.6%, C = 1.5M, and CGFRP = 0.8C). 142

Figure 7.9. Effect of using SCMs on the life cycle performance of black steel RC structure (considering the baseline scenario where r=0.6%, C=1.5M, and w/cm ratio is fixed at 0.47). 144

CHAPTER 1: INTRODUCTION

1.1 Background

Freshwater scarcity is increasingly an issue of global concern. Recently, it has been estimated that around two-thirds of the global population live under conditions of severe water scarcity for at least one month every year [1]. Consequently, desalination is used worldwide in regions with freshwater shortages: the global capacity of desalination plants has increased from 5 million m^3/day in 1980 to 80.9 million m^3/day in 2013 [2]. However, desalination is energy-intensive, making the desalted water relatively expensive, and generates a brine waste stream which negatively impacts on the environment [3]. The average cost of reverse osmosis (RO), the most commonly-used desalination technique worldwide [2], ranges between 0.50 and 1.20 \$/m^3 [4] and is associated with an energy consumption of 3–4 kWh/m^3 as well as emitted CO_2 levels of 1.4–1.8 kg/m^3 of product water [3]. The annual volume of brine generated is estimated to reach 156 km^3 by 2050 [2].

One important step towards overcoming the challenge of freshwater scarcity and the corresponding increasingly high demand for desalination is reducing the unnecessary use of freshwater for construction purposes. Concrete is the most commonly used construction material worldwide, and is typically produced by mixing cement, freshwater, aggregates, and often mineral/chemical admixtures [5]. The construction industry uses over two billion tons of potable water every year to produce concrete [6], with the use of reinforced concrete increasing globally every year: this accounts for approximately 9% of the global industrial water demand [7]. Predictions show that, in 2050, 75% of the water demand for concrete production will occur in regions most likely to experience water shortages [7]. Seawater can represent a valid alternative to freshwater in concrete production but, despite it being more a sustainable

water source, the use of seawater in concrete is currently prohibited because its high salinity promotes corrosion of steel reinforcement [8]. Seawater has an average total salinity of 3.5%, of which typically around 78% is sodium chloride (NaCl) [9].

Construction and demolition wastes make up about 30% of the total waste worldwide (over two billion tons annually [10]). In the US alone, the annual construction and demolition waste has been estimated at ~480 million tons, of which more than 50% is primarily concrete [11]. Without recycling, the yearly accumulation of these wastes is likely to lead to significant economic and environmental problems [12]. Furthermore, the global construction industry consumes over 40 billion tons of natural aggregates every year [10]. Using recycled concrete aggregate (RCA) can largely reduce the negative effects of the demolition waste and control the harvesting of natural aggregates (*Figure 1.1*) while potentially providing acceptable properties of the resulting concrete [13,14]. However, one of the main concerns in using RCA is the likelihood of saline contamination, given the high diversity in RCA sources, again promoting corrosion of the steel reinforcement [15].

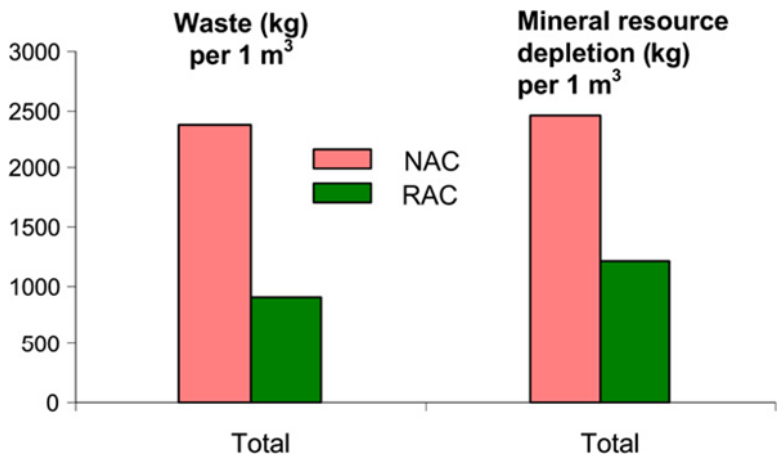

Figure 1.1. The waste produced and mineral resource depletion per 1 m^3 of natural aggregate and recycled-aggregate concretes [14].

It is postulated from the existing literature that the salt, existing either in seawater or potentially in RCA, has no significant negative effects on plain concrete characteristics [15–17]; the negative effect in such a case appears to be limited to the corrosion of steel reinforcement. This can be addressed by using fiber-reinforced polymer (FRP) to reinforce concrete structures [18], this material being corrosion-resistant [19,20] and lightweight while still providing sufficient mechanical strength [21]. Despite the higher cost of FRP reinforcement compared to that of black steel, the implementation of economic and environmental studies on FRP-reinforced concrete indicates significant cost savings in the long term [22–24]. Amongst all FRP types applicable to reinforce concrete, glass-FRP (GFRP) is the most common, being less expensive while having acceptable mechanical properties [25,26].

Existing literature postulates direct environmental benefits associated with the use of seawater or RCA in structural concrete. For instance, Arosio et al. [27] reported that mixing concrete with seawater would lead to reductions up to 12% in its water footprint. Hossain et al. [28] reported that using RCA in concrete mixtures can result in approximately 65% savings in greenhouse gas emissions and up to 58% reductions in non-renewable energy consumption. These findings have been corroborated by other studies on RCA environmental benefits [12,14,29]. Studies have shown that FRP also provides clear environmental benefits in concrete structures due to the increased service life [30–33]. For instance, Cadenazzi et al. [31] performed a life-cycle-assessment study (at the design stage) on a GFRP-reinforced concrete bridge in Florida. It was reported that the cradle-to-grave environmental impacts of the GFRP-RC bridge are lower than that of the black-steel-reinforced counterpart in terms of global warming (by 25%), photochemical oxidant creation (by 15%), acidification (by 5%), and eutrophication (by 50%). The shorter service life of the black steel-RC bridge was a relevant factor for its

lower performance. Also, Amnon [34] concluded that the environmental load of FRP-reinforced pavement is significantly lower than that of the steel-reinforced counterpart, mainly due to the absence of maintenance activities related to steel corrosion during the pavement service life.

In light of the aforementioned background, the present thesis investigates a seawater-mixed concrete incorporating RCA and corrosion-resistant reinforcement (GFRP). Indeed, the probable corrosion concerns associated with chloride ions in seawater and/or possibly contaminated RCA are avoided through the use of GFRP. The rest of Chapter 1 is organized as follows: at first, a literature appraisal is presented in Section 1.2 to identify research gaps to be bridged in the current thesis. After that, Section 1.3 highlights the objectives of the thesis, and Section 1.4 presents the thesis outline.

1.2 Literature Appraisal

1.2.1 Seawater in plain concrete

Despite the common belief that seawater is improper for use in structural concrete, a number of structures were successfully built using seawater concrete (seawater-mixed concrete and seawater concrete are used interchangeably in the text) during the last century [35] or even earlier [36,37]. This can be regarded as intuitive evidence for the potential use of seawater to produce durable concrete. The issue of steel corrosion can be addressed either by using seawater in non-reinforced concrete applications or alternatively by using non-corrosive material such as fiber-reinforced polymer (FRP) to reinforce concrete structures [18]. In effect, durability studies have verified the long-term strength performance of GFRP bars in seawater concrete [38–40].

While using seawater in concrete mixtures appears viable, there is a need to determine the fresh, hardened, and durability characteristics of such concrete. Existing

literature postulates no significant negative effects on the mechanical properties of seawater concrete [16,41]. Starting from early works, Narver [42] reported a higher compressive strength for seawater concrete during the first month, and then, from the third month, the strength was 6% lower when compared to that of freshwater concrete. Similarly, Steinour [43] showed an increase in the early strength followed by a later strength reduction of 8–15% for seawater concrete. These results are in conformity with more recent studies [16,35,44–46]. In contrast, the research conducted by Griffin and Henry [47] showed a strength increase not only at early ages but also in the long term. A gain in strength was also reported by Dewar [48], who underlined that the concrete strength increased with the salinity content of mixing water. Shi et al. [49] reported a 22% increase in the 28-day compressive strength of seawater concrete compared to that of freshwater-mixed counterpart. Park et al. [50] evaluated concrete mixtures with different chloride contents (0–1.2% of cement weight) in terms of concrete shrinkage and mechanical characteristics. While an insignificant influence of NaCl content was reported on the mechanical characteristics, the presence of chloride led to a notable increase in the drying shrinkage and cracking [50]. Seawater concrete was found to achieve better characteristics with the addition of mineral admixtures such as blast furnace slag [16,51–53], fly ash [17,54,55], and metakaolin [49,56,57]. In this context, Nishida et al. [16] conducted a comprehensive survey of about 85 references published between 1974 and 2013 and pertaining to the effects of using seawater in concrete mixture: it was reported that over 38% of the preceding research had shown promising outcomes, more particularly in the case of using blast furnace slag (*Figure 1.2*). When considering fresh concrete properties, it was generally reported that the existence of salt in seawater concrete leads to a decrease in the workability and the setting time [51,58–

60]. Some studies suggested that the use of suitable chemical admixtures leads to an improvement in the workability of seawater concrete [35].

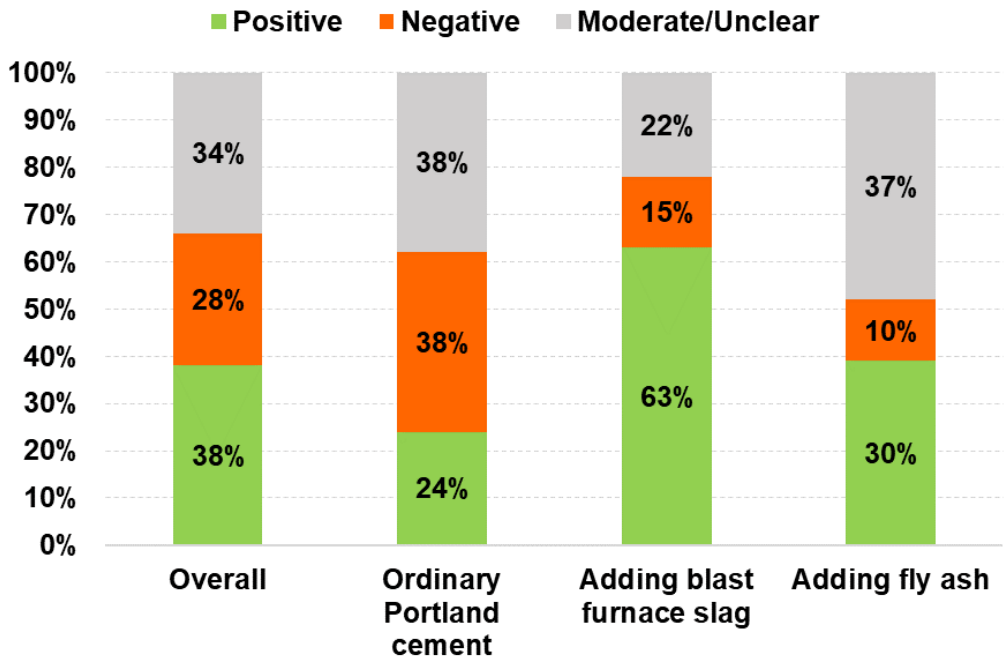

Figure 1.2. Positive and negative responses regarding seawater-mixed concrete, collected from previous research (adapted, with modifications, from [16]).

From the aforementioned literature survey, it is apparent that the reports concerning seawater concrete are, to a certain degree, contradictory. While the majority of studies concluded a slight negative effect on the concrete strength, some revealed otherwise [47–49]. It is likely that the exact effect of mixing using seawater on the compressive strength depends on the seawater composition, cement chemistry, concrete mixture proportions, and curing conditions. Nonetheless, further studies are needed before accepting the use of seawater concrete in structural applications. Further research is also needed to generate well-established design provisions in this regard and thus maximize the potential use of seawater for concrete production.

1.2.2 Combining seawater and RCA in plain concrete

The idea of producing RCA from demolished concrete structures was first introduced in Europe around the time of World War II [61], after which RCA usage has gained popularity and general acceptance. Currently, around 10% of the aggregate used in Europe is RCA; out of this amount, 65% and 35% are used to produce new concrete for buildings and infrastructure, respectively [10]. The first recorded use of seawater to produce concrete in modern times is traced back to World War II – structures were built along the coasts of California and Florida using seawater-mixed concrete [35]. However, some have suggested that the ancient Romans pioneered the use of seawater in concrete made with natural pozzolans [36].

Previous studies generally show negative impacts of RCA on the fresh and hardened properties of concrete (see the literature surveys [15,62–68]). Examples include reductions in workability, strength, and durability (more studies pertaining to recycled-aggregate concrete and its mechanisms are discussed in Chapter 4). For instance, a complete replacement of natural coarse aggregates (NCA) by RCA in plain concrete results in reductions up to 30% in compressive strength, 24% in tensile strength, and 45% in the elastic modulus [15,64,65,67]. In principle, such drawbacks are generally attributed to the relatively inferior physical and mechanical performance of RCA compared to NCA [69]. However, these negative impacts may potentially be mitigated by adjustments in the concrete mixture design [70,71] or by using supplementary cementitious materials and chemical admixtures [72–74]. For example, Marinković et al. [14] indicated that a slight increase in cement concentration (~5%) is sufficient for the recycled-aggregate concrete to achieve a compressive strength comparable to that of conventional concrete as shown in *Figure 1.3* (although this

highly depends on other several factors such as RCA quality, curing regime, type of cementitious materials, etc.).

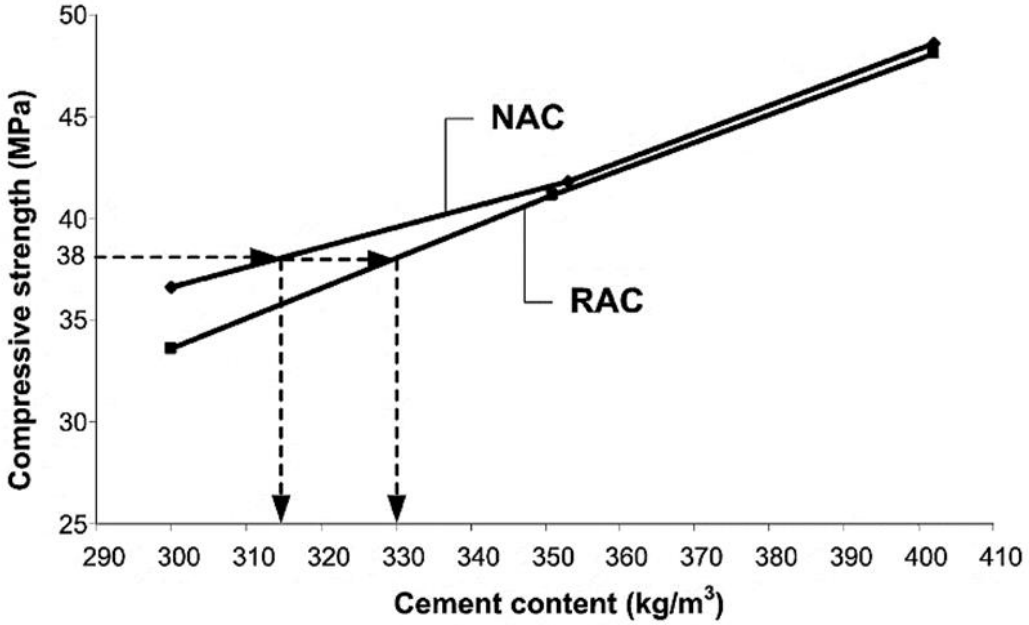

Figure 1.3. Relationship between compressive strength and cement content for natural-aggregate concrete (NAC) and recycled aggregate concrete (RAC) [14].

Whilst a significant amount of research has been performed in the last two decades on the sole effect of mixing concrete with seawater [16,41] or RCA [15,62–68], studies concerning the combined effect of seawater and RCA are relatively very scarce [51]. In this context, Etxeberria et al. [51] reported an approximately 30% reduction in the compressive strength of concrete while using both seawater and RCA in the mixture at 100% replacement level. Nevertheless, further research is needed to understand the fresh and hardened properties of seawater-mixed concrete made with RCA, primarily to address the shortcomings expected in the performance of such concrete. While various aspects of such novel and sustainable concretes need to be studied and understood before widespread implementation, this research is focused on

understanding and quantifying the negative impacts of the combined use of seawater and RCA on a large range of concrete properties, and on mitigating these negative impacts.

1.2.3 Flexural performance of RC beams

Studies on the flexural performance of RC beams with seawater-mixed concrete are limited [75] with a clear lack of addressing durability related issues. In this context, Dong et al. [75] reported a change in the failure mode of seawater concrete beams reinforced with steel/FRP composite bars and subject to aggressive exposure (over 6-month immersion in 50 °C seawater) from concrete crushing to rebar tensile rupture, associated with ~11% reduction in the flexural capacity.

The effects of using RCA on the flexural performance of RC beams have received significant attention among researchers worldwide [76–84]. Alnahhal and Aljidda [76] underlined that the use of RCA has no remarkable impact on the flexural capacity of RC beams. Likewise, Sunayana and Barai [77] demonstrated application of 100% RCA in RC beams without compromising flexure performance. This finding was corroborated by preceding works from other researchers [78–84], who conclusively reported no significant difference in flexural capacity and service-load deflections between NCA and RCA reinforced concrete beams having the same reinforcement percentage and concrete strength.

GFRP has shown high potential as an alternative non-corrosive reinforcement material given its high strength-to-weight ratio [21], excellent durability performance [85], and relatively lower cost compared to carbon FRPs [23]. Therefore, GFRP has globally attracted the interest of the construction industry. Design guidelines have also been developed for the use of GFRP in RC elements [86,87]. As such, successful implementations have been reported on the use of GFRP-RC in several types of

structures such as bridges [88,89], parking garages [90], as well as tunnels and marine structures [91]. Over the last decade, a significant amount of research has been carried out to investigate the flexural performance of GFRP-RC beams [92–101], demonstrating a higher flexural strength yet lower stiffness and ductility of GFRP-RC beams compared to their steel-reinforced counterparts. Indeed, this is attributable to the linear elastic behavior and the relatively lower elastic modulus of GFRP bars [21].

The main research gap identified from the above literature survey is the lack of understanding of the flexural behavior of seawater-mixed recycled-aggregate GFRP-reinforced concrete beams – which is an aim of the present thesis. To achieve this, twelve RC beams with varying concrete mixture design and reinforcement material were constructed and tested under four-point loading.

1.2.4 Life cycle cost analysis

In principle, to quantitatively measure the sustainability of a product, the economic and environmental impacts associated with it are obtained on a life-cycle assessment basis (i.e., cradle-to-grave); starting from raw materials collection and assembly, and extending to fabrication, operation, transport, and waste management [102]. Life-cycle cost analysis (LCCA) is an established tool to optimize the cost of a certain product when the focus is on measuring the economic aspects of sustainability. Classically, the LCCA of an RC structure involves four key cost items (*Figure 1.4*), namely, initial, functional, repairs, and disposal at the end of the life-cycle [103,104].

The existing literature shows a clear advantage of individually using recycled concrete aggregate [14,105,106] or FRP reinforcement [22–24] in structural concrete in terms of cost performance. The main research gap to be bridged here is to assess the life-cycle cost implications of combining seawater, RCA, and GFRP reinforcement in concrete structures (particularly high-rise buildings). In addition, as elaborated in the

literature survey of Chapter 7, there is a perceptible need to compare the cost performance of GFRP with that of other corrosion-resistant reinforcements in concrete structures other than bridges. In this thesis, we established a comparative cost analysis among four reinforcement materials, namely, black steel, stainless steel, epoxy-coated steel, and GFRP for an RC water chlorination tank.

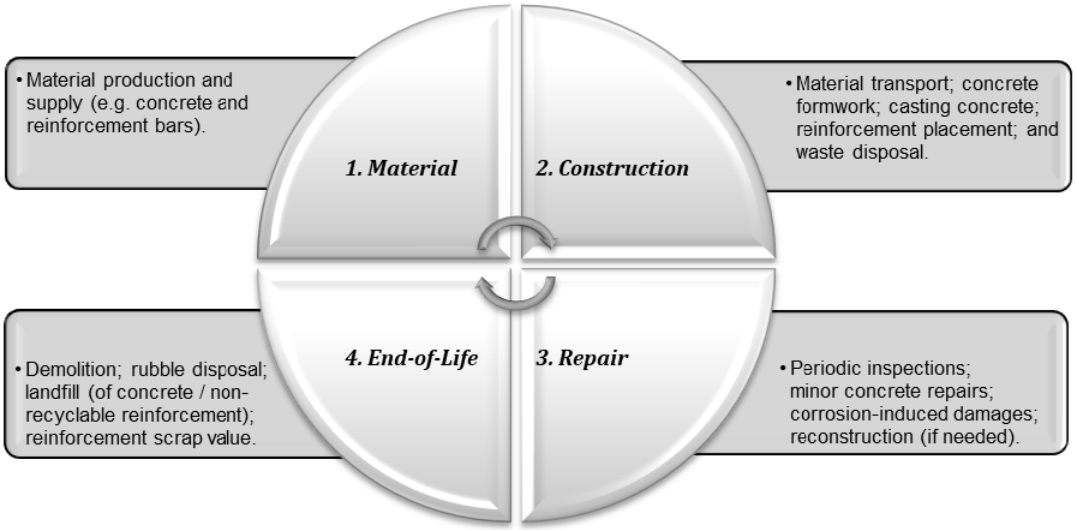

Figure 1.4. Components of the life-cycle cost model for an RC structure.

1.3 Research Objectives and Significance

The current research represents a step towards redefining sustainable/green concrete as shown in *Figure 1.5*. It is apparent that combining seawater and RCA in concrete mixtures is significantly advantageous from a sustainability perspective, considering the increasing global concerns of freshwater scarcity, desalination impacts, construction and demolition waste, and the possible depletion of natural aggregate. However, the expected high concentration of chlorides in such mixtures potentially resulting in steel reinforcement corrosion is an undeniable challenge. This challenge may be addressed by using the proposed mixtures in plain concrete applications or with

non-corrosive reinforcement such as FRPs. The relatively higher initial direct cost of FRP reinforcement can be recompensed in the long term by the savings associated with corrosion alleviation. Therefore, combining seawater, RCA, and FRP in structural concrete is a novelty, and is potentially viable from technical, environmental, and economic standpoints.

The main objective of this research is to establish the experimental scientific evidence on the safe utilization of both seawater and recycled aggregates that, when combined with GFRP reinforcement, can be used to construct sustainable and economic concrete structures. In light of *Figure 1.5*, and based on the research gaps identified in Section 1.2, this thesis aims at fulfilling five key tasks:

(a) To carry out a wide-range experimental study on the fresh and hardened properties of seawater-mixed concrete.

(b) To study the effect of combining seawater and recycled coarse aggregates on the performance of the resulted concrete.

(c) To investigate the flexural performance of seawater-mixed recycled-aggregate GFRP-reinforced concrete beams.

(d) To conduct a life cycle cost analysis in order to measure the cost effectiveness of the proposed combination (i.e., seawater + RCA + GFRP reinforcement) as compared to traditional RC structures.

(e) To establish a comparison among different reinforcement materials for structural concrete in terms of their cost effectiveness.

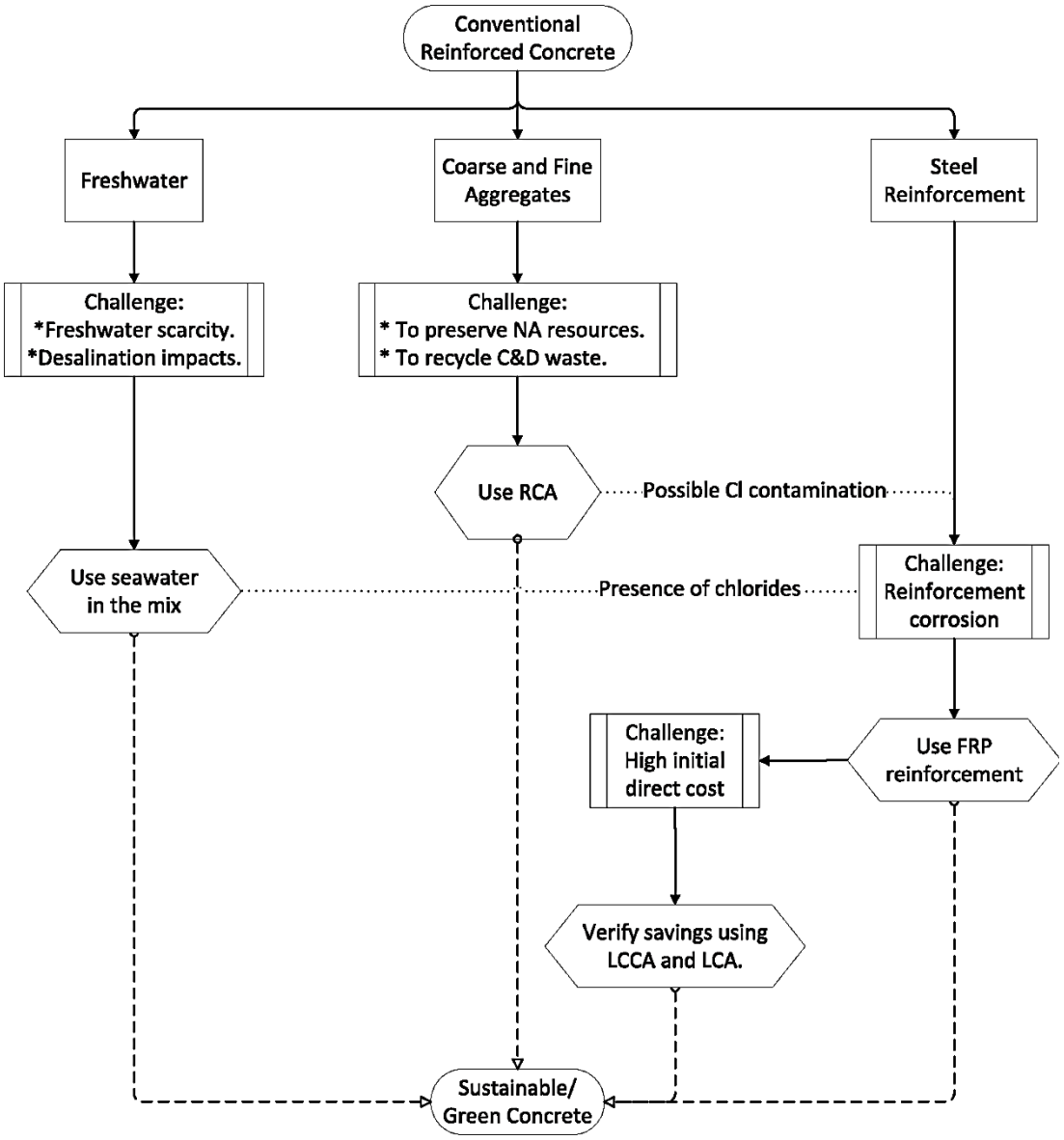

Figure 1.5. A perspective towards sustainable concrete structures (NA stands for natural aggregates; C&D for construction and demolition; LCCA for life cycle cost analysis; and LCA for life cycle assessment).

1.4 Thesis Outline

In line with the objectives listed in Section 1.3, the main body of this thesis consists of three main parts (*Figure 1.6*), namely, concrete characterization, RC beams testing, and life cycle cost analysis, overall encompassing five core studies. Each of the five studies has been submitted (by the thesis date) for consideration for a journal publication.

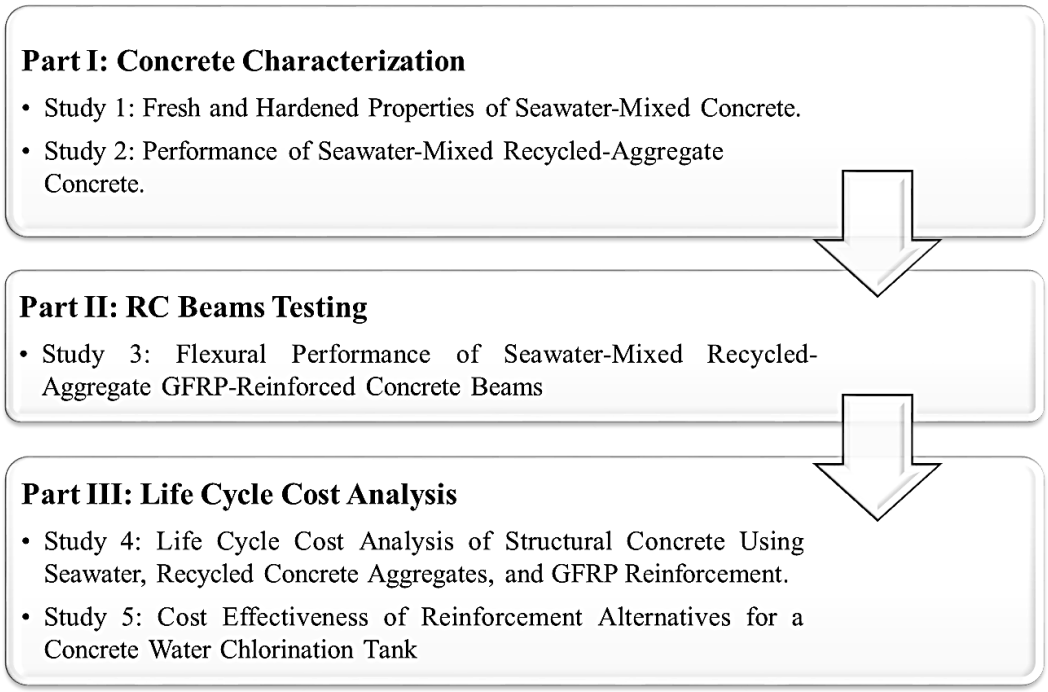

Figure 1.6. Outline of the thesis body.

Chapter 2 details the concrete characterization methodology in the first and second studies of the thesis. Material characterization results for the concrete mix constituents were presented. In addition, methods implemented to measure fresh and hardened properties of concrete were explained.

Chapter 3 (Study 1) reports on the results of an extensive experimental study to compare the fresh and hardened properties of freshwater- and seawater-mixed concretes. The experimental program included the following tests: (a) characterization

of fresh concrete (slump flow, density, yield, air content, and setting time tests); (b) mechanical characterization of hardened concrete (compressive strength, splitting tensile strength, and shrinkage tests); and (c) permeability performance of hardened concrete (rapid chloride permeability, chloride migration, and water absorption tests). Scanning electron microscopy and isothermal calorimetry were used as supplementary tools to better explain the experimental observations. Based on the study results, remedial measures were proposed based on lab trials to improve the properties of seawater concrete.

Likewise, **Chapter 4 (Study 2)** investigates the fresh and hardened properties of a proposed "green" concrete mixed using seawater and recycled coarse aggregates. Fresh and hardened properties of the two concretes including workability, strength gain, drying shrinkage, permeability, and microstructure were characterized and compared. Finally, strategies to improve the performance of such concrete are suggested.

Chapter 5 (Study 3) reports on the results of an experimental study on the flexural performance of seawater-mixed recycled-aggregate concrete reinforced with GFRP bars. A total of 12 medium-scale reinforced concrete (RC) beams ($150 \times 260 \times 2200$ mm) were tested under four-point loading. The test variables included the mixing water (seawater/freshwater), aggregate type (conventional/recycled), and reinforcement material (black steel/GFRP). A wide range of flexural properties, including failure mode, cracking behavior, load-carrying capacity, deformation, energy absorption, and ductility were characterized and compared among the beam specimens.

In **Chapter 6 (Study 4)**, a life cycle cost analysis (LCCA) has been conducted to establish the relative cost savings of structural concrete combining seawater, RCA, and GFRP reinforcement in high-rise buildings compared with a traditional concrete mix and reinforcement material (i.e., black steel).

Chapter 7 (Study 5) addresses the use of non-corrosive reinforcement in a concrete water chlorination tank using life cycle cost analysis (LCCA) that aims to evaluate the cost effectiveness of different reinforcement alternatives. A comparison was established between four concrete reinforcing materials, namely, black steel, epoxy-coated steel, stainless steel, and GFRP through a 100-year analysis period.

Finally, based on the outcomes of this thesis, the final conclusions, as well as recommendations for future work, are presented in **Chapter 8**.

CHAPTER 2: CONCRETE CHARACTERIZATION METHODOLOGY

Chapter 2 details the experimental program for the first part of this thesis (**Part 1: Concrete Characterization**). This chapter presents the concrete mixtures to be investigated, details the material characterization of concrete constituents as well as concrete mixture proportions, and describes the test and observation methods used to measure the performance of fresh and hardened concrete.

2.1 Concrete Mixtures

Three concrete mixtures were prepared as shown in Table 2.1. Mix A represents the conventional concrete mixed with freshwater and natural coarse aggregates (NCA) and is considered as a reference. Mix B is made with the use of seawater and NCA. Mix C represents the use of concrete mixed with seawater and recycled coarse aggregate (RCA) at 100% replacement level.

Table 2.1

Concrete Mixtures.

Concrete Mix	Water	Coarse Aggregate
Mix A	Freshwater	Conventional
Mix B	Seawater	Conventional
Mix C	Seawater	Recycled

2.2 Material Characterization of Concrete Constituents

2.2.1 Water

Seawater was pumped from Al-Khor coastal area in Qatar to a portable tank. After that, the seawater was delivered to the concrete plant, fabric-filtered, and stored in chemical tanks to be used for concrete mixing and curing. Chemical characterization was performed for both types of mixing water, including the determination of chlorides, sulfates, alkalinity, total dissolved solids, and pH (at 25 ºC). Table 2.2 summarizes the chemical characterization results for both water types as per the corresponding methods/standards. As shown in the table, the pH values were comparable. Alkalinity measurements were within acceptable limits as per Qatar Construction Specifications (QCS) [107] for both water types. However, the sulfates, chlorides, and dissolved solids in seawater were significantly higher than those of the conventional freshwater or the allowable limits. The relatively high concentrations of chlorides and sulfates in Qatari seawater compared to those of the global average [41] can be attributed to extensive desalination activities which result in high disposal rates of the generated brine. Accordingly, this research evaluates the implications of using such water in concrete, with an attempt to provide remedial measures, if needed, to achieve properties comparable to that of the conventional concrete.

Table 2.2

Chemical Characterization of the Two Types of Mixing Water.

Test	Unit	Method/Standard	Maximum Limit [107]	Results	
				Freshwater	Seawater
Chloride (Cl^-)	mg/L	BS 1377 PART 3 [108]	1000	14.1	18600
Sulfate (SO_4^{-2})	mg/L	BS 1377 PART 3 [108]	2000	20.9	2359
Total alkalinity	mg/L	BS 6068-2.51 [109]	500	69.5	149
Total dissolved solids	mg/L	BS 1377 PART 2 [110]	2000	62.0	30300
pH (at 25 ºC)	-	BS 6068-2.50 [111]	6.5 – 9.0	8.1	8.20

2.2.2 Aggregates

Locally-available washed sand was used in all concrete mixtures. The natural coarse aggregates used in Mix A and Mix B were Gabbro crushed rock (imported from Oman to Qatar to meet local demands). Recycled concrete aggregates (produced and used in Qatar since 2009 from demolished concrete structures and discarded concrete from construction [112]) were used as coarse aggregates in Mix C. Gradation analysis was carried out on the coarse and fine aggregates as per BS EN 933-1 [113], for which *Figure 2.1* presents the particle size distributions. The size of the RCA used was between 5–20 mm: 75% of the RCAs were 10-mm in size or more.

Table 2.3 presents the physical and chemical characteristics of the fine and coarse aggregates used in the current research. In general, the measured properties of the aggregates were within the acceptable limits [107], except the RCA water absorption, which was significantly higher than the 2% limit [107]. Indeed, this high water absorption is due to the high porosity of the RCA, the presence of adhered mortar on the RCA surface, and the relatively high percentage of clay lumps and friable particles in the RCA. RCA showed a lower particle density than the NCA. Results from

the Los Angeles abrasion and 10%-fines-value tests revealed an increase in the material loss for RCA as compared to NCA. Aggregate soundness test showed that RCA had potentially less resistance to disintegration by weathering compared to the NCA. Flakiness and particle-shape indices suggested that, compared to NCA, RCA had a rougher surface texture with an irregular shape. These results taken together indicate that the RCA generally showed inferior physical and mechanical performance compared to the NCA, which is somewhat expected. However, RCA showed similar results to NCA in tests for organic impurities, acid-soluble chloride, acid-soluble sulfate, and percentage of lightweight particles.

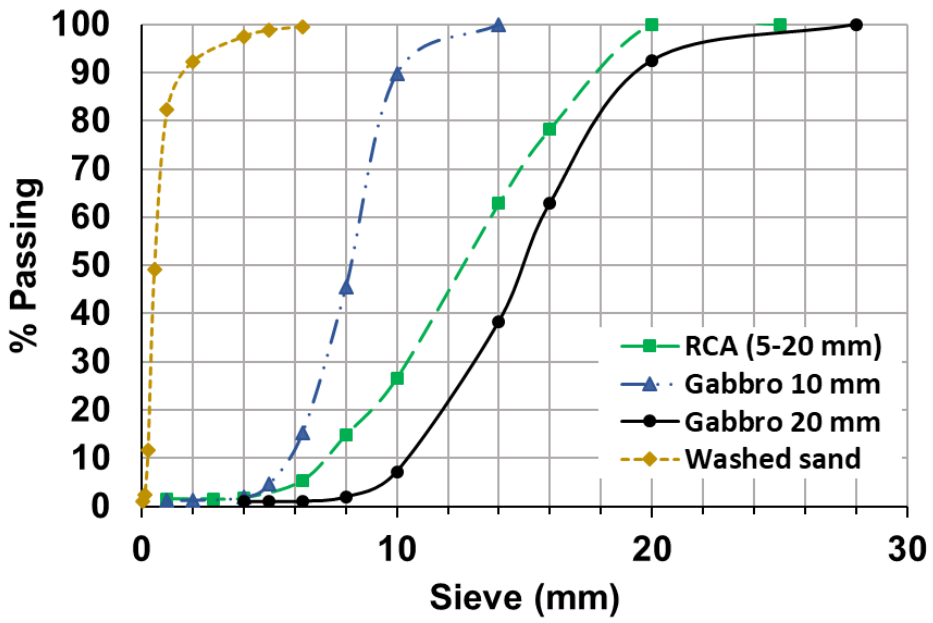

Figure 2.1. Particle size distributions for the aggregates used.

Table 2.3

Physical and Chemical Characterization of Aggregates.

Test	Method	Results (Coarse Aggregates)				Results (Fine Aggregates)	
		20-mm Gabbro	10-mm Gabbro	RCA	Limit [107]	Washed Sand	Limit [107]
Material finer than 63 µm	BS EN 933-1 [113]	0.8%	1%	0.3%	2.0% max.	1.1%	3.0% max.
Particle density (kg/m^3)							
(a) Oven dried	BS EN 1097-6 [114]	(a) 2980	(a) 2930	(a) 2440	2000 min.	(a) 2620	2000 min.
(b) Saturated surface dried		(b) 2960	(b) 2950	(b) 2552		(b) 2630	
(c) Apparent		(c) 2940	(c) 2980	(c) 2746		(c) 2650	
Water absorption	BS EN 1097-6 [114]	0.4%	0.6%	4.6%	2.0% max.	0.6%	2.3% max.
Clay lumps & friable particles	ASTM C142 [115]	0.10%	0.10%	0.29%	2.0% max.	0.10%	2.0% max.
Flakiness index	BS EN 933-3 [116]	6.9%	11.7%	5.2%	35.0% max.	-	-
Particle shape index	BS EN 933-4 [117]	8.2%	7.7%	3.4%	15.0% max.	-	-
% of lightweight particles	ASTM C123 [118]	0.0%	0.0%	0.0%	0.5% max.	0.0%	0.5% max.
10% Fines value	BS 812-111 [119]	360 kN	360 kN	189 kN	150 kN min.	-	-
Los Angeles abrasion test	BS EN 1097-2 [120]	9%	10%	24%	30% max.	-	-
Aggregate soundness	BS EN 1367-2 [121]	1.2%	2.9%	12.6%	15.0% max.	10.3%	15% max.
Organic impurities	ASTM C40 [122]	None	None	None	-	None	-
Acid-soluble chloride	BS EN 1744-5 [123]	0.02% wt.	0.02% wt.	0.02% wt.	0.03% wt. max.	0.02% wt.	0.06% wt. max.
Acid-soluble sulfate	BS EN 1744-1 [124]	0.1% wt.	0% wt.	0.19% wt.	0.3% wt. max.	0.3% wt.	0.4% wt. max.

2.2.3 Cementitious materials

Ordinary Portland cement (OPC) and blast furnace slag were used as cementitious materials. Table 2.4 lists the chemical composition of the ordinary Portland cement obtained as per BS EN 196-2 [125]. Blast furnace slag (referred to as "slag" in the rest of the thesis) was used at 65% supplementary cementitious material replacement level in all mixtures as it is known to improve the performance of fresh and hardened seawater-mixed concrete [126] or recycled-aggregate concrete [51]. In accordance with BS EN 15167 [127], the chemical composition of the slag was determined by X-ray fluorescence and listed in Table 2.4. The chemical composition of the slag conforms with previous research [128] and acceptable criteria [127]. The calcium oxide (CaO) content in slag (41.1% wt.) was lower than that of the ordinary Portland cement (61.8% wt.) but higher than typical values for fly ash [129] or metakaolin [49]. Accordingly, the CaO/SiO_2 ratios calculated for the slag and cement were 1.25 and 3.11, respectively. The fineness obtained by Blaine air permeability test [130] was measured as 4510 and 3350 cm^2/g for the slag and ordinary Portland cement, respectively.

Table 2.4

Chemical Characterization of the Cement and Slag.

Chemical composition (% wt.)	Slag	Cement
SiO_2	32.77	19.90
Al_2O_3	13.49	4.30
Fe_2O_3	0.44	3.21
CaO	41.10	61.84
MgO	5.84	4.49
Na_2O	0.24	0.51 (combined)
K_2O	0.35	
TiO_2	0.38	-
MnO	0.14	-
Mn_2O_3	0.16	-
S	0.82	2.70
Cl	0.004	0.051
Loss on Ignition	0.77	2.34
$C_2S + C_3S$	-	69.98
C_3A	-	5.96
C_4AF	-	9.76

2.3 Concrete mixture proportions

Ready-mix concrete, with a 28-day design compressive strength of 60 MPa and a water-to-cementitious material (w/cm) of 0.34, was used. Table 2.5 presents the mixture design quantitates for each concrete mixture according to BS EN 206 [131]. The mixture proportions for concrete per cubic meter were 750 kg of sand, 1190 kg of gravel, 158 kg of ordinary Portland cement, 292 kg of slag, and 165 kg of water. In Mix B, seawater fully displaced freshwater as mixing water of concrete. In Mix C, NCA was fully replaced by RCA on a volume basis. It is noted that while the three mixtures have the same w/cm, the water contents in Table 2.5 are different as additional mixing water was used in Mix C to account for the higher water absorption of the RCA. Commercial superplasticizer (Glenium 110M) at a dosage of 3.8 kg/m^3 was used in all mixtures to maintain a minimum of 550-mm slump flow for 60 minutes in the control mixture.

Table 2.5

Concrete Mixture Proportions.

Component	Mix A (kg/m^3)	Mix B	Mix C (kg/m^3)
OPC	158	158	158
Slag	292	292	292
Gabbro 20 mm	700	700	-
Gabbro 10 mm	490	490	-
5-20 mm RCA	-	-	990
Washed sand	750	750	750
Freshwater	165	-	-
Seawater	-	165	205

2.4 Test and Observation Methods for Concrete

2.4.1 Characterization of fresh concrete

Fresh concrete properties were measured and compared among the three concrete mixtures. The slump test was used as a measure of workability. The density, yield, and air content were measured for fresh concrete, along with the initial setting time of the corresponding mortar. The following standards were adopted: (a) ASTM C143/C143M [132] for the slump flow test; (b) ASTM C138/C138M [133] for the density, yield and air content; and (c) ASTM C403/C403M [134] for the setting time test.

2.4.2 Mechanical characterization of hardened concrete

The compressive strength and the splitting tensile strength for concrete cylinders, 150 mm diameter and 300 mm height, were measured using the following standards: (a) ASTM C39/C39M [135] for the compressive strength test and (b) ASTM C496/C496M [136] for the splitting tensile strength test. Two curing conditions were considered, namely:

(a) Standard/control curing (E1): in which the specimens were demolded after 24 hours and cured with freshwater for a 28-day period, and then left to be exposed to the outdoor/ambient environment (of Doha, Qatar);

(b) Seawater curing (E2): in which the specimens were kept in a fiberglass curing tank after demolding and immersed in seawater until the testing time. This condition can provide some insight into the effect of seawater exposure in case of marine concrete structures.

Samples were tested to investigate the effect of four variables, namely: (a) mixing water (seawater/freshwater); (b) coarse aggregates (natural/recycled); (c) testing age (3,7, 28, 56, and 365 days following mixing); and (d) curing condition (E1/E2). Three specimens were considered for each test point.

Concrete shrinkage test was performed on the concrete mixtures in accordance with ASTM C157/C157M [137] (*Figure 2.2*). Three concrete prisms ($100 \times 100 \times 500\ mm$) were cast for each mixture. After 24 hours, concrete prisms were demolded and immersed in water for 30 minutes, then initial length measurements were taken. Concrete specimens were then stored in a room with air-drying conditions (i.e., temperature of 25 ± 1°C and humidity less than or equal 50%). The concrete shrinkage was measured at Days 4, 7, 14, 21, 28, 56, 112, 224, and 365 following concrete mixing. For each measurement, the length difference (ΔL) was determined between a reference bar and the concrete prism. The concrete shrinkage at time t, S_t, is calculated as the change in ΔL_t with respect to that initially measured (ΔL_0) divided by the gauge length ($G = 25.4\ mm$) as follows:

$$S_t\ (\%) = \frac{\Delta L_t - \Delta L_0}{G} x100 \tag{2.1}$$

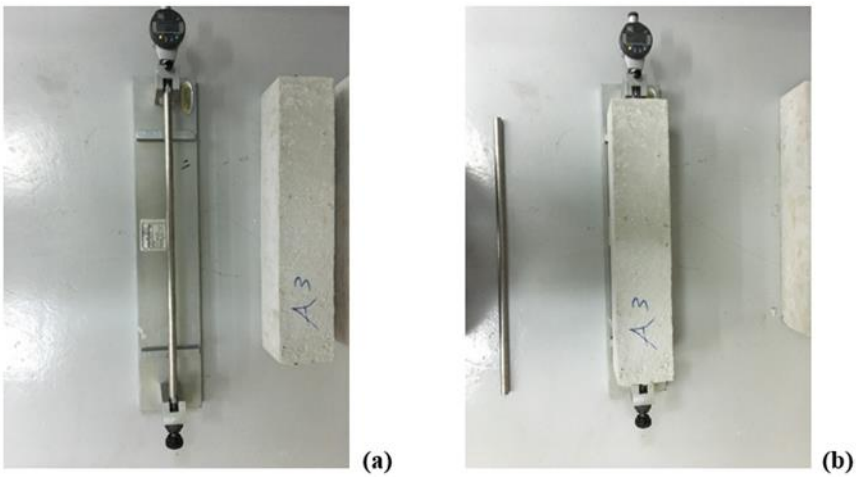

Figure 2.2. Concrete shrinkage test—measurement of (a) reference bar length and (b) specimen's length.

2.4.3 Permeability performance of hardened concrete

Three tests were performed to partially assess the durability performance of hardened concrete, namely:

(a) rapid chloride permeability (RCP) test: in which the electrical conductance of concrete was determined to provide a rapid indication of its resistance to the penetration of chloride ions.

(b) chloride migration (CM) test: in which the resistance of concrete to chloride penetration was also measured but via a different and relatively longer procedure that includes the determination of the non-steady-state migration coefficient. This provides additional information with respect to chloride penetration resistance, which can be compared to that provided by the RCP test.

(c) water absorption (WA) test: in which the ingress of water through the surface of hardened concrete was determined. This test is important given that the performance of concrete subjected to aggressive environments can be strongly related to the penetrability of its pore system [138,139].

These permeability tests provide indications about the quality of hardened concrete and its resistance to chemical attack. It is emphasized that, as Mix B and Mix C concretes are naturally not supposed to be used with steel reinforcement, resistance to chloride penetration is not important per se; however, it is used as a general indicator of the concrete quality.

Rapid chloride permeability test was performed in accordance with ASTM C1202 [140] (*Figure 2.3*). In this test, the total amount of electrical current passing through a concrete cylinder of 100 mm in diameter and 50 mm in depth was measured over a period of 6 hours. The potential difference was maintained at 60 V between the two ends of the specimen, of which the first was immersed in an NaCl solution and the

second in an NaOH solution. The total charge passed in Coulombs can be related to the resistance of the specimen to chloride penetration and thus to the concrete permeability/quality.

Figure 2.3. Rapid chloride permeability test.

Chloride migration test was performed in accordance with NT BUILD 492 [141] (*Figure 2.4*). In this test, the external chloride ions were forced to migrate into the specimen by applying an external electric potential across the specimen. After a certain period (24 hours), the specimen was axially split, and a silver nitrate solution was sprayed on both freshly-split sections. The depth of chloride penetration was then measured from the visible white precipitation of silver chloride. Using these measurements, the chloride migration coefficient was determined for the specimen as an indication to its resistance to chemical attack.

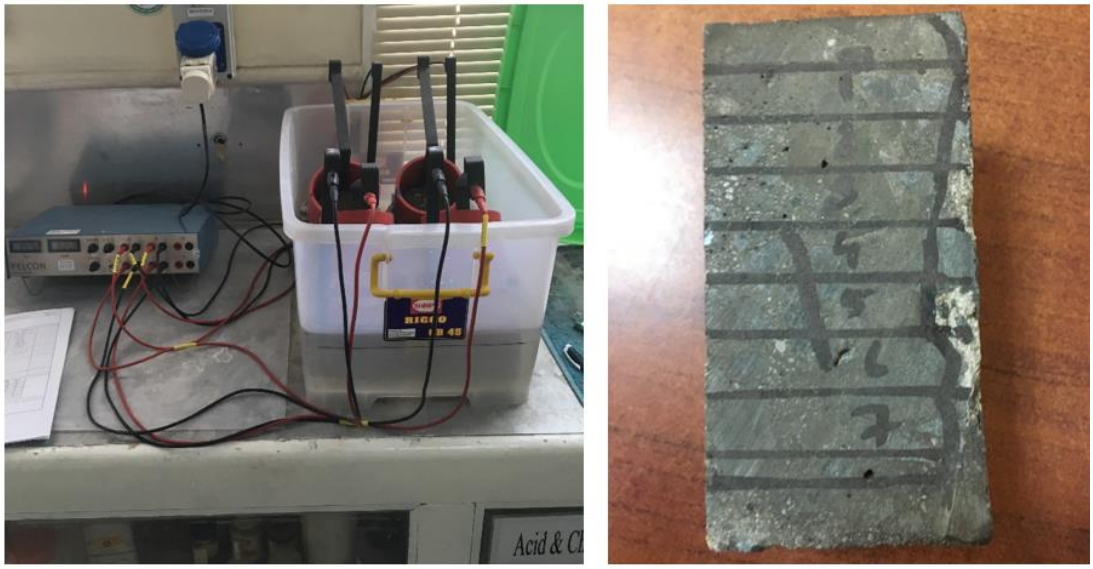

Figure 2.4. Chloride migration test.

Water absorption test was performed in accordance with BS 1881-Part 122 [142]. Three cylindrical cores, 75 mm in diameter and 47 mm deep, were extracted from the top, middle, and bottom of a 150 mm concrete cube. The samples were then placed in a 110 ºC drying oven for three days. The samples were then cooled for one day in a dry airtight vessel. After that, the initial weight for each sample was measured (W_1), and the samples were then immersed in water for 30 minutes. The samples were dried with a cloth (i.e., saturated surface-dried) and weighed again (W_2). The water absorption was calculated as follows:

$$WA\ (\%) = \frac{W_2 - W_1}{W_1} \times 100 \tag{2.2}$$

2.4.4 Isothermal calorimetry

Isothermal calorimetry was performed at the University of Miami as per ASTM C1679 [143] on freshwater and seawater-mixed pure cement pastes with the same w/cm ratio (0.34). As soon as the water was mixed with cement, the paste was poured into a glass ampoule, with an approximate amount of 6–7 g, and then gently tamped to ensure

proper consolidation. The glass ampoule was then sealed and placed in an isothermal calorimeter preconditioned at 23 ± 0.05 °C. The heat flow and the cumulative heat release were measured for a 7-day period following mixing and normalized to the mass of cementitious material. Further details of isothermal calorimetry testing can be found elsewhere [144,145].

2.4.5 Microstructure investigation

The microstructure of hardened concrete was investigated using scanning electron microscopy (SEM) to provide a basis upon which certain experimental observations can be explained. Scanning electron microscopy was performed in accordance with ASTM C1723 [146] with the use of a NOVA NANO SEM 450 machine located at Qatar University. Three types of analysis techniques were utilized, namely [147]:

(a) Secondary electron (SE) imaging: in which the secondary electrons - that are produced due to the collision with the primary electrons of the passing electron beam - were detected. Secondary electrons are low-energy and thus cannot travel far enough from the specimen surface once emitted without being reabsorbed. Consequently, SE imaging primarily provides information about the morphology of the specimen surface. Hence, the specimens used for this technique were surface-fractured.

(b) Backscattered electron (BSE) imaging: in which the backscattered electrons were detected. Backscattered electrons are primary electrons re-emerged from the specimen surface with relatively much higher energy than that of the SE counterparts. The proportion of the detected backscattered electrons from the primary electrons is strongly dependent on the atomic number of the specimen. Therefore, BSE imaging can provide a general indication of the atomic number

distribution for the specimen by means of the difference in surface brightness. The specimens used for this technique have a flat/polished surface, for which section polishing was performed as per ASTM C1723 [146] in the Center of Advanced Material at Qatar University.

(c) Energy-dispersive X-ray microanalysis (EDX): in which the X-rays - that are generated due to the interaction between the specimen and the projected electron beam - were detected. The analysis of the resulting X-ray spectra can be used as an effective tool to identify the chemical composition.

CHAPTER 3: FRESH AND HARDENED PROPERTIES OF SEAWATER-MIXED CONCRETE

This chapter reports on the results of an extensive experimental study on the effect of using seawater in concrete mixtures. A comparison between freshwater and seawater concretes (referred to as Mix A and Mix B, respectively) in terms of their fresh, mechanical, and permeability characteristics is detailed, supported by analytical testing including scanning electron microscopy and isothermal calorimetry.

3.1 Fresh Concrete Properties

The density and yield of the fresh concrete were similar in both mixtures (2555 kg/m^3 and 101.6%, respectively). As expected, densities of Mixes A and B were similar, as the density of seawater is only 2 – 3 % greater than freshwater and the rest of the concrete ingredients are the same. A slight difference in the air content was observed (1.40% and 1.65% for Mix A and Mix B, respectively).

As shown in *Figure 3.1*, the use of seawater reduced the initial slump flow to a value that was 20% lower than that of the reference mix. The use of seawater also impacted the slump retention, where Mix B lost slump faster than Mix A. *Figure 3.2* shows the penetration resistance for the fresh concrete as a function of time. The initial setting time - which is the time corresponding to a penetration resistance of 3.5 MPa - was obtained as 395 and 285 minutes for Mix A and Mix B, respectively. The use of seawater reduced the initial setting time of the fresh concrete by approximately 30%. These observations may be explained by the acceleration in the cement hydration induced by seawater – the faster hydration reduces slump, slump retention, and setting time. These results are consistent with other studies in the literature showing an initial accelerating effect of seawater [58–60].

In principle, chlorides are known to accelerate cement hydration [148,149]. A possible mechanism is the reaction between NaCl existing in seawater and the $Ca(OH)_2$ formed from cement hydration to form $CaCl_2$ as per Eq. (3.1) [53,150]. Calcium chloride is a strong accelerator of cement hydration as discussed elsewhere [151,152].

$$Ca(OH)_2 + 2NaCL \rightarrow CaCL_2 + 2Na^+ + 2OH^- \tag{3.1}$$

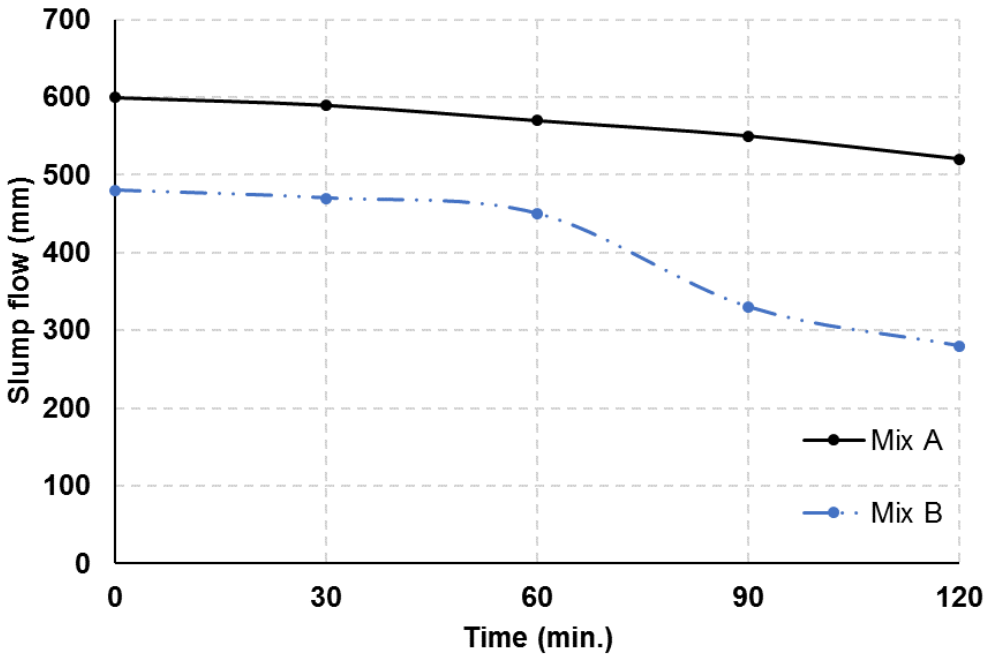

Figure 3.1. Slump flow for Mixes A and B as a function of time.

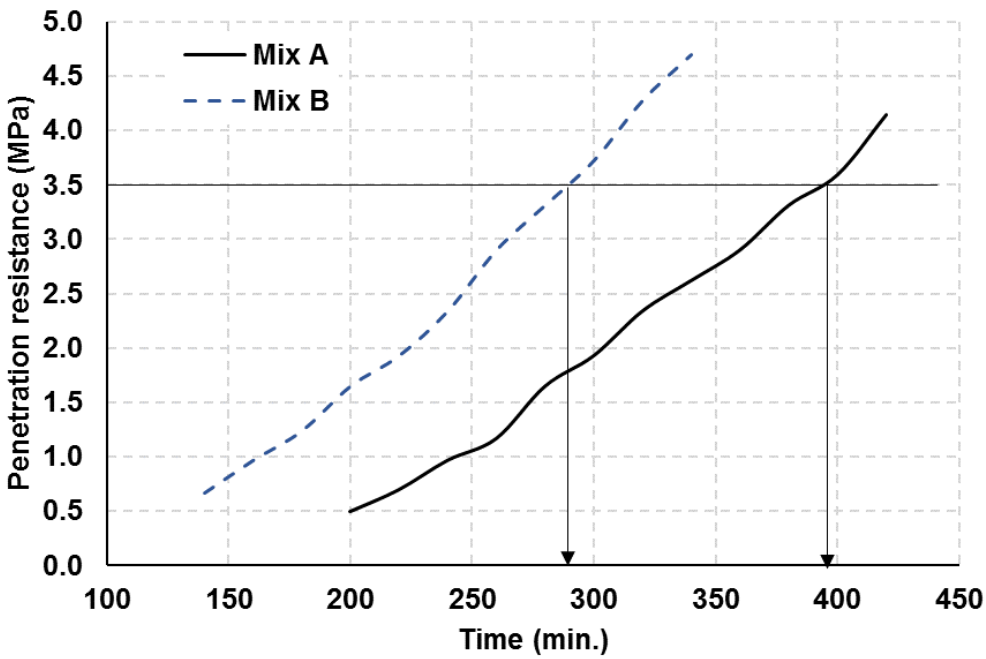

Figure 3.2. Initial setting time measurements for Mix A and Mix B.

3.2 Mechanical Characteristics of Hardened Concrete

Figure 3.3 and *Figure 3.4* present the compressive and tensile strength measurements for the tested specimens, respectively. As shown in *Figure 3.3*, using seawater resulted in a slight increase (~5%) in the compressive strength of the concrete at early ages (3 and 7 days). At 28 days (and later) following mixing, the compressive strength of Mix B was 7-10% lower than that of Mix A. These results are in agreement with previous research [16,17,50,153,154]. As suggested by Kaushik and Islam [35], the higher early-age strength of seawater concrete can be attributed to lower porosity because of the acceleration in the hydration, while the lower long-term strength could be due to the leaching of hydration products. Wegian [44], however, suggested that the lower long-term strength of seawater concrete could be due to salt crystallization in concrete. According to Wegian [44], magnesium sulfates ($MgSO_4$) in seawater react with calcium hydroxide ($Ca(OH)_2$) in the pore solution to form soluble magnesium hydroxide ($Mg(OH)_2$) and gypsum ($CaSO_4.2H_2O$). These phases may cause expansive

crystallization pressure which results in a decrease in the concrete strength. While various explanations have been proposed, the strength decrease likely depends on cement and seawater chemistry, the use of supplementary cementitious materials, and the curing regime used. We note here that the strength decrease is not substantial (7-10%). On the other hand; tensile strength test results of seawater concrete were 10–20% lower (depending on the test age) than those of freshwater-mixed counterpart (*Figure 3.4*).

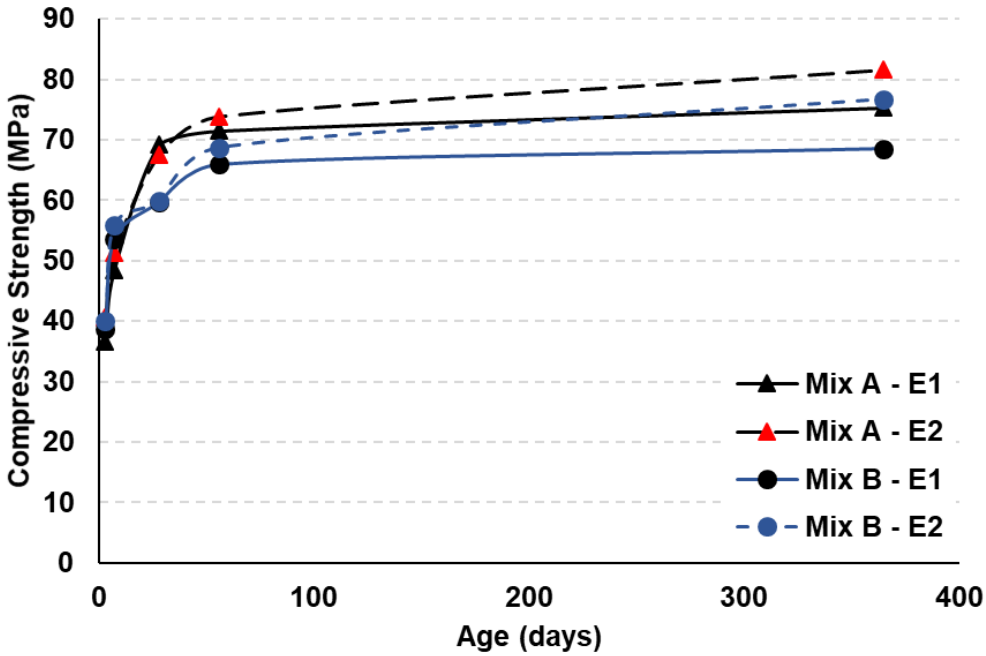

Figure 3.3. Compressive strength test results for Mix A and Mix B concretes.

Note: standard deviations (Days 3, 7, 28, 56, 365) in MPa are (0.31, 0.11, 1.05, 2.40, 0.67) for Mix A-E1; (1.13, 2.62, 0.49, 2.58, 1.70) for Mix B-E1; (0.40, 0.96, 2.44, 0.80, 0.62) for Mix A-E2; and (1.12, 1.17, 0.17, 1.48, 1.53) for Mix B-E2.

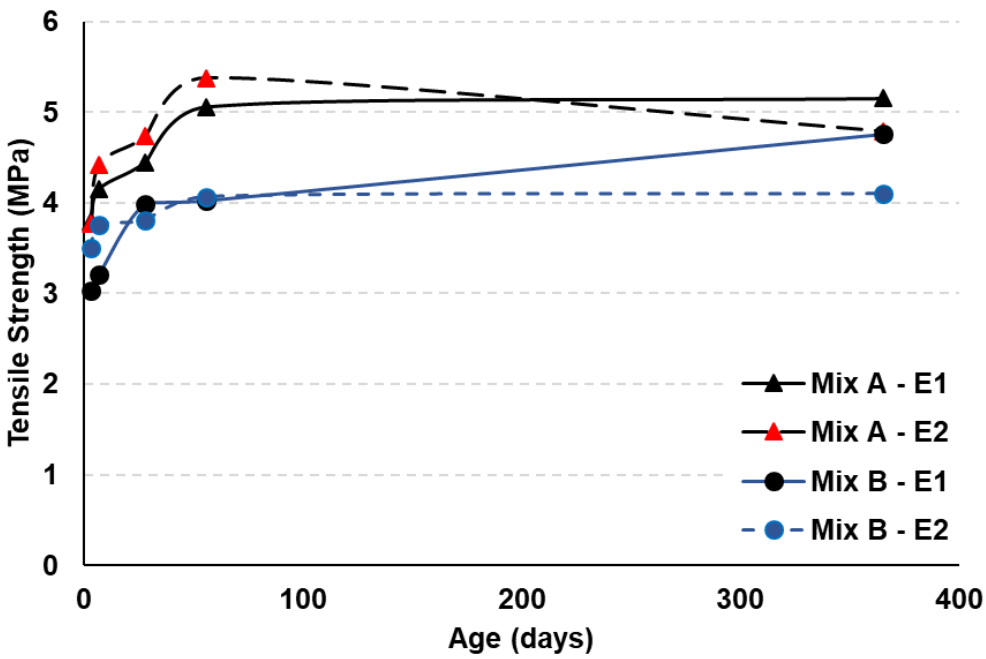

Figure 3.4. Tensile strength test results for Mix A and Mix B concretes.

Note: standard deviations (Days 3, 7, 28, 56, 365) in MPa are (0.19, 0.14, 0.53, 0.10, 0.88) for Mix A-E1; (0.40, 0.36, 0.12, 0.19, 0.67) for Mix B-E1; (0.27, 0.20, 0.13, 0.25, 0.20) for Mix A-E2; (0.23, 0.42, 0.34, 0.11, 0.33) for Mix B-E2.

In general, continuous seawater curing resulted in greater compressive strength of concrete when compared to that kept under ambient conditions. After one year, the compressive strengths of the E2 specimens were on average 10% higher than those of the E1 counterparts (*Figure 3.3*). It is possible that continuous moist curing further enhanced the cement hydration in the E2 specimens compared to the E1 specimens (under ambient conditions). This suggests that seawater-mixed concretes with the current design mixture could show good performance under marine conditions. The tensile strengths of the E2 specimens, on the other hand, were observed to reduce after 56 days, being 12–20% lower than those of the E1 counterparts after one year (*Figure 3.4*). Similarly, Wegian [44] reported long-term reductions in the tensile strength of

concrete as a result of continuous seawater curing (comparing 3-month and 28-day results).

Figure 3.5 shows the concrete shrinkage (%) as a function of time for each concrete mixture. Each test point is the average of three measurements. In general, the rate of increase in concrete shrinkage is reduced after a period of 28 days following mixing. Mix B showed a slightly higher drying shrinkage (<5%) than that of Mix A until Day 56, after which the shrinkage rate between Mix A and Mix B became comparable. The observed slight influence of seawater on the drying shrinkage could be due to the presence of chloride in the pore solution, or due to the formation of a finer pore structure in the seawater-mixed concrete [49,50,57]. Still, comparing the two shrinkage diagrams between Mix A and Mix B, it can be reasonably said that the effect of seawater mixing on shrinkage was negligible.

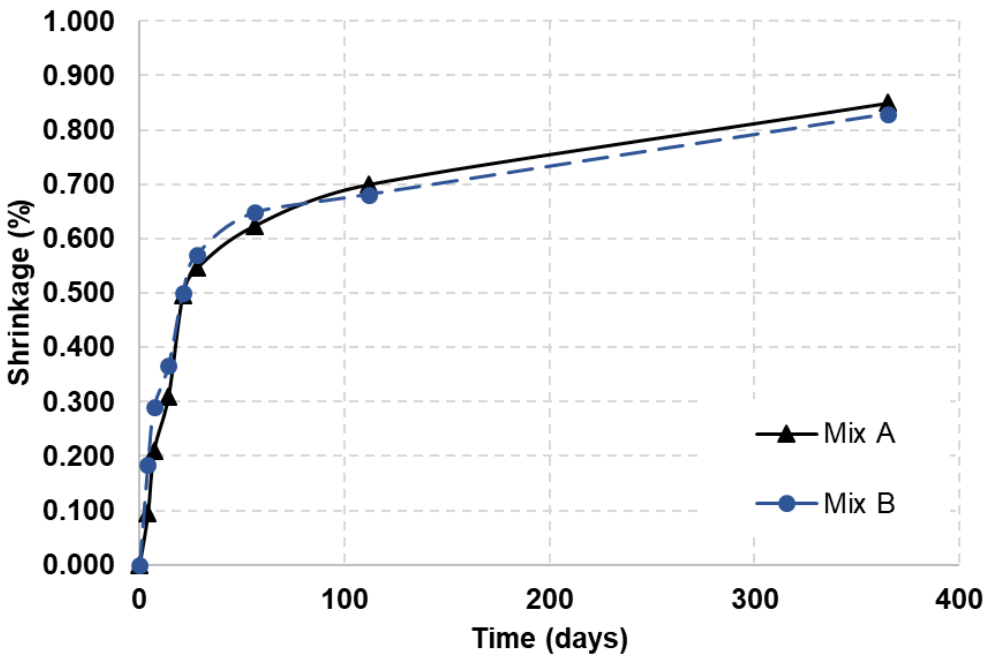

Figure 3.5. Shrinkage test results for Mix A and Mix B concretes.

Note: standard deviations are 0.041% for 3-day, 0.082% for 7-day, 0.068% for 14-day, 0.078% for 21-day, 0.01% for 28-day, 0.098% for 56-day, 0.088% for 112-day, 0.12% for 224-day, and 0.097% for 1-year measures on average.

3.3 Permeability Performance of Hardened Concrete

Table 3.1 summarizes the results of rapid chloride permeability, chloride migration, and water absorption tests. Each concrete mixture was tested after 28-day and 56-day periods following mixing. Each test point represents the average of two samples. It can be observed that the measurements of chloride permeability, chloride migration, and water absorption at 28-day age are lower than those corresponding to the 56-day age. This can be attributed to the general improvement in concrete properties due to the ongoing hydration of cement. Also, the measurements obtained for Mixes A and B are comparable, indicating an insignificant effect of using seawater on the permeability performance of hardened concrete.

Table 3.1

Summary of Permeability Performance Test Results for Mixes A and B.

Specimen	RCP		CM		WA
	Charge passed (coulombs)	Permeability Class	Non-steady-state migration coefficient ($x10^{-12}$ m^2/s)	Resistance to chloride ingress	
Mix A – 28d	407	Very low	2.07	Good	1.79
Mix A – 56d	369	Very low	1.49	Very Good	1.58
Mix B – 28d	439	Very low	1.81	Very Good	1.69
Mix B – 56d	349	Very low	1.48	Very Good	1.56

3.4 Isothermal Calorimetry

Figure 3.6-a presents the heat flow results for the freshwater- and seawater-mixed pastes. As illustrated in the figure, the seawater accelerated the hydration reaction (kinetics) of the cementitious pastes. This is evident from the larger magnitude and the earlier occurrence time of the peak of the seawater paste curve as compared to those of the freshwater counterpart. The maximum heat flow was measured as 4.0 and 5.4 mW/g for the freshwater and the seawater pastes, respectively, associated with a silicate peak time of 8.25 hours for the former and 6.52 hours for the latter. This acceleration is related to the various ions existing in seawater, and explains the earlier setting time as well as the lower slump retention in Mix B as compared to those in Mix A. On the other hand, no difference was observed in the heat flow (i.e., rate of reaction) between seawater and freshwater pastes at later ages.

Figure 3.6-b shows the results of the cumulative heat release for both cementitious pastes. As shown in the figure, the seawater paste has a higher cumulative heat at early ages: the 3-day cumulative heat was measured as 260 J/g for freshwater paste and 280 J/g for the seawater counterpart. However, this difference was observed to decrease with time and, in seven days after mixing, almost no difference was realized in the cumulative heat between seawater and freshwater pastes (measured as approximately 300 J/g for both cement pastes). Given that the cumulative heat release is a direct indicator of the cement hydration and thus of the attained compressive strength, these results validate the higher early strength measured in seawater concrete as compared to that of the freshwater-mixed counterpart (*Figure 3.3*).

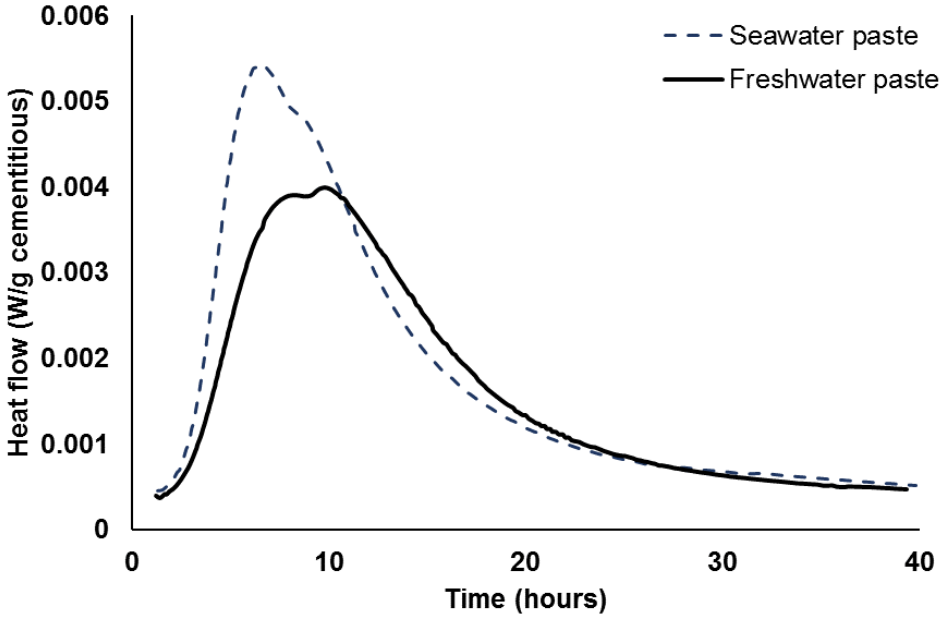

(a)

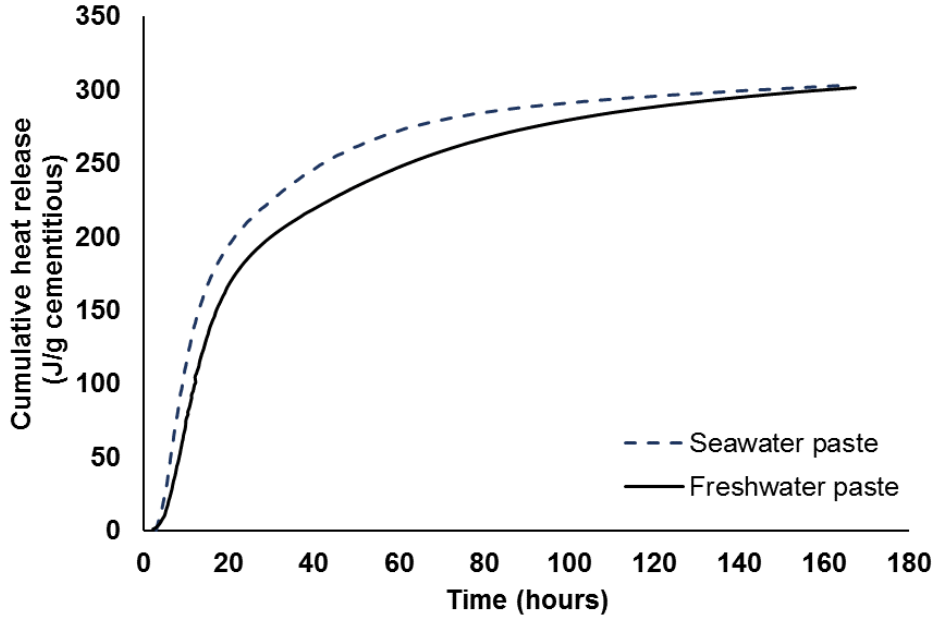

(b)

Figure 3.6. (a) Heat flow and (b) Cumulative heat release of the paste samples.

3.5 SEM Results

3.5.1 Cement paste

Figure 3.7-a and *Figure 3.7*-b show the difference between the back-scattered electron (BSE) images for 3-day freshwater and seawater pastes of the same w/cm ratio (0.34). In general, the microstructure of the seawater paste appeared to be more densified and solid than that corresponding to the freshwater counterpart, with the following qualitative observations being noticed: (a) greater number of pores (black-colored [155]) with larger size in the freshwater paste than that in seawater-mixed counterpart; (b) the amount of anhydrous cement (white-colored [155]) in the freshwater paste was more than that in seawater-mixed counterpart. These observations can explain the more advantageous mechanical characteristics of the seawater concrete during the first 7 days (*Figure 3.3*). Furthermore, the semi-quantitative EDX microanalysis for the sections corresponding to *Figure 3.7* revealed clearly higher amounts of sodium and chloride in seawater paste than those of the paste with freshwater. The proportion of iron atoms - which generally indicates the anhydrous cement - in the freshwater paste was generally higher than that of the seawater-mixed counterpart.

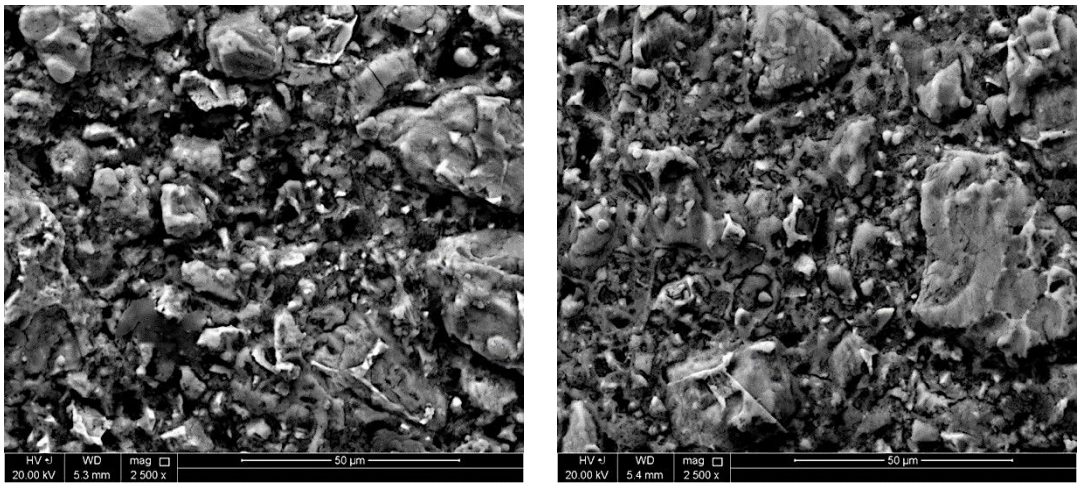

(a) (b)

Figure 3.7. BSE images taken for the (a) 3-day freshwater paste and (b) 3-day seawater paste.

Such advantages observed for the early-age seawater paste can also be evidenced by the secondary electron (SE) imaging. *Figure 3.8*-a and *Figure 3.8*-b show the morphological behavior of the fractured surface for freshwater and seawater cement pastes, respectively. As shown in *Figure 3.8*-a, the C-S-H needles (as so named in [156]) were less densified and highly distributed in case of freshwater paste. Against this, the seawater paste showed a more densified structure (*Figure 3.8*-b). Similar observations on the early-age pastes were reported by Katano et al. [60] and Shi et al. [49] concluding that, in case of seawater paste, ettringite and gypsum crystals are formed so as to fill in the voids and further densify the microstructure. However, the microstructure of the freshwater and seawater cement pastes was similar at 28-day of mixing and, as intuitively expected, was more densified than that of the early-age paste as illustrated from the BSE (*Figure 3.9*-a and *Figure 3.9*-b) and SE (*Figure 3.9*-c and *Figure 3.9*-d) images.

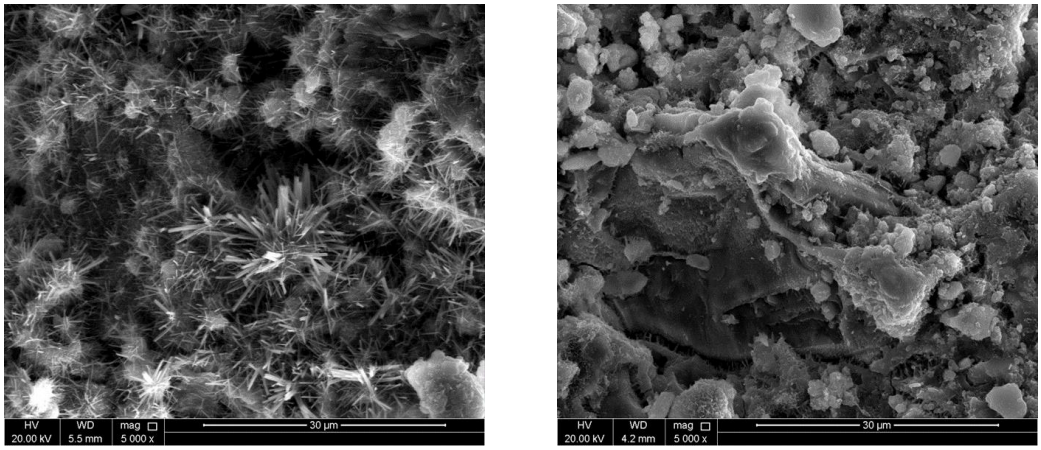

(a) (b)

Figure 3.8. SE images taken for the (a) 3-day freshwater paste and (b) 3-day seawater paste.

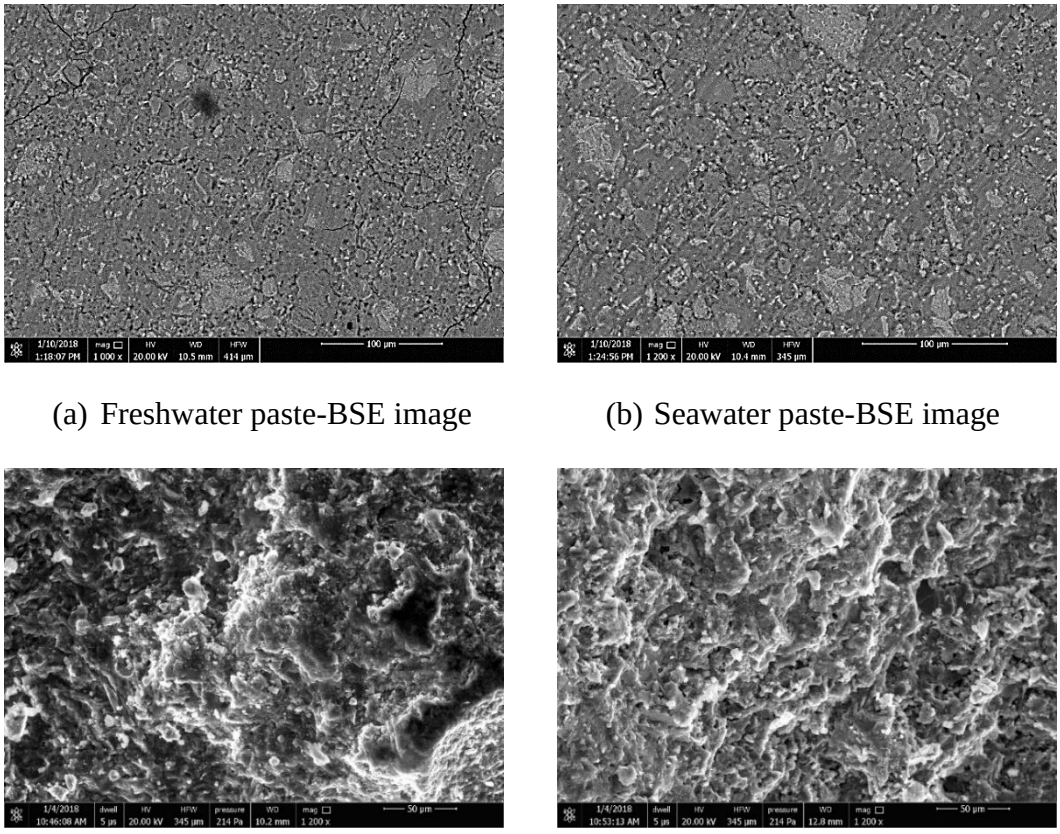

(a) Freshwater paste-BSE image (b) Seawater paste-BSE image

(c) Freshwater paste-SE image (d) Seawater paste-SE image

Figure 3.9. Typical microstructure for seawater- and freshwater-mixed 28-day cement pastes.

3.5.2 Mature, hardened concrete

The BSE images of the 56-day hardened concrete were comparable for Mixes A and B (*Figure 3.10*-a and *Figure 3.10*-b, respectively). The BSE images generally showed low porosity (black color) as compared to the early-age paste (*Figure 3.7*), with the distribution of slag (the irregular-shaped grey particles) and very little anhydrous cement (white color) [155]. The overall grey-colored matrix represents the hydrated cement [155]. The difference between the two mixtures could only be observed using EDX microanalysis, where the Na and Cl atoms are found in greater amounts in Mix B (*Figure 3.11*). Also, the SE images accompanied by EDX microanalysis indicated that part of the calcium in Mix B reacted with the sulfate ions of seawater forming salt impurities (most likely gypsum [157]) as shown in *Figure 3.12*); this could be related to the high concentration of sulfate ions existing in seawater. Such phases could be regarded as a possible explanation for the slight reduction in the mechanical performance of the mature hardened concrete of Mix B as compared to that of Mix A.

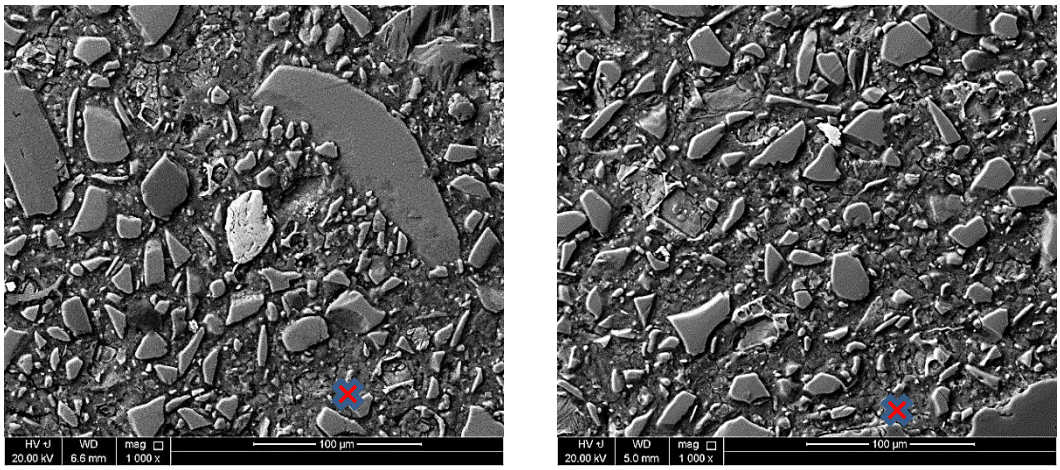

(a) (b)

Figure 3.10. BSE images taken after 56 days for concrete of (a) Mix A and (b) Mix B (refer to Figure 3.11 for the ‘x’ mark).

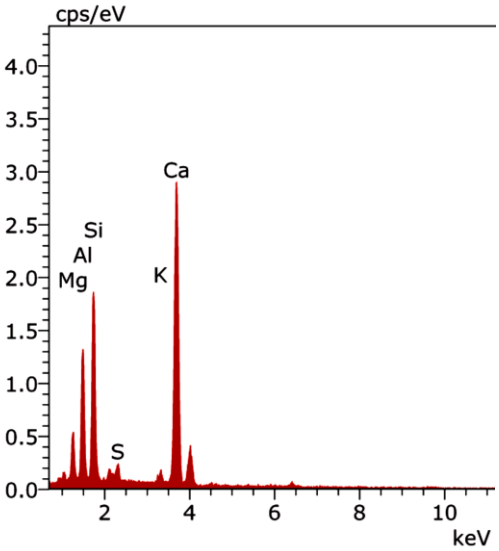

El	AN	Series	unn. C [wt.%]	norm. C [wt.%]	Atom. [at.%]
Mg	12	K-series	3.42	5.38	7.47
Al	13	K-series	5.50	8.67	10.84
Si	14	K-series	15.95	25.14	30.20
S	16	K-series	0.89	1.40	1.47
K	19	K-series	0.44	0.69	0.59
Ca	20	K-series	37.26	58.72	49.43
		Total:	63.46	100.00	100.00

(a)

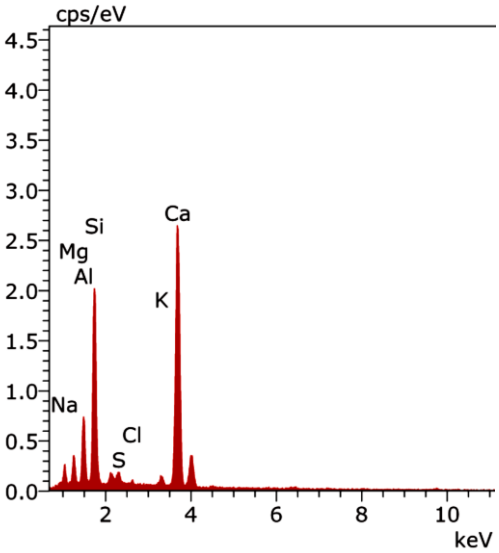

El	AN	Series	unn. C [wt.%]	norm. C [wt.%]	Atom. [at.%]
Na	11	K-series	1.77	3.26	4.83
Mg	12	K-series	1.91	3.52	4.92
Al	13	K-series	4.20	7.74	9.77
Si	14	K-series	11.19	20.63	25.00
S	16	K-series	0.91	1.68	1.78
Cl	17	K-series	0.21	0.39	0.38
K	19	K-series	0.80	1.48	1.29
Ca	20	K-series	33.23	61.29	52.04
		Total:	54.23	100.00	100.00

(b)

Figure 3.11. Typical EDX microanalysis for the hydrated cement ('x' sign location in *Figure 3.10*) in the 56-day concrete of (a) Mix A and (b) Mix B.

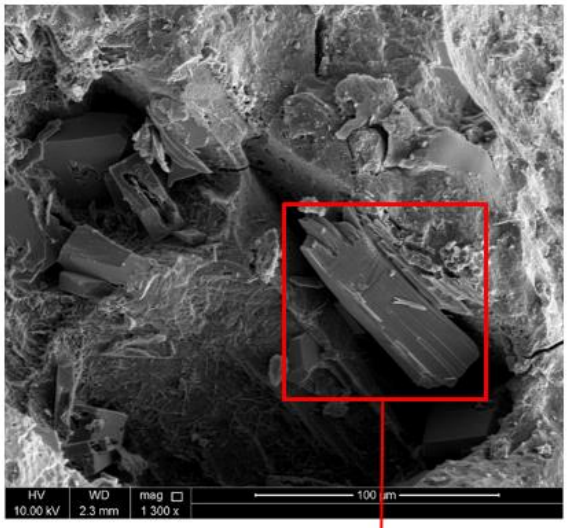

(a) SE image

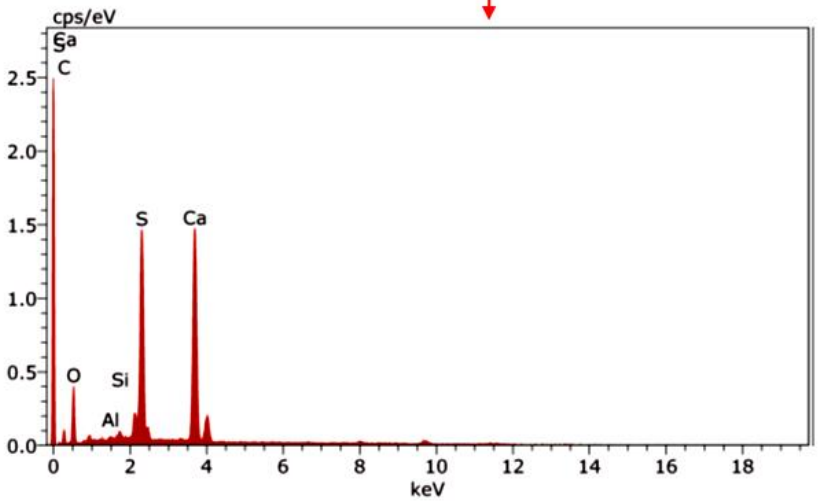

(b) EDX analysis

Figure 3.12. Observation of salt impurities in the SE image of the 56-day seawater concrete.

3.6 Remedial Measures

Seawater had some negative effects on the fresh concrete, and to a less extent the hardened concrete. Lab trials were performed to mitigate such potential drawbacks in seawater concrete, during which the effects on the fundamental concrete properties (i.e., slump flow and compressive strength) were evaluated. Consequently, it was found that using retarder and superplasticizer in the concrete mixture improved the fresh properties of seawater concrete. Here, about 0.25 L/m^3 of a commercial retarder (CHRYSOPlast CQ240) in the seawater concrete mix was used. Also, the superplasticizer dosage used in seawater concrete mix was 15% higher than that of freshwater concrete leading the workability of Mix B to be comparable to that of Mix A (*Figure 3.13*-a). The compressive strength of Mix B was enhanced after implementing the countermeasures. *Figure 3.13*-b depicts the compressive strength test results at Days 7, 28, and 56 for Mixes A and B, under standard curing conditions. It is possible that the elimination of the accelerating effects in seawater concrete improved its strength performance. Likewise, other studies indicated the positive effect of superplasticizers on compressive strength of concrete [158,159]. This can be regarded as a direct evidence of the applicability of using seawater for mixing concrete, with the consideration of proper chemical admixtures to achieve properties comparable to those of conventional concrete.

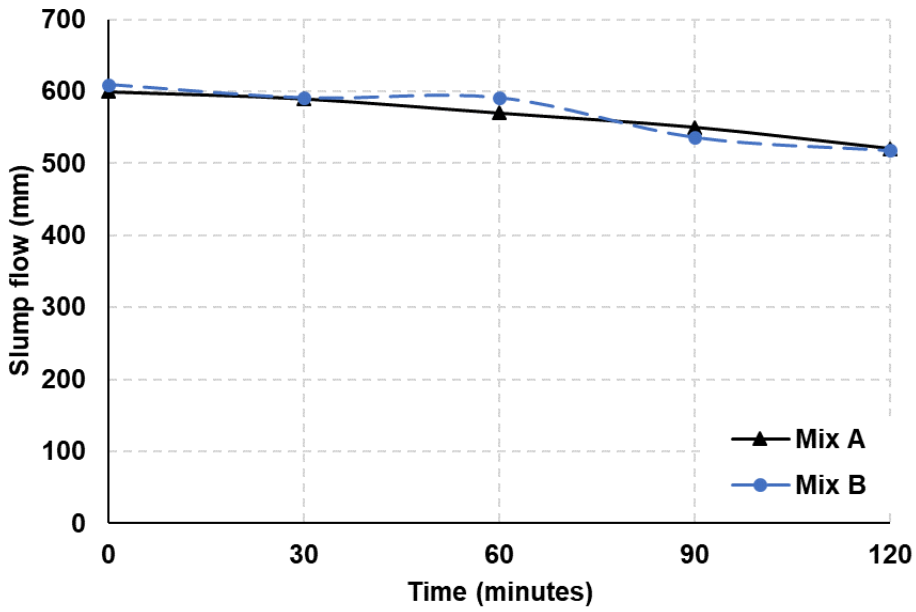

(a)

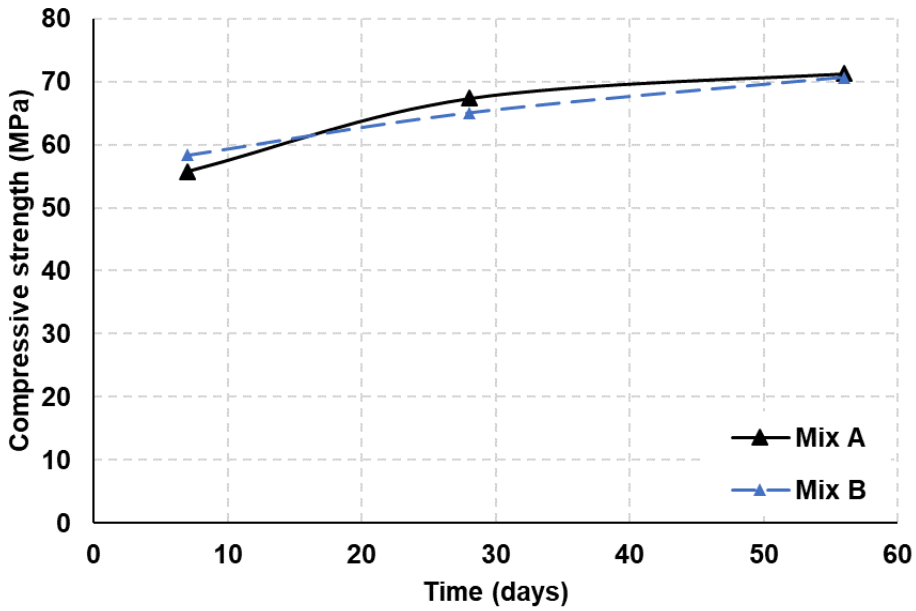

(b)

Figure 3.13. (a) Slump flow and (b) compressive strength results for seawater concrete after remedial actions.

Note: standard deviations for compressive strength (Days 7, 28, 56) in MPa are (0.54, 1.16, 1.74) for Mix A and (0.18, 0.035, 2.38) for Mix B.

3.7 Summary and Conclusions

Two concrete mixtures were compared; namely, Mix A denoting the freshwater concrete and Mix B denoting the seawater-mixed concrete. Based on the results of this study, the following conclusions have been drawn:

- Using seawater in concrete mixtures had almost no effect on the density, yield, and air content measurements of the fresh concrete.
- A notable reduction in the workability, workability retention, and initial setting time measurements was observed when using seawater in concrete. The initial slump flow of Mix B was approximately 20% lower than that of Mix A. The initial setting time measured for Mix B was 30% lower than that of Mix A.
- Using seawater in concrete resulted in an initial slight increase in the compressive strength of the hardened concrete until Day 7 following mixing. Then, a reduction of around 7–10% was observed in the compressive strength results of Mix B as compared to those of Mix A after 28 days. Seawater concrete had averagely 10–20% lower tensile strength than that of freshwater mixed counterpart. The shrinkage of Mix B concrete was comparable to that of Mix A.
- Using seawater in concrete mixtures had no effect on the permeability and/or resistance to chloride ingression of hardened concrete. The two mixtures under comparison (i.e., Mixes A and B) had almost the same results for the RCP, CM, and WA tests.
- Results from isothermal calorimetry revealed the heat flow (i.e., rate of hydration) of the seawater paste to be higher than that of the freshwater-mixed counterpart at early ages (up to Day 7). However, at later ages, the heat flow was almost the same for both cement pastes.

- Results from scanning electron microscopy revealed a more densified microstructure of the seawater paste at early ages as compared to that of the freshwater counterpart; however, at later ages, the microstructure was similar for the two cement pastes. Salt impurities were observed in Mix B mature concrete as a result of seawater ions.
- Using chemical admixtures in seawater concrete was found to be effective to achieve concrete properties in Mix B comparable to those of Mix A. Based on lab trials, we proposed a specific procedure for this purpose which includes adding 0.25 L/m^3 of a commercial retarder (in this study CHRYSOPlast CQ240) and increasing the superplasticizer amount by 15%.

Finally, it should be emphasized that the above conclusions are solely based on the materials and the specimens used in this study. Future research could be directed towards investigating different concrete compositions and other aspects of durability such as water permeability under pressure. Furthermore, as the current study focuses on plain concrete characteristics, the above conclusions are of most use for non-reinforced concrete structures or for concrete with non-corrosive reinforcement.

CHAPTER 4: PERFORMANCE OF SEAWATER-MIXED RECYCLED-AGGREGATE CONCRETE

In Chapter 3, we investigated the performance of plain concrete mixed with seawater. This chapter details the results of an experimental study on the effects of using seawater and RCA together in concrete mixtures. This chapter presents a comparison between two concrete mixtures, namely: (a) Mix A, which represents the conventional mixture produced with freshwater and natural coarse aggregate (NCA) and is regarded as a reference; and (b) Mix C, which is produced with seawater and RCA.

4.1 Fresh Concrete

4.1.1 Density

The density of Mix C concrete (2400 kg/m^3) was approximately 5% lower than that of Mix A (2555 kg/m^3). As previously reported in Chapter 3, mixing with seawater has no effect on the fresh concrete density: this suggests that the replacement of NCA by RCA reduced the concrete density of Mix C. This can be attributed to the presence of adhered mortar on the surface of RCAs, which makes RCAs less dense than NCAs [15]. This result is in agreement with the literature [62], which shows a 5–8% lower concrete density when using 100% RCA. In accordance with Bravo et al. [160], the decrease in concrete density is strongly related to the physical properties of RCAs: those with lower density and higher water absorption generally yield further loss in the fresh density of concrete.

4.1.2 Air content

The use of seawater and RCA together in Mix C resulted in an increase in the air content (1.85%) when compared to the conventional Mix A (1.40%). Existing literature on seawater-mixed concrete [41] and RCA concrete [62] suggest that increases in the air content are generally attributed to the use of RCA rather than the

use of seawater. In addition to their higher porosity, RCAs also possess a rougher surface with greater angularity, as a result of the recycling process, which can lead to air become trapped on the aggregate surface [62,161]. As the RCAs were not pre-saturated in this study, it is possible that the air inside the mortar of the RCA was also being measured. Previous research has shown similar impact of using RCA on the concrete air content, with the air content increasing with RCA replacement levels [70].

4.1.3 Workability and setting

Figure 4.1 depicts the slump flow as a function of time for both concrete mixtures. In Chapter 3, we noted that the use of seawater reduced the initial slump flow of fresh concrete by approximately 20% compared to the reference, and resulted in somewhat lower slump retention. Here, combining seawater and RCA resulted in a more significant reduction in the workability. Mix C not only showed an initial slump 25% lower than that of Mix A, but also it remained flowable for only half the period (i.e., 60 minutes in Mix C versus 120 minutes in Mix A). The initial setting time for Mixes A and C was 395 and 210 minutes, respectively (*Figure 4.2*). While the sole use of seawater was observed to reduce the initial setting time by almost 30% in Chapter 3, the combined effects of seawater and RCA in Mix C resulted in an approximately 50% lower initial setting time compared to Mix A. These observations conform with previous studies indicating the accelerating effects induced by seawater [162] and RCA [163].

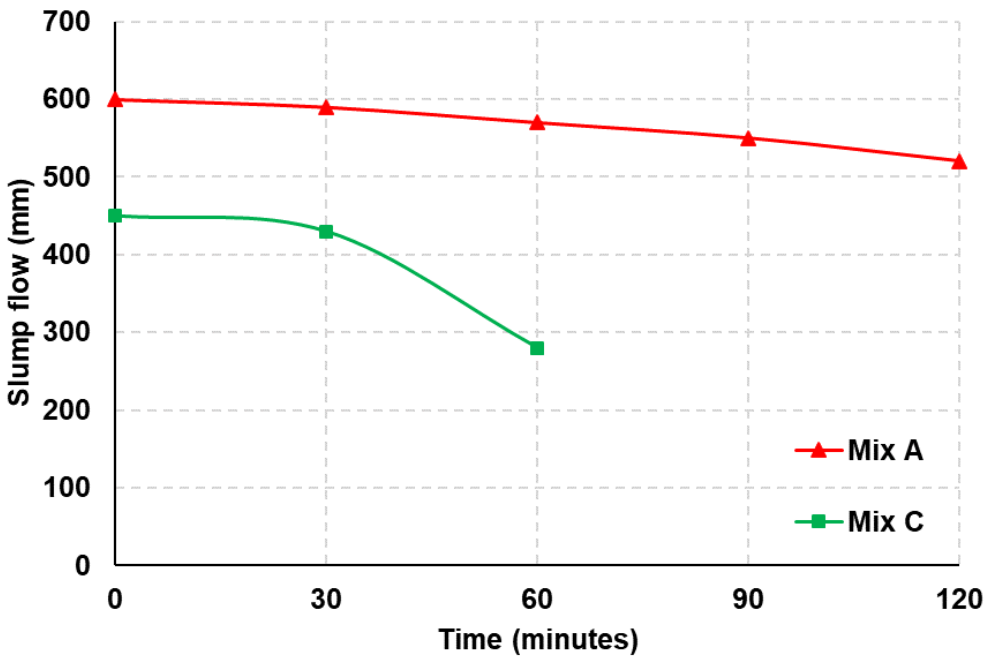

Figure 4.1. Slump flow as a function of time for Mix A and Mix C concretes.

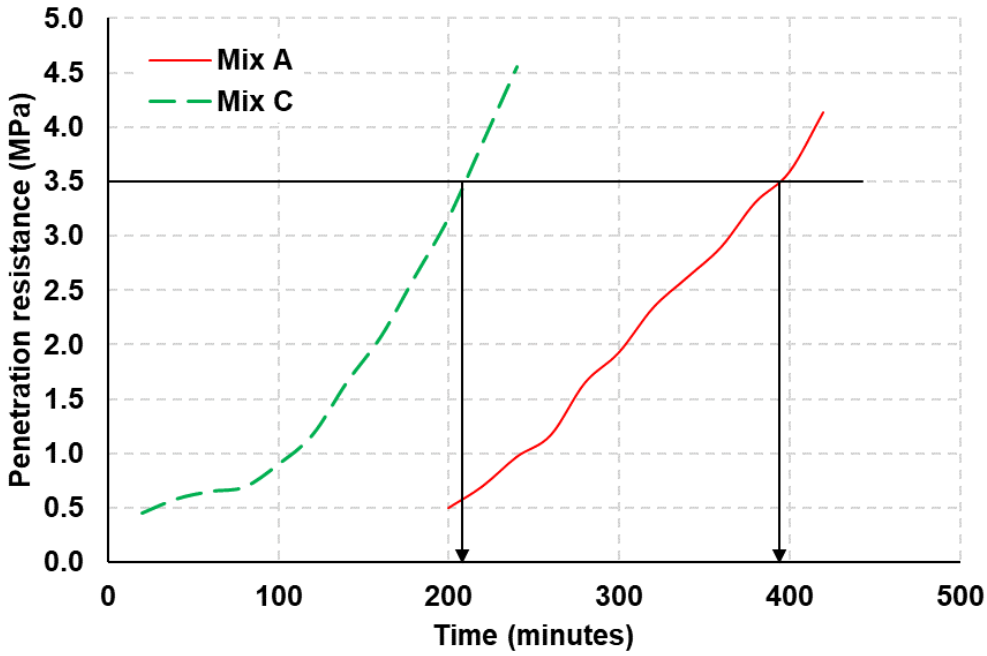

Figure 4.2. Setting time test results for Mix A and Mix C concretes.

As indicated in Chapter 3, the reduction in workability and setting time in seawater concrete is attributed to the presence of large amounts of chloride accelerating the cement hydration [53]: isothermal calorimetry comparison between freshwater and seawater cement pastes revealed that the heat flow (i.e., the rate of hydration) and the heat release of the latter are higher than that of the former at early ages [162,164]. Here, incorporation of RCA in Mix C resulted in a significantly higher water demand and thus a slump loss greater than in Mix A. In general, RCA has harsh/granular texture because of the adhered porous mortar on its surface; hence, more water (or effort) are required for compaction due to the inter-particle friction [15,165]. While not overlooking the simultaneous accelerating effects of seawater, it is apparent that using 100% RCA in an air-dry condition hampered the concrete workability to a great extent despite the additional mixing water. Therefore, it is recommended in this particular case to consider pre-soaked recycled aggregates [51,166,167] or greater amounts of superplasticizer [74] to mitigate such reductions in workability performance. Koenders et al. [168] reported that using RCA in a saturated surface dry condition resulted in relatively lower heat flow (i.e., rate of hydration) and a slightly longer induction period, possibly due to the unabsorbed mixing water.

4.2 Hardened Concrete

4.2.1 Strength

Figure 4.3 and *Figure 4.4* show the compressive and tensile strength results of the studied mixtures, respectively. Mix A achieved the 60-MPa design compressive strength after 28 days, whereas Mix C did not. With the sole use of seawater (refer to Chapter 3), we noted a slight increase (within 5%) in the strength at early ages (up to 7 days) attributable to the reduced porosity due to the acceleration in cement hydration. At later ages (28 days or later), seawater concrete showed strength values 8–10% lower than those of the conventional concrete, suggested to be due to leaching of hydrates.

Here, Mix C showed significantly lower compressive and tensile strength values compared to those of the conventional Mix A at all ages. For instance, the compressive strength value of Mix C concrete was approximately 35% lower than that of Mix A after one year (*Figure 4.3*). It is evident that the combined negative effects from mixing seawater and RCA worsen the mechanical behavior of Mix C. These results are in agreement with previous research on RCA concrete [15,65], which generally shows a reduction up to 30% in the concrete compressive strength with the use of 100% RCA. In principle, RCA concrete has lower strength than conventional concrete due to the increased porosity, the lower strength and density of RCA, the weak interfacial bond between RCA and the matrix, and/or the presence of microcracks and fissures within the RCA because of crushing and recycling processes [15].

Similar to the observations reported in Chapter 3, continuous seawater curing generally resulted in greater compressive strength of concrete when compared to that kept under ambient conditions (*Figure 4.3*). Also, the tensile strengths of the E2 specimens were observed to reduce after 56 days following mixing as shown in *Figure 4.4*.

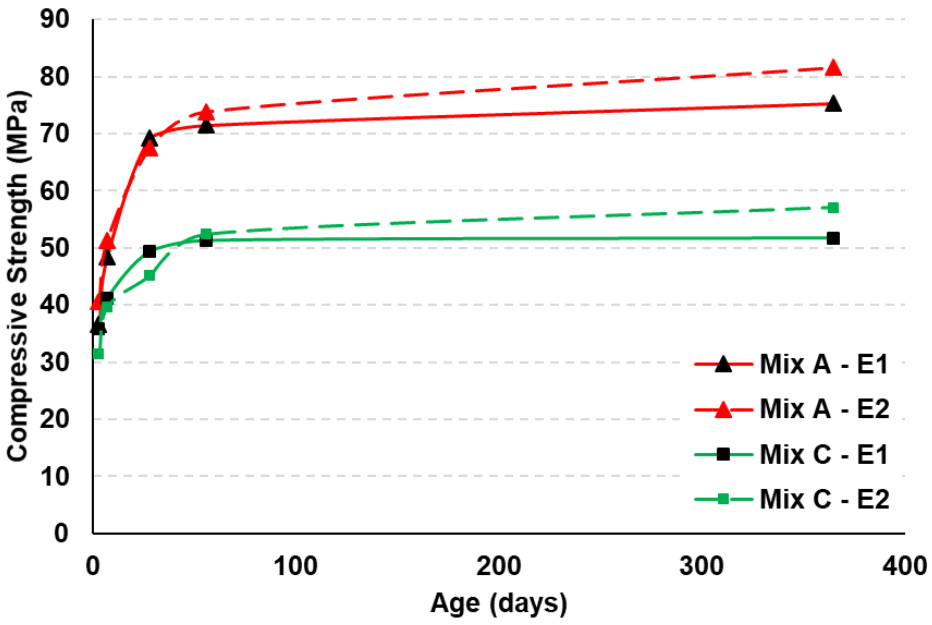

Figure 4.3. Compression test results for Mix A and Mix C concretes.

Note: standard deviations (Days 3, 7, 28, 56, 365) in MPa are (0.31, 0.11, 1.05, 2.40, 0.67) for Mix A-E1; (1.47, 0.72, 1.88, 1.74, 1.71) for Mix C-E1; (0.40, 0.96, 2.44, 0.80, 0.62) for Mix A-E2; and (1.14, 1.48, 2.70, 2.24, 0.76) for Mix C-E2.

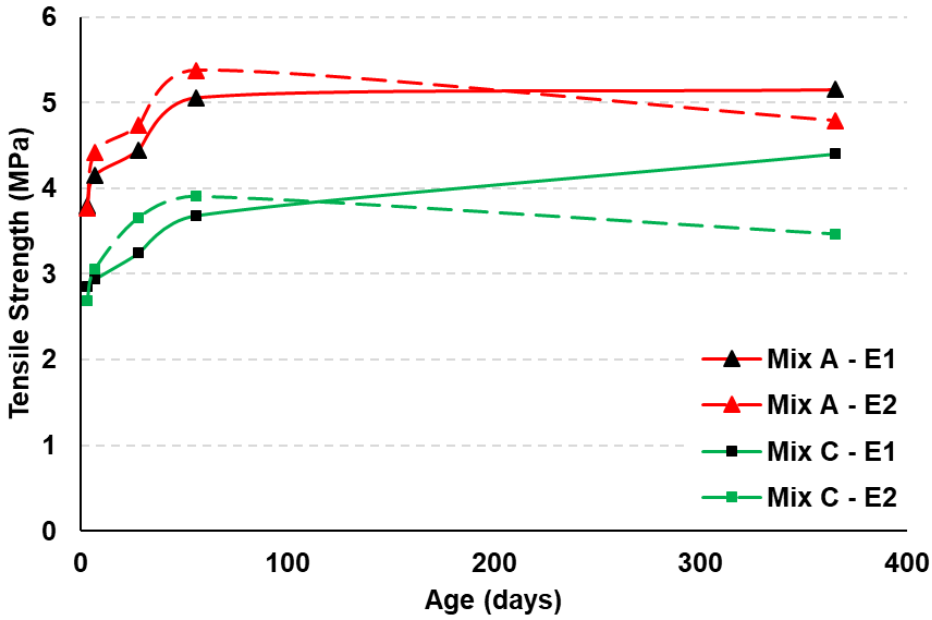

Figure 4.4. Splitting tensile test results for Mix A and Mix C concretes.

Note: standard deviations (Days 3, 7, 28, 56, 365) in MPa are (0.19, 0.14, 0.53, 0.10, 0.88) for Mix A-E1; (0.31, 0.19, 0.23, 0.83, 0.10) for Mix C-E1; (0.27, 0.20, 0.13, 0.25, 0.20) for Mix A-E2; (0.15, 0.30, 0.21, 0.14, 0.32) for Mix C-E2.

4.2.2 Microstructure

Figure 4.5 shows the BSE images of 56-day hardened concrete for the two mixtures. In general, the microstructure of the two mixtures appeared to be similar, although this was not quantified. In a qualitative manner, both mixtures showed low porosity (black color) and little anhydrous cement (white-colored). The majority of the space was covered by hydrated cement (grey color) and slag (irregular-shaped grey particles) [155]. The SE images; however, showed relatively a less dense microstructure of Mix C as compared to Mix A (*Figure 4.6*). Several microcracks and fissures were observed in the microstructure of Mix C: those, as suggested by Xiao et al. [169], are

likely to exist within the RCA as a result of crushing the parent concrete and recycling processes.

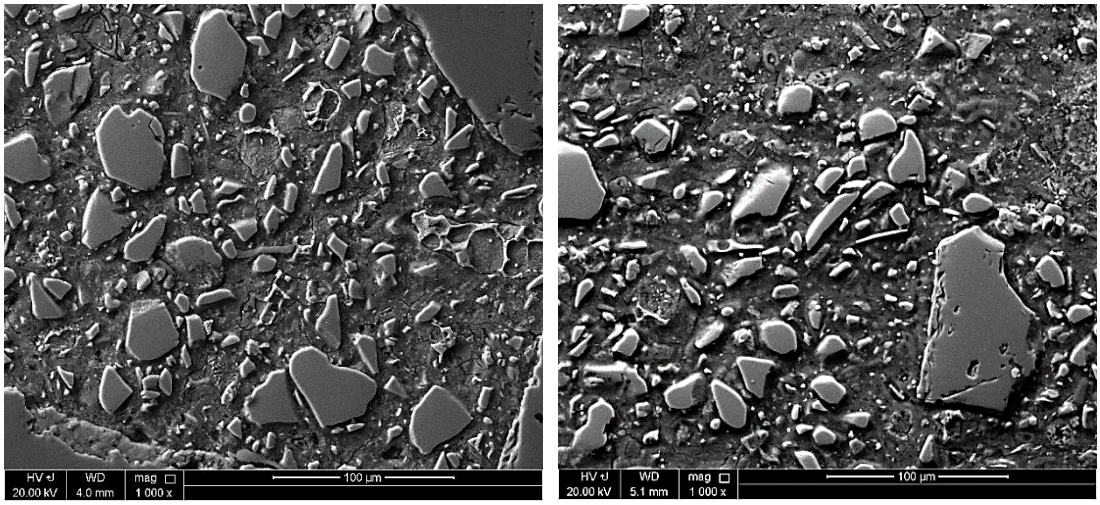

(a) (b)

Figure 4.5. BSE images taken after 56 days for concrete of (a) Mix A and (b) Mix C.

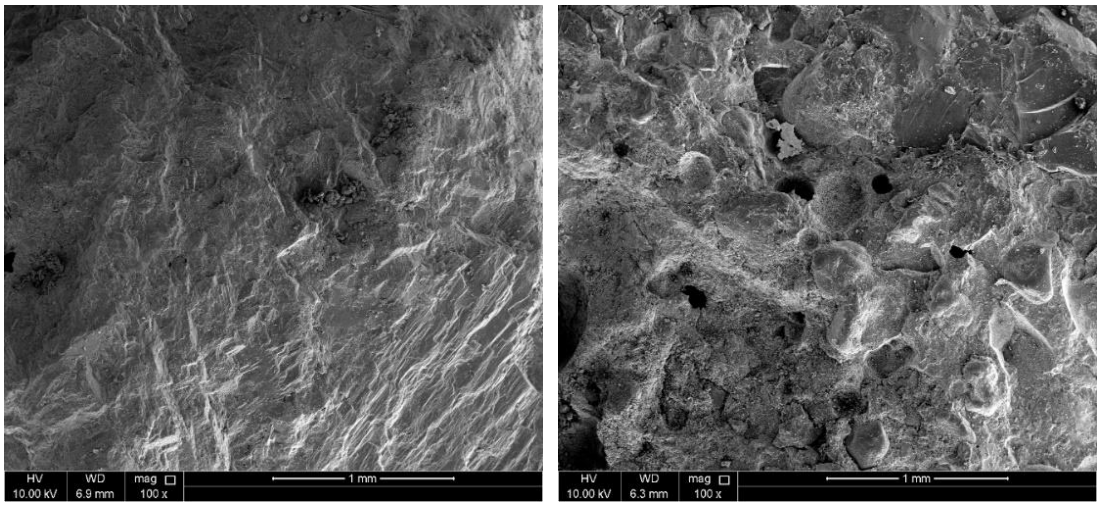

(a) (b)

Figure 4.6. SE images of the 56-day-aged concrete for (a) Mix A and (b) Mix C.

At higher magnifications, crystalline products were observed in concrete mixed with seawater (see *Figure 3.12* in Chapter 3), suggesting that part of the calcium in the

pore solution reacted with the sulfate ions (abundant in seawater) to form such phases (mostly gypsum as per the EDX). While not directly confirmed, gypsum formation could possibly yield expansive crystallization pressures that result in decreases in concrete strength, which explain in part the reduction in the strength of Mix C compared to Mix A.

Apart from the negative effects of salt crystallization and RCA microcracks, the dual interfacial transition zone (ITZ), normally existing in RCA concrete [170], likely plays a role in the inferior properties of Mix C. This dual ITZ (i.e., coarse aggregate/old mortar and RCA/new mortar interfaces as shown in *Figure 4.7*) represents a weak link (hence a load-transfer barrier within the concrete matrix) that limits the strength of Mix C. Further discussion about the microstructure of recycled-aggregate concrete can be found in [171–173].

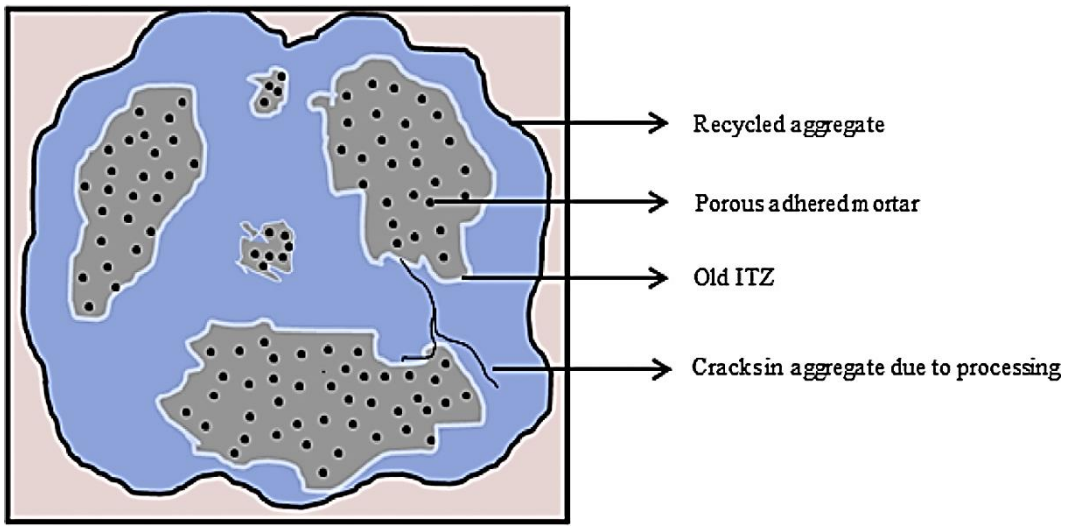

Figure 4.7. Pictorial representation of RCA micro cracks and dual ITZ [15].

4.2.3 Permeability

The results of rapid chloride permeability (RCP) test and water absorption (WA) are shown in Table 4.1. Tests were performed on hardened concrete at 28 and 56 days following mixing. The permeability performance of hardened concrete at Day 56 was better than that at Day 28, because of the reduction in porosity due to increased hydration of cement and reaction of slag. RCP test results for both concrete mixtures were within the acceptable limits [107]; however, there was a 100% higher charge passed when comparing Mix C with Mix A. Similarly, WA test results revealed a poor performance for Mix C compared to Mix A or even the standard limits (2.5% max. [107]). While seawater mixing showed almost no effect on the permeability performance of hardened concrete (refer to Section 3.3 in Chapter 3), incorporating RCA in Mix C reduced its permeability performance. This is attributed to the inferior quality of RCA given the existence of microcracks, the high porosity, and the adhered old mortar, which make concrete more vulnerable to permeation [63].

Table 4.1

Summary of Permeability Performance Test Results for Mixes A and C.

Specimen	RCP result (as the charge passed in coulombs)	WA (%)
Mix A – 28d	407	1.79
Mix A – 56d	369	1.58
Mix C – 28d	1100	2.87
Mix C – 56d	844	2.63
Mix C – 28d (improved)	616	1.18

4.2.4 Shrinkage

Figure 4.8 shows the concrete drying shrinkage (%) as a function of time for the two mixtures. In general, the shrinkage curve followed a bilinear trend that consisted of two portions. The first portion showed a rapid increase in shrinkage up until Day 28 (at which concrete gains most of its strength); the second portion, after 28 days, showed a lower slope (i.e., a slower shrinkage rate). Similar drying shrinkage of concrete has been reported elsewhere [174].

Mix C showed higher drying shrinkage at all ages compared to Mix C: an approximate difference of 10% was reported at Day 365. Seawater appeared to have little-to-no effect on the drying shrinkage as reported in Chapter 3, especially in the long term. However, incorporating RCA in Mix C increased its drying shrinkage due to the higher water absorption, higher porosity, and lower modulus of elasticity, which in turn resulted in greater mass loss and shrinkage stresses. Other researchers have also reported higher drying shrinkage for recycled-aggregate concrete compared to the conventional counterpart [66,175]; however, the effect of RCA here seemed to be relatively less significant (only within 10%), possibly due to the use of slag as supplementary cementitious material [72].

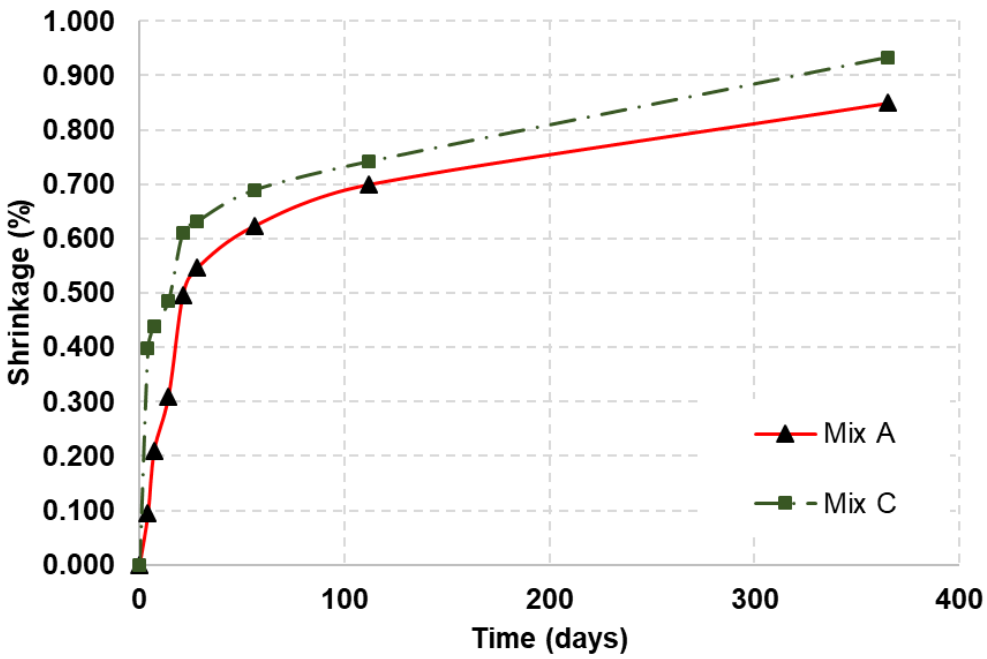

Figure 4.8. Shrinkage test results for Mix A and Mix C concretes.

Note: standard deviations are 0.041% for 3-day, 0.082% for 7-day, 0.068% for 14-day, 0.078% for 21-day, 0.01% for 28-day, 0.098% for 56-day, 0.088% for 112-day, 0.12% for 224-day, and 0.097% for 1-year measures on average.

From the results reported in Sections 4.1 and 4.2, the strong negative effect of the combined use of seawater and RCA on concrete properties is apparent. While this is somewhat expected, the quantification of these negative impacts is important, as it allows for the design of appropriate strategies that may be used to reduce these impacts. Several such strategies could be envisioned, but only some are explored here, and further studies on the feasibility and sustainability of such changes are being carried out.

4.3 Improving Performance of Concrete with Seawater and RCA

In order to improve the performance of concrete made with RCA and seawater, changes in mixture design for Mix C were performed to improve the slump flow, compressive strength, water absorption, and chloride permeability. The following changes were made in Mix C: (i) a dosage of 0.75 L/m³ of commercial retarder (CHRYSOPlast CQ240) was used in the mixture, (ii) the superplasticizer dosage was increased by 40% compared to the conventional mix, and (iii) the w/cm was reduced from 0.34 to ~0.30 by increasing the cement content (by ~10%). These changes led to a significant improvement in the workability (*Figure 4.9*), strength (*Figure 4.10*), and permeability (Table 4.1) of Mix C concrete. The resulting properties of Mix C concrete were comparable to those of the conventional Mix A.

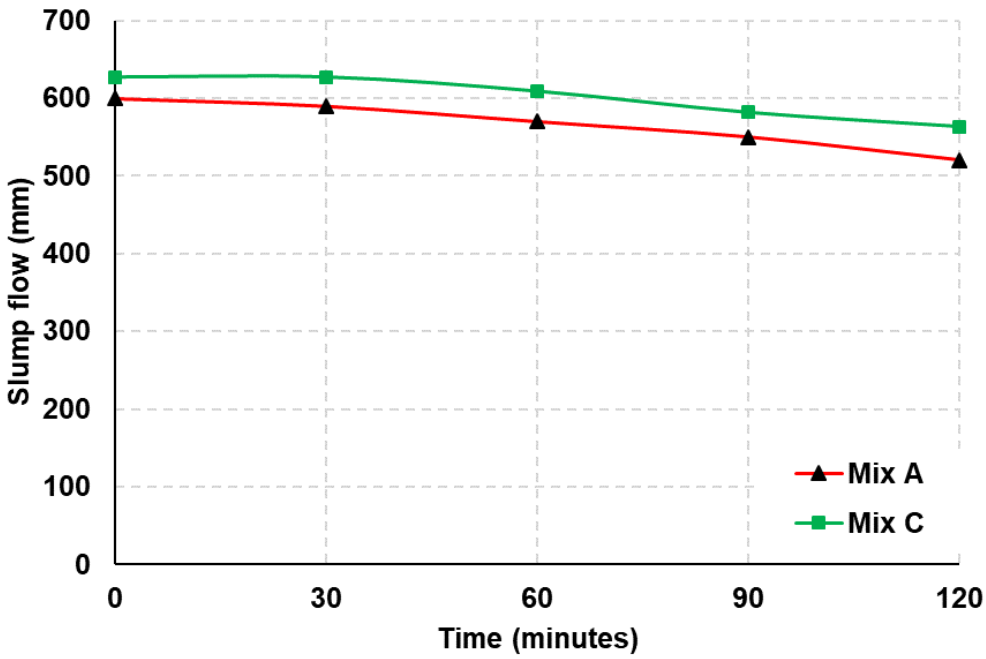

Figure 4.9. Slump flow after changes in mixture design for Mix C.

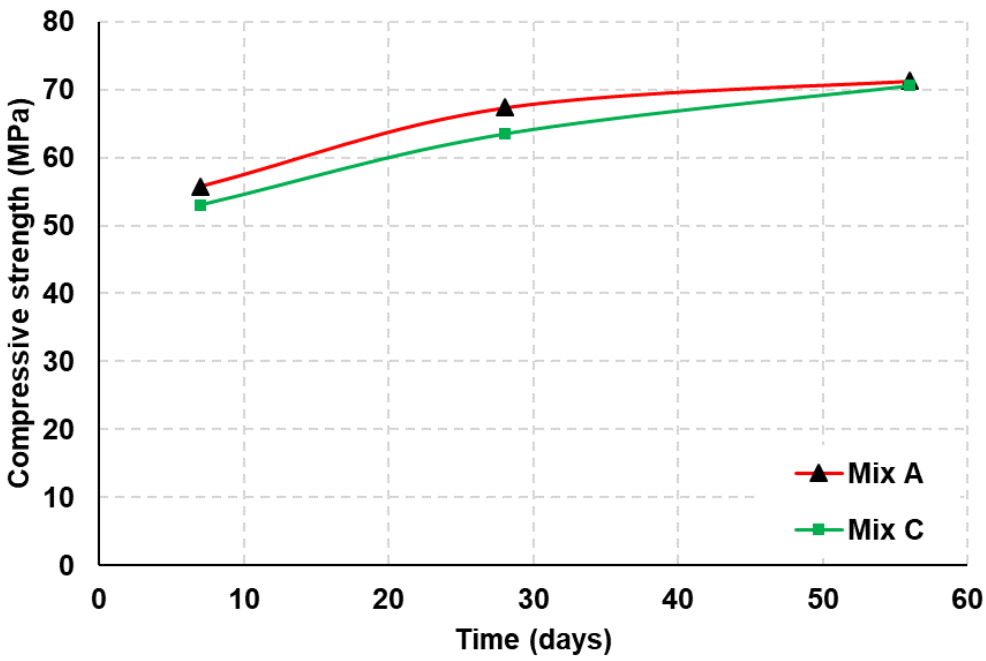

Figure 4.10. Compressive strength results for Mix C concrete after applying mixture design improvements, considering standard curing conditions.

Note: standard deviations (Days 7, 28, 56) in MPa are (0.54, 1.16, 1.74) for Mix A and (0.67, 0.88, 0.40) for Mix C.

The improvement in fresh concrete properties of Mix C can be mainly attributed to the use of chemical admixtures [74], while the improvement in hardened properties likely resulted from reducing the w/cm [14]. These results provide evidence of the applicability of using seawater and RCA in concrete mixtures, especially with appropriate consideration of chemical admixtures and mixture proportions. Yet, the methods implemented here, despite being effective, are not necessarily "green". Life-cycle analysis and similar analyses are likely required before optimal improvement strategies for the use of concrete combining seawater and RCA can be fully understood. Recent research efforts suggest that the carbonation treatment of RCA may represent a

more viable solution that not only improves the performance of RCA concrete but also represents a more environmentally-friendly approach [69,176,177].

4.4 Summary and Conclusions

This chapter compared two concrete mixtures, namely, conventional concrete (Mix A) and seawater-mixed recycled-aggregate concrete (Mix C). Based on the results of this study, the following conclusions have been drawn concerning the effects of combining seawater and RCA in concrete (compared to conventional concrete):

- Combining seawater and RCA reduced the concrete density (by approximately 5%) and increased the air content of the fresh concrete. This is attributed to the effects of RCA rather than seawater.
- Combining seawater and RCA resulted in a significant reduction in the slump flow (25%), initial setting time (50%), and also the workability retention (Mix C remained flowable for only half the time as Mix A).
- Combining seawater and RCA resulted in a significant reduction in the strength gain of hardened concrete (approximately 35%) at all ages. Scanning electron microscopy results showed some changes in microstructure between Mix C and Mix A which could potentially explain the poor strength performance.
- Long-term seawater curing (up to one year) increased the compressive strength of hardened concrete but led to reductions in the tensile strength.
- Mix C showed slightly an increase in the drying shrinkage (approximately 10%) compared to Mix A, mostly due to the effects of having RCA in the mixture.
- Combining seawater and RCA resulted in a reduced permeability performance, evidently from the increase in charge passed and also from the increase in water absorption of Mix C concrete over the allowable limits.

- Mixture design modifications were proposed to overcome the performance issues associated with the use of seawater and RCA, using chemical admixtures and adjusting w/cm.

While the fundamental observations in terms of behavior may be generalized, the above conclusions and specifically the numbers listed are valid for the materials and the specimens used herein. Future research is required to shed further light onto the effect of combining seawater and RCA in concrete mixtures while considering different compositions and test methods. Other “greener” approaches, such as RCA carbonation treatment, can also be investigated to improve the performance of the proposed concrete mixture.

CHAPTER 5: FLEXURAL PERFORMANCE OF SEAWATER-MIXED RECYCLED AGGREGATE GFRP-REINFORCED CONCRETE BEAMS

Following the concrete-characterization program carried out in Chapters 2–4, Chapter 5 investigates the flexural performance of seawater-mixed recycled-aggregate concrete reinforced with GFRP bars. Twelve RC beams with varying concrete mixture design and reinforcement material were constructed and tested under four-point loading. It is emphasized here that the concrete mixtures incorporating seawater and RCA are those "improved" mixtures proposed in Chapter 3 and Chapter 4.

5.1 Experimental Program

5.1.1 Concrete mixtures

Ready-mix concrete, with a 28-day design compressive strength of 60 MPa, was used to cast the RC beam specimens. Three concrete mixtures were considered, as shown in Table 5.1. Mix A (reference) is the conventional mix with freshwater and NCA. In Mix B, seawater replaced freshwater as mixing water. Mix C represents concrete mixed with seawater and RCA at 100% replacement level. Blast furnace slag was used in all mixtures as supplementary cementitious material (at 65% Portland cement replacement level) as it is known to improve the durability of seawater and/or RCA concrete [16,51]. Chemical and mechanical characterization details for the mix constituents can be found in Chapter 2.

Table 5.1 presents the mix proportions (per cubic meter) as per BS EN 206 [131] for each mixture. Direct volume replacement was used to determine the amount of RCA replacing NCA in Mix C (refer to Chapter 2). Additional mixing water was used in Mix C to compensate for the higher water absorption of RCA (compared to NCA), as explained in Chapter 2. Remedial measures were adopted in Mix B and Mix C to address the performance reductions expected due to the use of seawater and RCA, using chemical admixtures and/or reducing the water-to-cementitious material (w/cm) ratio

as detailed in Chapter 3 (for Mix B) and Chapter 4 (for Mix C). Consequently, Mix B and Mix C concretes showed performance comparable to the conventional Mix A for both workability and strength (Table 5.1).

Table 5.1

Concrete Mixtures Adopted in Study 3.

Property	Mix A	Mix B	Mix C
1. Concrete mixture proportions			
Water	165 kg/m³ (Freshwater)	165 kg/m³ (Seawater)	200 kg/m³ (Seawater)
Coarse aggregates	Conventional — 700 kg/m³ (Gabbro 20 mm) + 490 kg/m³ (Gabbro 10 mm)	Conventional — 700 kg/m³ (Gabbro 20 mm) + 490 kg/m³ (Gabbro 10 mm)	Recycled concrete — 990 kg/m³ (5-20 mm RCA)
Fine aggregates	750 kg/m³ (Washed sand)	750 kg/m³ (Washed sand)	750 kg/m³ (Washed sand)
Cementitious material	450 kg/m³ (35% OPC + 65% Slag)	450 kg/m³ (35% OPC + 65% Slag)	490 kg/m³ (35% OPC + 65% Slag)
Retarder (CHRYSOPlast CQ240)	-	0.25 L/m³	0.75 L/m³
Super plasticizer (Glenium 110 M)	4.05 L/m³	4.46 L/m³	5.57 L/m³
2. Concrete fresh properties and compressive strength			
Fresh concrete temperature	28.7 °C	30.0 °C	30.0 °C
Initial slump	250 mm	260 mm	270 mm
Initial slump flow	610 mm	650 mm	660 mm
28-day compressive strength	$64.1 \pm 0.4\ MPa$	$68.5 \pm 1.0\ MPa$	$59.7 \pm 0.4\ MPa$

5.1.2 RC beam specimens

Table 5.2 presents the test matrix for the RC beam specimens used in the current study. Twelve RC beam specimens were tested under four-point loading to assess their flexural performance. Two test variables were considered, namely, the concrete mixture (Mix A, B, or C) and the reinforcement material (steel/GFRP). Two identical samples were tested for each beam specimen. It is emphasized that the reinforcement ratio was kept the same among beam specimens with different concrete mixtures, with an intent to investigate the effects of mixing with seawater and RCA.

As shown in *Figure 5.1*, the beam specimens were 2.2 m in length (L), 150 mm in width (b), and 260 mm in height (h). GFRP/steel bars of 8 mm in diameter were used as transverse and top reinforcement, while 12 mm diameter bars were used as main flexural reinforcement. A 25 mm clear cover to reinforcement was maintained from all sides of the beam specimen, resulting in an effective depth (d) of 221 mm. The beams' dimensions and reinforcement details were typically aimed to produce an under-reinforced section (i.e., tension-controlled failure).

Steel bars of grade 500B (BS 4449:2005 [178]) were used as reinforcement in steel-RC beam specimens. Based on a tested sample of the steel bars, the yield stress, yield strain, and modulus of elasticity were measured as 594 MPa, 0.27%, and 220 GPa, respectively [179]. The GFRP bars had a tensile modulus of 45 GPa, a guaranteed tensile strength (f_{fu}^{*}) of 760 MPa, and a maximum strain of 1.7% as provided by the manufacturer [180].

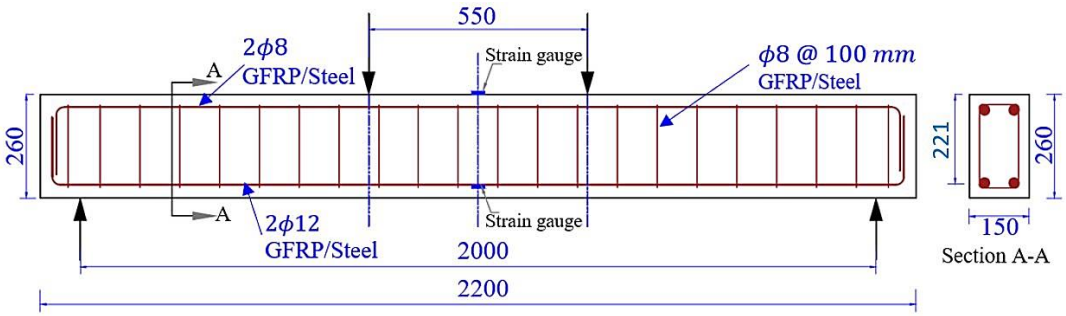

Figure 5.1. Schematic drawing for a typical RC beam used in this study.

Table 5.2

Test Matrix for the RC Beams.

Specimen ID	Concrete Mixture	Reinforcement
A-S-1 & A-S-2	Mix A	Steel
B-S-1 & B-S-2	Mix B	Steel
C-S-1 & C-S-2	Mix C	Steel
A-F-1 & A-F-2	Mix A	GFRP
B-F-1 & B-F-2	Mix B	GFRP
C-F-1 & C-F-2	Mix C	GFRP

5.1.3 Test setup

Figure 5.2 illustrates the test setup and instrumentation for a typical specimen. After two months following casting, each specimen was tested under four-point bending with monotonic loading using the Instron 1500 HDX Static Hydraulic Universal Testing Machine. Displacement-controlled loading was applied at a rate of 1 mm/min until failure. The vertical deflection at mid-span was monitored using a Linear Variable Displacement Transducer (LVDT). The beam specimen midspan was instrumented with a 60-mm strain gauge bonded at the top concrete surface and with two 5-mm strain gauges bonded to the rebars in tension. Additionally, a clip-type displacement transducer was placed at the side of the beam to measure the crack width

as shown in *Figure 5.2*. Data acquisition of the measurements was performed at a frequency of 1 Hz.

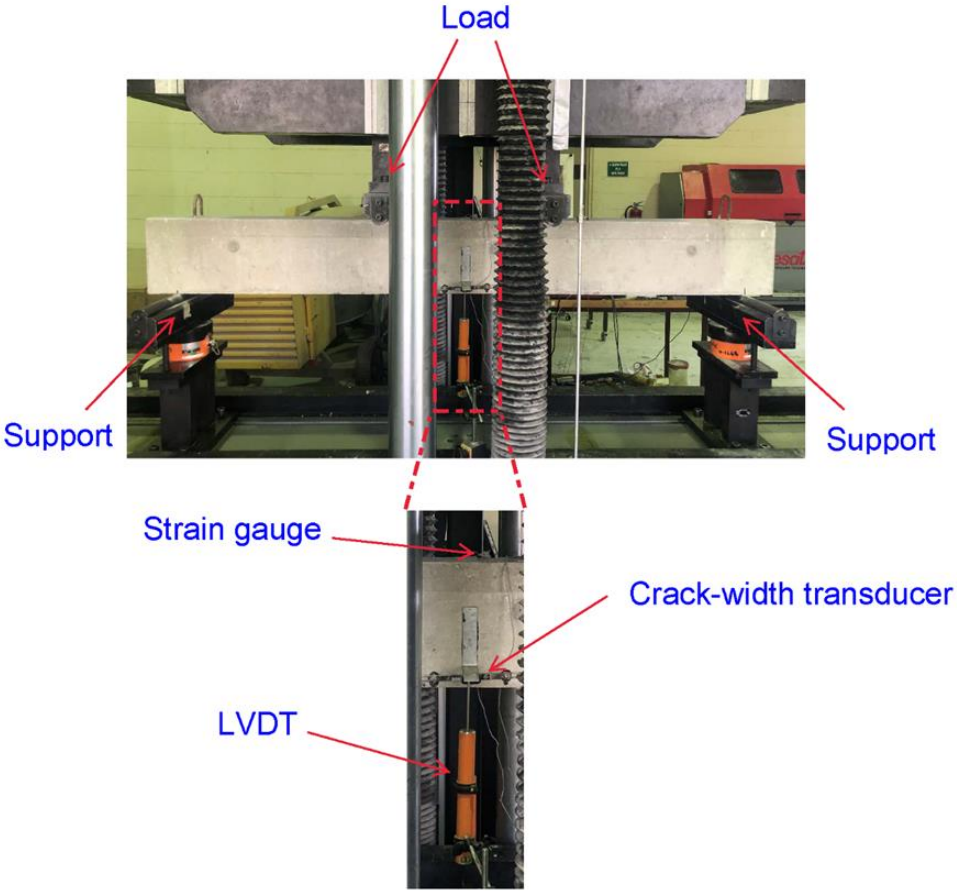

Figure 5.2. Test setup and instrumentation for RC beams.

5.2 Experimental Results

Table 5.3 presents a summary of the experimental results. In general, using seawater and/or RCA in the concrete mix had ultimately little-to-no effect on the flexural performance of RC beams, consistent with previous studies on recycled-aggregate RC beams [76,77]. This is perhaps unsurprising as the workability and strength were comparable among the concrete mixtures (Table 5.1). Reinforcement material, however, showed a notable effect on the flexural capacity as well as the deformational characteristics of the RC beams tested, conforming with previous studies on FRP-RC beams [92–101]. The following sub-sections (5.2.1–5.2.7) provide a detailed discussion on the experimental results.

5.2.1 Modes of failure

Column 13 of Table 5.3 presents the failure modes of the tested beams. The concrete mixture had no effect on the flexural failure behavior of RC beams, and the failure was a function of the reinforcement material. Two distinct failure modes were observed, namely, (a) concrete crushing following reinforcement yielding (denoted CC+Y) in steel-RC beams (*Figure 5.3*) and (b) rebar tensile rupture (denoted TR) in GFRP-RC beams (*Figure 5.4*). The concrete-crushing failure mode in steel-RC beams was verified via the concrete compressive strain values at the top soffit, that were generally close to or often exceeded the 0.003 maximum strain specified by ACI-318 [181] (Column 5 of Table 5.3). On the other hand, the tensile-rupture failure mode of GFRP-RC beams was confirmed by the rebar tensile strains reaching the ultimate value provided by the supplier ($\varepsilon_{fu}^{*} = 1.7\%$) (Column 4 of Table 5.3), in addition to the relatively small concrete compressive strains at failure (Column 5 of Table 5.3).

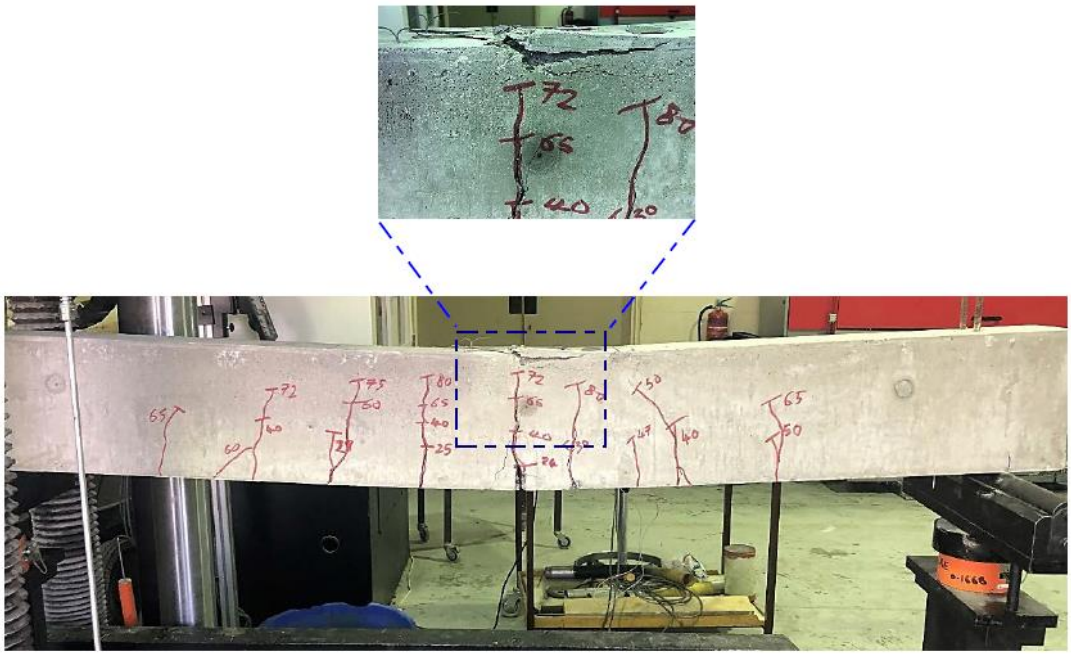

Figure 5.3. Concrete crushing in Specimen B-S-2.

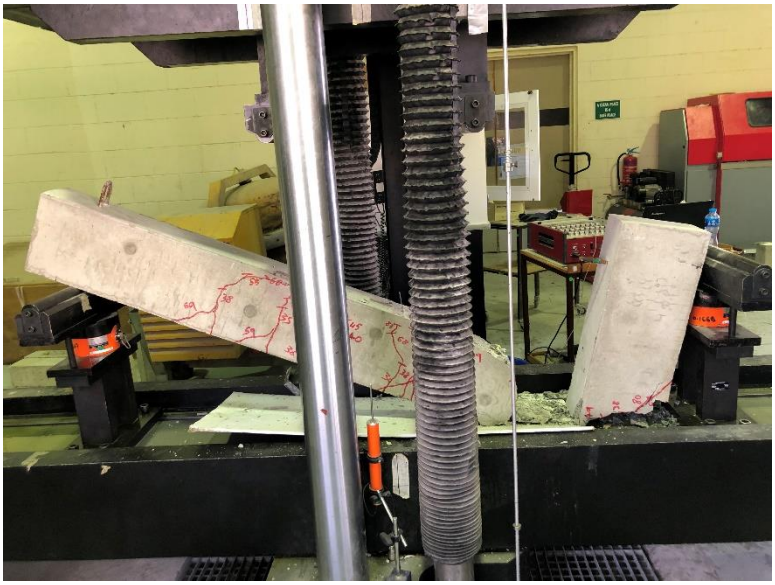

Figure 5.4. GFRP tensile rupture in Specimen B-F-2.

Table 5.3

Summary of the Test Results.

1	2	3	4	5	6	7	8	9	10	11	12	13
Specimen	P_u (kN)	δ_u (mm)	ε_{t-max} (%)	ε_{c-max} (%)	P_{cr} (kN)	No. of cracks	w_u (mm)	Expected S_i (kN/mm)	S_{cr} (kN/mm)	ψ (kN.mm)	μ	Failure Mode
A-S-1	79.3	50.6	1.49	0.279	19.0	12	3.60	58.5	6.5	3497	12.17	CC+Y
A-S-2	89.6	56.2	-	0.334	20.4	11	4.40	58.5	7.1	4314	12.20	CC+Y
B-S-1	83.5	47.8	1.95	0.243	22.2	12	4.87	60.4	6.7	3372	12.35	CC+Y
B-S-2	81.1	39.0	1.21	0.246	20.6	10	-	60.4	6.2	2680	9.88	CC+Y
C-S-1	87.3	59.1	0.98	0.245	22.1	10	-	56.7	7.9	4548	14.36	CC+Y
C-S-2	86.1	44.6	2.30	0.293	16.7	12	3.30	56.7	6.25	3255	8.33	CC+Y
A-F-1	103.2	36.9	1.79	0.158	14.8	9	1.53	55.4	2.3	2181	2.54	TR
A-F-2	103.2	37.4	1.94	0.151	17.1	8	-	55.4	2.4	2277	2.89	TR
B-F-1	99.7	40.5	1.71	0.156	19.1	9	1.55	57.1	2.2	2382	3.65	TR
B-F-2	116.2	47.5	1.88	0.185	16.7	10	1.93	57.1	2.7	3309	3.19	TR
C-F-1	92.5	30.5	1.82	0.168	20.4	8	1.88	53.5	2.4	1674	3.19	TR
C-F-2	102.4	44.3	1.67	0.153	19.2	9	-	53.5	2.7	2986	4.36	TR

5.2.2 Load-carrying capacity

Column 2 of Table 5.3 lists the values of the load-carrying capacity (P_u) of all beams. The difference in P_u was insignificant ($\leq 5\%$) among the companion specimens with different concrete mixtures. Taking the six steel-RC beams as an example, the two-beam average P_u values were calculated as 84.5, 82.3, and 86.7 kN for Mixes A, B, and C, respectively. As expected, the effect of the reinforcement material was substantial on the flexural capacity of the tested RC beams. The average load-carrying capacity of GFRP- and steel-reinforced concrete beams was 103 and 85 kN, respectively — i.e., the GFRP-RC beams outperformed their steel-reinforced counterparts by approximately 25%. This is attributed to the fact that the reinforcement in GFRP-RC beams had fully attained its tensile strength ($f_{fu}^{*} = 760\ MPa$) at failure, as opposed to their steel-reinforced counterparts whose reinforcement only yielded at $f_y = 594\ MPa$.

5.2.3 Deformational characteristics

Figure 5.5-a and *Figure 5.5*-b present the load-deflection responses for steel- and GFRP-RC beams, respectively. As shown in *Figure 5.5*-a, the load-deflection diagram of steel-RC beams typically consisted of three phases: (a) the uncracked phase, (b) the post-cracking/reduced-stiffness phase, and (c) the yield plateau that had a very small stiffness. On the other hand, the GFRP-RC beams showed a typical bilinear load-deflection response that represented two distinct phases, namely, the uncracked phase and the reduced-slope/post-cracking phase (*Figure 5.5*-b). These observed load-deflection behaviors were the same among beams with different concrete mixtures. *Figure 5.6*-a and *Figure 5.6*-b show an idealization of the load-deflection response for steel- and GFRP-RC beams, respectively.

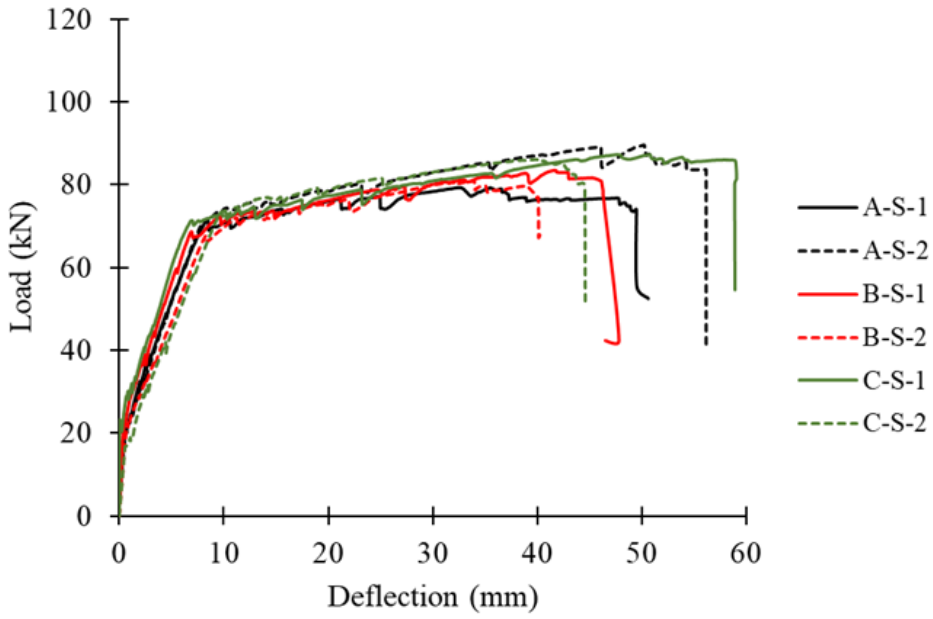

(a)

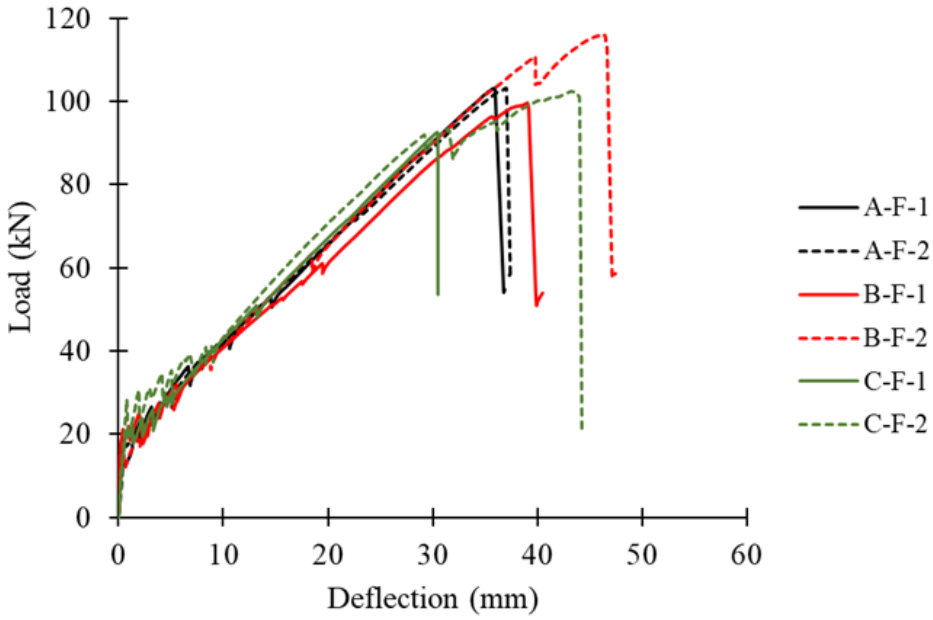

(b)

Figure 5.5. Load vs. deflection diagrams for (a) steel and (b) GFRP reinforced concrete beams.

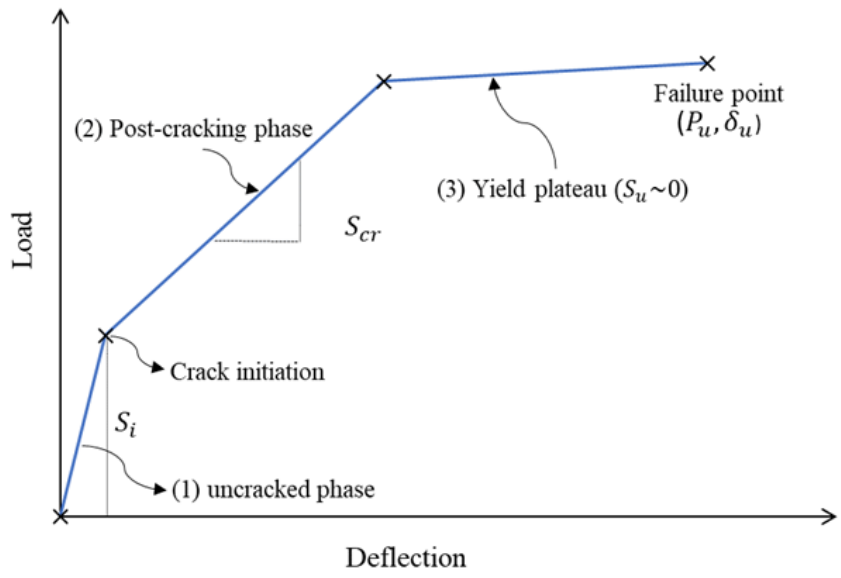

(a)

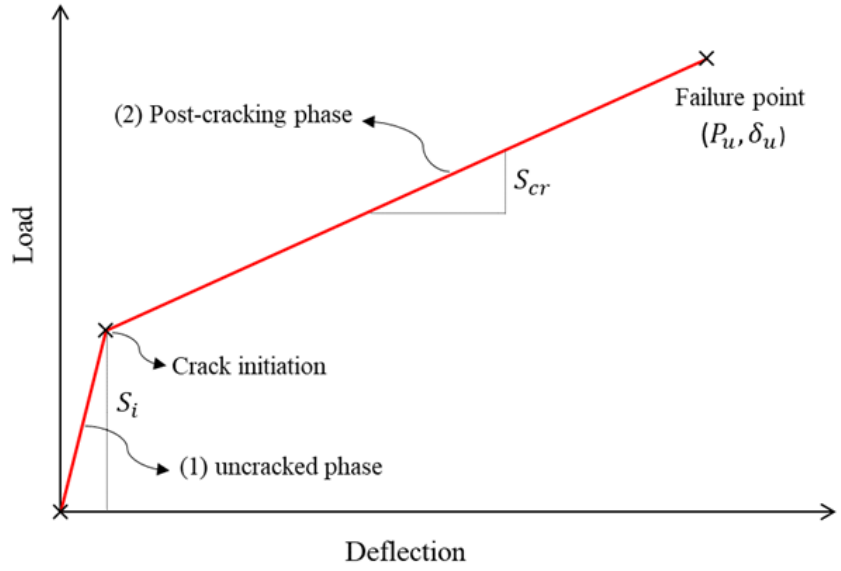

(b)

Figure 5.6. Idealization of load-deflection diagrams for (a) steel and (b) GFRP reinforced concrete beams.

The uncracked stiffness (S_i) widely varied among the tested beams without showing a specific pattern among different reinforcements or concrete mixtures, with an overall average of 48.0 kN/mm (compared to average expected value 56.9 kN/mm). The post-cracking stiffness (S_{cr}) values are listed in Column 10 of Table 5.3. The post-cracking stiffness of steel-RC beams (6.78 ± 0.64 kN/mm) was higher than that of the GFRP-reinforced counterparts (2.45 ± 0.21 kN/mm). This means that the GFRP-RC beams exhibited higher amounts of deflection at service-load conditions compared to their steel-reinforced counterparts. Indeed, this can be attributed to the higher tensile modulus of steel compared to GFRP. No effect of using seawater and/or RCA was observed, though, on the stiffness values of the tested beams.

The deflection values measured at failure (δ_u) for the tested beams are listed in Column 3 of Table 5.3. GFRP-RC beams had generally lower δ_u values as compared to those of their steel-reinforced counterparts. On average, the maximum deflection measured for GFRP- and steel-reinforced concrete beams was approximately 40 and 50 mm, respectively. This can be attributed to the more ductile behavior of steel-RC beams. As shown in *Figure 5.5*-a, most of the steel-RC beam's deflection occurred after the steel yielded. On average, the deflection at the yield plateau for steel-RC beams ($\delta_u - \delta_y$) was approximately 86% from the total deflection (δ_u).

5.2.4 Strain characteristics

The tensile strain of the flexural reinforcement (ε_t), as well as the concrete compressive strain at the top surface (ε_c), were continuously (and simultaneously) measured at the mid-span of the tested beams, until failure. The maximum tensile (ε_{t-max}) and compressive (ε_{c-max}) strains measured at failure are listed in Columns 4 and 5 of Table 5.3, respectively. In general, the effect of the concrete mix on strain characteristics was negligible when compared to that of the reinforcement material. As

expected, steel-RC beams had ε_{t-max} values higher than the yield strain ($\varepsilon_y = 0.27\%$) at failure ($\varepsilon_{t-max} = 1.586\%$ on average), associated with high compressive strains at the top soffit ($\varepsilon_{c-max} = 0.273\%$ on average). The ε_{t-max} values of GFRP-RC beams (1.8% on average) have had approached or exceeded the ultimate strain value provided by the supplier ($\varepsilon_{fu}^{*} = 1.7\%$), and were associated with relatively lower ε_{c-max} values (0.162% on average) compared to those of steel-RC beams. These results taken together verify the tension-controlled failure mode exhibited by steel- and GFRP-RC beams.

Figure 5.7-a and *Figure 5.7*-b depict the increase in the rebar tensile strain with the applied load for steel- and GFRP-RC beams, respectively. In general, the tensile strain of the flexural reinforcement started to significantly develop just after the crack initiation (at $P = P_{cr}$). After that, the tensile strain increased with the applied load, taking a shape matching the constitutive law of the reinforcement material — i.e., linear elastic to failure for GFRP (*Figure 5.7*-b) and bi-linear for steel (*Figure 5.7*-a). Likewise, *Figure 5.8*-a and *Figure 5.8*-b present the load versus concrete-compressive-strain diagrams for steel- and GFRP-RC specimens, respectively. In general, the $P - \varepsilon_c$ curves of the tested beams had profiles similar to their load-deflection diagrams (i.e., tri-linear for steel-RC beams and bi-linear for GFRP-RC beam specimens), with approximately the same load values at pivot points.

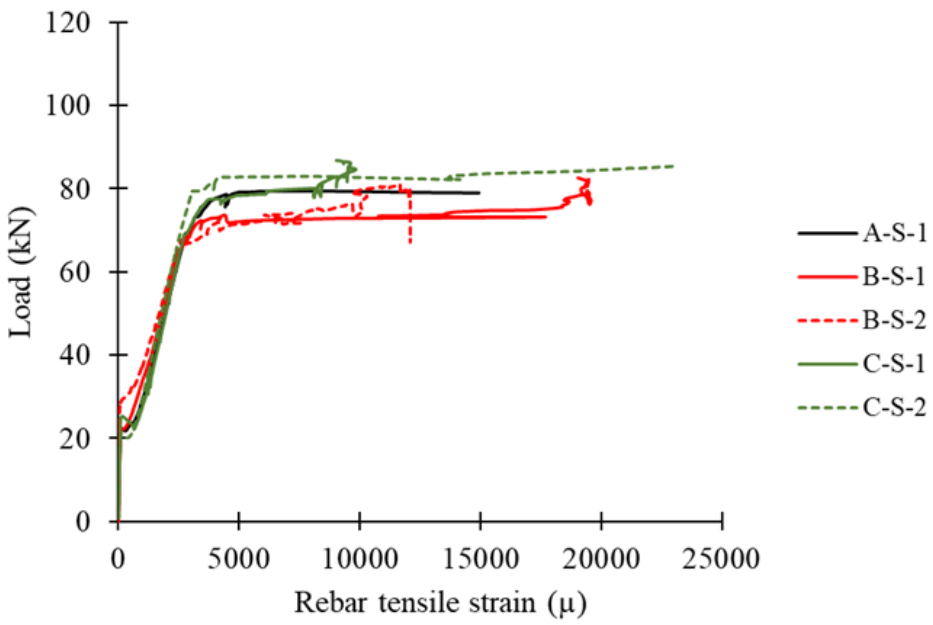

(a)

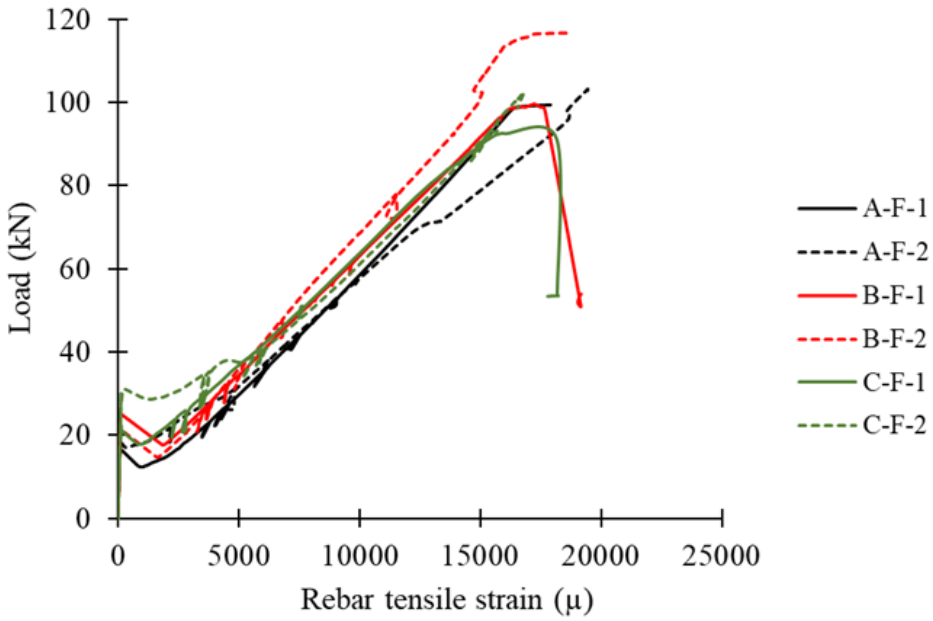

(b)

Figure 5.7. Load vs. rebar strain diagrams for (a) steel and (b) GFRP reinforced concrete beams.

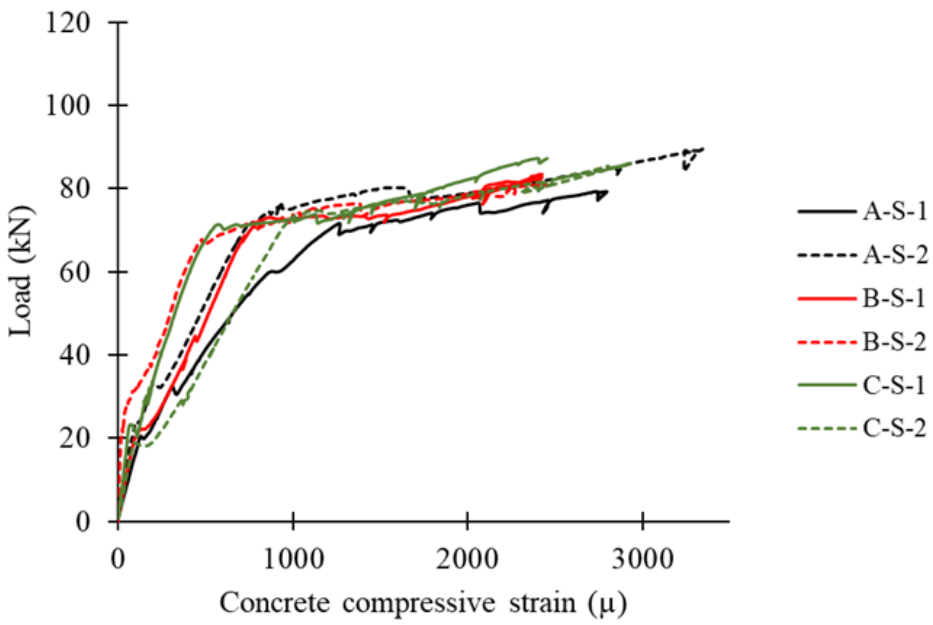

(a)

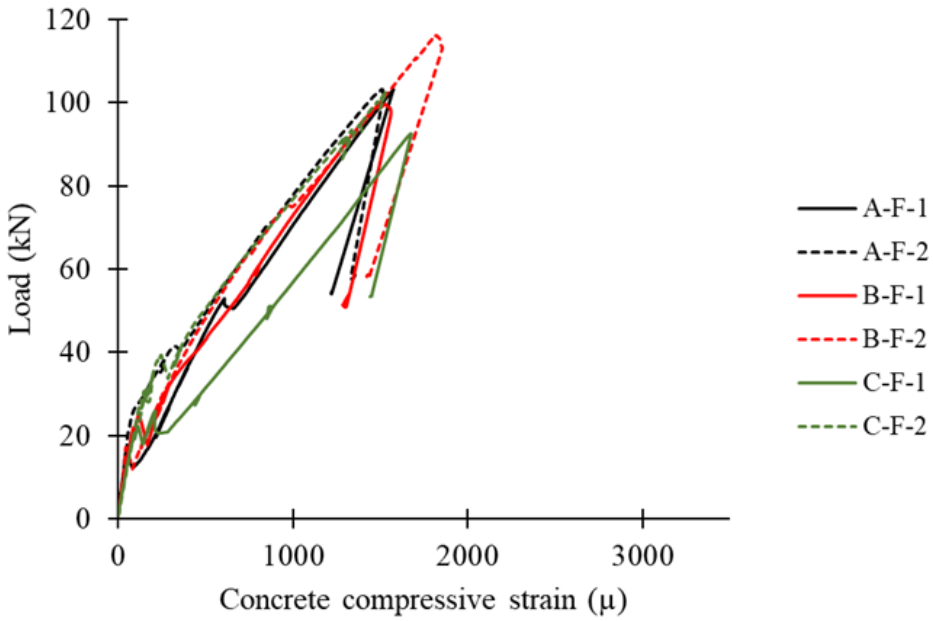

(b)

Figure 5.8. Load Vs. concrete compressive strain diagrams for (a) steel and (b) GFRP reinforced concrete beams.

5.2.5 Energy absorption

Energy absorption (ψ) is defined as the total area under the load-deflection curve up until the failure point (δ_u, P_u) [182]. Column 11 of Table 5.3 lists the energy absorption values determined for the beam specimens. The concrete mixture type showed no clear effect on the energy absorption of the tested beams when compared to that of the reinforcement material. The ψ values calculated for steel- and GFRP-RC beam specimens (expressed as average $\pm$ standard deviation) were 3611 $\pm$ 698 and 2468 $\pm$ 588 kN.mm, respectively, indicating the superior flexural performance of the steel-RC beams due to their ductile behavior as demonstrated in load-deflection diagrams (*Figure 5.5*).

5.2.6 Ductility index

In steel-RC beams, the ductility index (μ) is classically defined as the ratio of the deflection at ultimate (δ_u) to that at steel yielding (δ_y). However, in the case of FRP-RC beams, such interpretation of ductility (i.e., on the basis of reinforcement yielding) may be misleading since FRP bars exhibit a linear stress-strain relationship until failure without an intermediate yielding point. Alternatively, Naaman and Jeong [183] proposed an energy-based approach to calculate μ that is applicable to both steel- and FRP-reinforced concrete beams, thus providing a common basis for comparison. In this energy-based approach, the ductility index can be calculated as follows [183]:

$$\mu = 0.5\left(\frac{\psi}{\psi_{el}} + 1\right) \tag{5.1}$$

where ψ is the total energy absorption, and ψ_{el} is the elastic energy calculated as illustrated in *Figure 5.9*. The P_1 in *Figure 5.9* refers to the cracking load, P_{cr} (Column 6 of Table 5.3); P_2 refers to the load at which the beam's stiffness changes prior to failure (and is usually close to P_u); S_1 here is taken as the expected value of uncracked

stiffness (Column 9 of Table 5.3); and S_2 refers to the post-cracking stiffness (Column 10 of Table 5.3).

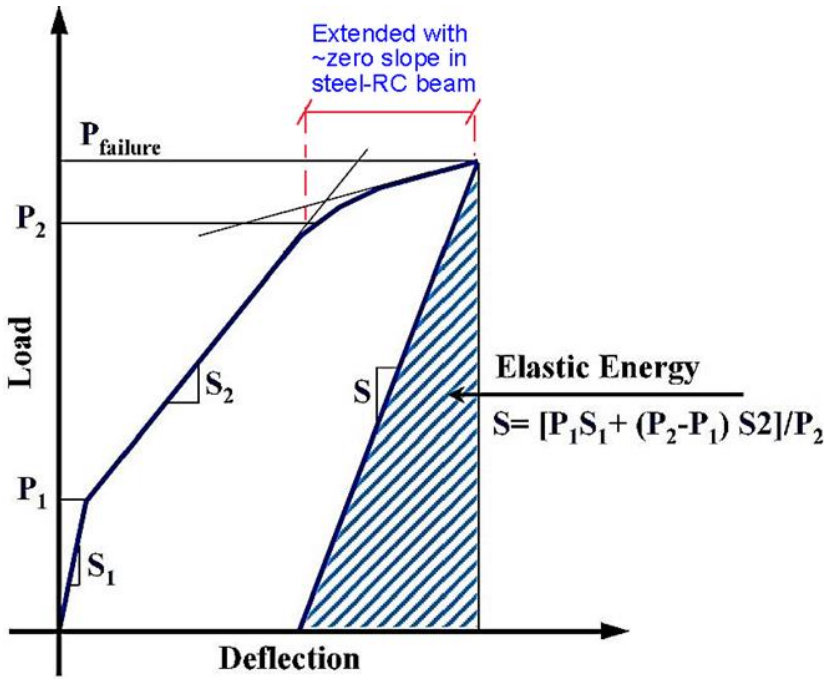

Figure 5.9. Schematic description of ductility index for RC beams based on energy concept [183].

Column 12 of Table 5.3 lists the μ values calculated as per Eq. (5.1) for the tested specimens. Using seawater and/or RCA appeared to have almost no significant effect on μ when compared to that of the reinforcement material. Comparing μ values between steel and GFRP-RC beams verifies the ductile behavior of the former as well as the brittle behavior of the latter. The ductility indices for steel- and GFRP-RC beams (expressed as average $\pm$ standard deviation) are 11.55 $\pm$ 2.12 and 3.30 $\pm$ 0.64, respectively.

5.2.7 Cracking behavior

All beams exhibited a steep load-deflection response until the applied load reached the cracking load (P_{cr}), at which crack initiated at the constant-moment zone of the beam span. Column 6 of Table 5.3 lists the P_{cr} values for the tested beams. The P_{cr} values ranged from 14.8 kN (Specimen A-F-1) to 22.2 kN (Specimen B-S-1), with an average value of 19.0 kN and a standard deviation of 2.3 kN. No clear or patterned effect of the concrete mix was observed on P_{cr} (given that $f_{c'}$ was comparable among concrete mixtures). Also, the cracking pattern was almost the same among specimens with different concrete mixtures.

The reinforcement material exhibited a clear effect on the cracking behavior of the tested specimen. *Figure 5.10*-a and *Figure 5.10*-b present the cracking pattern for steel- and GFRP-RC beams, respectively. Although both steel- and GFRP-RC beams showed the same flexural-shear crack pattern that is naturally expected for an RC beam subject to 4-point loading (idealized in *Figure 5.10*-c), the former had generally a greater number of cracks at failure (see *Figure 5.10*-a and Column 7 of Table 5.3). Furthermore, the crack-width values at failure (w_u) corresponding to steel-RC beams were higher than those of GFRP-reinforced counterparts (Column 8 of Table 5.3): the average w_u obtained for steel- and GFRP-RC beams was 4.04 and 1.72 mm, respectively. This can be attributed to the fact that the steel yields at the crack location allowing the cracks to widen. The effect of the beam ductility on the crack width can be demonstrated by comparing the $P - w$ diagrams between steel- and GFRP-RC beam specimens (*Figure 5.11*). Most of the increase in the crack width (approximately 90%) in the steel-RC beams had occurred after the steel yielded (*Figure 5.11*-a). Against this, the crack width (following P_{cr}) of GFRP-RC beams had a linear profile (*Figure 5.11*-b).

(a)

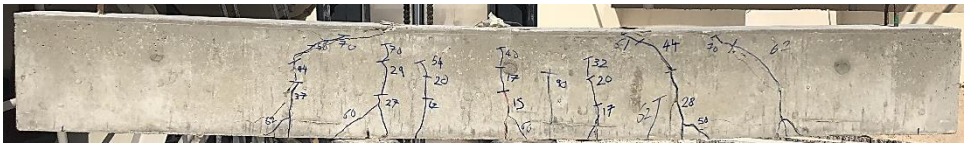

(b)

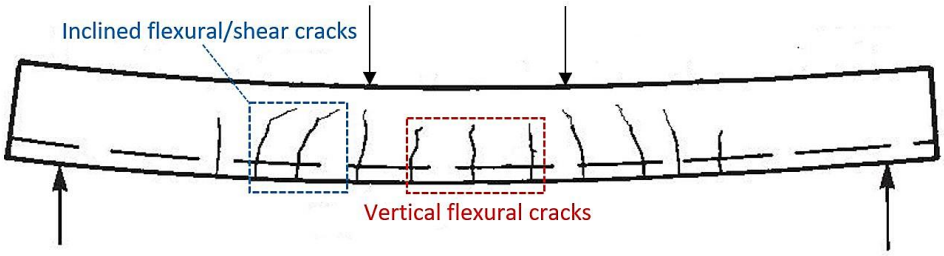

(c)

Figure 5.10. Crack pattern for Specimens (a) C-S-2 and (b) C-F-2; (c) idealization of the crack pattern in the RC beams tested.

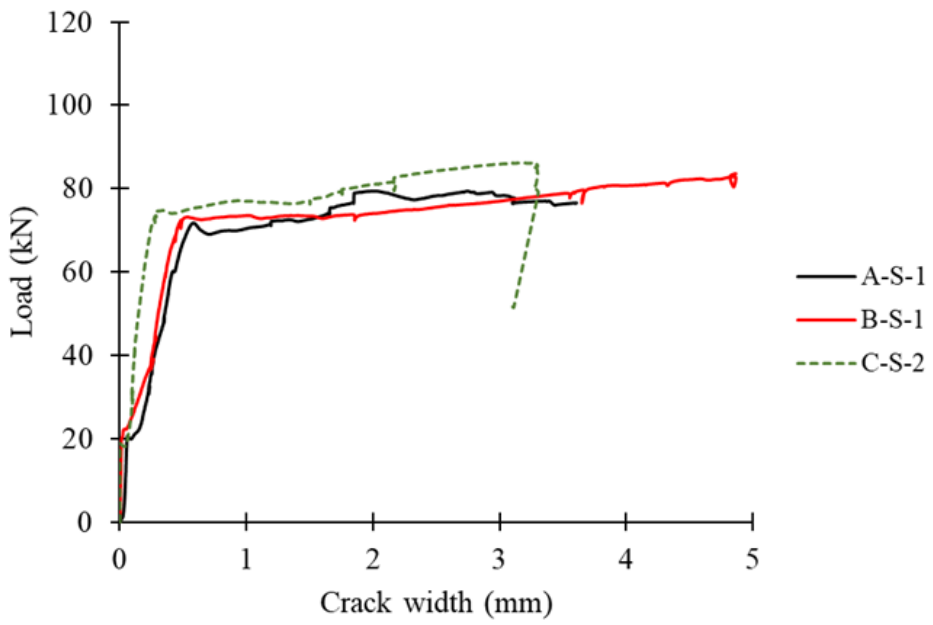

(a)

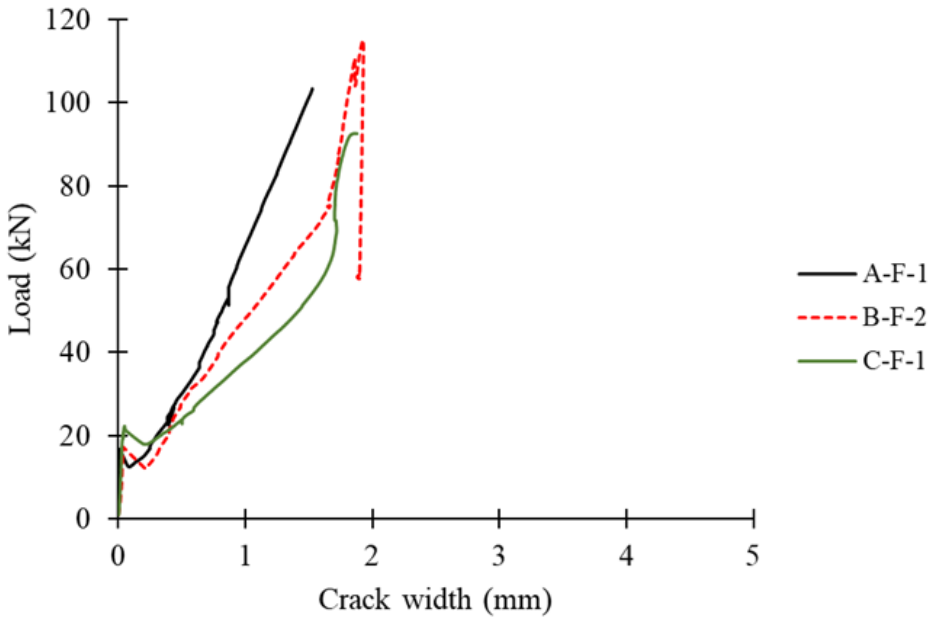

(b)

Figure 5.11. Load vs. crack-width diagrams for samples of (a) steel and (b) GFRP reinforced concrete beams.

5.3 Theoretical Formulation

5.3.1 Cracking and ultimate Loads

Theoretical values of cracking load (P_{cr-Th}) were obtained considering a concrete modulus of rupture (f_r) determined as per ACI-318 [181] ($f_r = 0.62\sqrt{f_c'}$), and accounting for the reinforcement stiffnesses in the gross moments of inertia. As shown in Column 4 of Table 5.4, the experimental P_{cr} values were lower (by 20% on average) than those predicted using ACI-318 [181].

Theoretical values of load-carrying capacity (P_{u-Th}) were obtained according to ACI 318 [181] for steel-RC beams and ACI 440.1 [86] for GFRP-RC beams. Based on the equilibrium illustrated in *Figure 5.12*, the moment capacity (M_n) of a typical steel-RC beam is obtained using Eq. (5.2):

$$M_n = T\left(d - \frac{\beta_1 c}{2}\right) \tag{5.2}$$

where β_1, α_1, and ε_c (see *Figure 5.12*) were taken as 0.65, 0.85, and 0.003, respectively, in compliance with ACI 318 provisions [181].

The same formula was used to calculate P_{u-Th} for GFRP-RC beams considering the GFRP tensile parameters ($E_f = 45\ GPa$ and $f_{fu} = f_{fu}^* = 760\ MPa$). The concrete compressive strain (ε_c), the depth of compression zone (c), and the rectangular stress block parameters (β_1 and α_1) were obtained by means of "equilibrium and compatibility" as per ACI 440.1 [86] provisions (for tension-controlled failure).

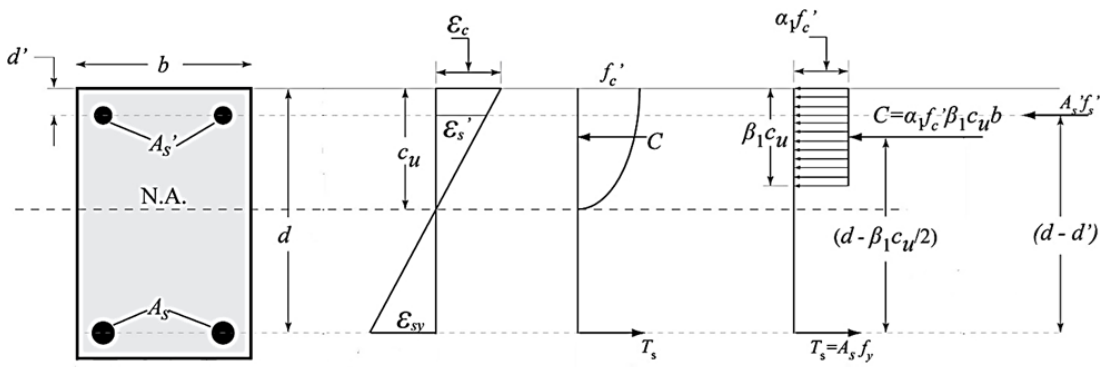

Figure 5.12. Equilibrium forces for a typical RC beam under flexure.

Columns 6 and 7 of Table 5.4 list P_{u-Th} values and P_u/P_{u-Th} ratios for the tested RC beams, respectively. The experimental values of load-carrying capacity were generally higher (except for C-F-1) than those predicted by the ACI design guides [86,181]. A reasonable agreement was obtained between the experimental and theoretical P_u values, with an approximate average difference of 7.5%.

Table 5.4

Comparison of Experimental and Theoretical Predictions.

1	2	3	4	5	6	7	8	9	10	11	12	13
Specimen	Cracking load			Load-carrying capacity			Deflection (Service)			Crack width (Service)		
	P_{cr} (kN)	P_{cr-Th} (kN)	$P_{cr}/P_{cr-\mathrm{Th}}$	P_u (kN)	P_{u-Th} (kN)	P_u/P_{u-Th}	δ_{ser} (mm)	δ_{ser-Th} (mm)	$\delta_{ser}/\delta_{ser-Th}$	w_{ser} (mm)	w_{ser-Th} (mm)	w_{ser}/w_{ser-Th}
A-S-1	19.0	24.5	0.78	79.3	78.8	1.006	1.72	1.23	1.40	0.217	0.141	1.539
A-S-2	20.4	24.5	0.83	89.6	78.8	1.137	1.92	1.23	1.56	0.205	0.141	1.454
B-S-1	22.2	25.3	0.88	83.5	79.0	1.057	1.27	1.13	1.13	0.152	0.140	1.078
B-S-2	20.6	25.3	0.81	81.1	79.0	1.027	2.10	1.13	1.88	-	-	-
C-S-1	22.1	23.7	0.93	87.3	78.6	1.111	1.26	1.33	0.95	-	-	-
C-S-2	16.7	23.7	0.70	86.1	78.6	1.095	2.49	1.33	1.87	0.097	0.141	0.688
A-F-1	14.8	23.2	0.64	103.2	97.4	1.060	4.85	6.06	0.80	0.505	0.905	0.558
A-F-2	17.1	23.2	0.74	103.2	97.4	1.060	5.52	6.06	0.91	-	-	-
B-F-1	19.1	24.0	0.80	99.7	96.4	1.034	5.02	5.69	0.88	0.499	0.904	0.551
B-F-2	16.7	24.0	0.70	116.2	96.4	1.205	5.87	5.69	1.03	0.571	0.904	0.631
C-F-1	20.4	22.4	0.91	92.5	98.5	0.939	5.57	6.45	0.86	0.719	0.905	0.794
C-F-2	19.2	22.4	0.86	102.4	98.5	1.040	5.08	6.45	0.79	-	-	-

5.3.2 Crack width

The ACI-318 design code [86] accounts for the crack-width control of steel RC beams by setting maximum limits for the reinforcement spacing, rather than using a specific formula to calculate the crack width. ACI 440.1 [184], however, recommends using Eq. (5.3) to calculate the maximum crack width for FRP-RC beams under flexure:

$$w = 2\frac{f_f}{E_f}\beta k_b\sqrt{d_c^2 + (s/2)^2} \tag{5.3}$$

where w is the maximum crack width (in mm); f_f is the reinforcement stress (in MPa); E_f is the reinforcement modulus of elasticity (in MPa); β is the ratio of the distance between neutral axis and extreme tension face to the distance between neutral axis and centroid of reinforcement; d_c is the thickness of cover from the extreme tension face to the center of closest bar (in mm); s is the bar spacing (in mm); and k_b is a coefficient that indicates the degree of bond between FRP bar and concrete. In accordance with ACI 440.1 [184], k_b was conservatively taken here as 1.4 given the lack of experimental evidence on the bond between concrete and the GFRP bars used here.

Columns 11–13 of Table 5.4 compare the predicted and experimental values of crack width at service load. The service load (P_{ser}) for GFRP-RC beams refers to the load at which the rebar tensile stress reaches the creep-rupture limit ($f_f = 0.3f_{fu}$ [185]), and was determined to be 30.2 kN. It is emphasized that the small difference in f_c' among the concrete mixtures had ultimately no effect on crack-width calculations. The predicted crack width at service load (w_{ser-Th}) was calculated as 0.90 mm, and was generally higher than that experimentally measured (0.60 mm on average). This discrepancy is probably attributed to the conservative use of $k_b = 1.4$. Considering a k_b of 1.2 (as recommended by ISIS [186]) reduced the gap between the predicted and

experimental w_{ser} values by 40%.

Likewise, the crack width was predicted for steel-RC beams using Eq. (5.3) considering the tensile parameters of steel bars and taking k_b as 1.0 (in compliance with ACI 440.1 [184]). The stress level at steel bars was taken as $0.4f_y$ (adopted in the allowable stress method [187]) and corresponded to $P_{ser} = 30.0\ kN$. The w_{ser} for steel-RC was predicted as 0.14 mm (compared to an average experimental value of 0.17 as shown in Column 12 of Table 5.4). The discrepancy observed among steel-RC beams in the experimental w_{ser} are likely attributed to deviations in their uncracked stiffness.

5.3.3 Deflection

The immediate mid-span deflection (δ_{Th}) of a simply supported RC beam subject to four-point loading is calculated as follows:

$$\delta = \frac{Pa}{48E_cI_e}(3L^2 - 4a^2) \tag{5.4}$$

where L is the total span length; a is the shear span; P is the total applied load; E_c is the concrete modulus of elasticity determined as $E_c = 4700\sqrt{f_c'}$ [86]; and I_e is the effective moment of inertia. Prior to concrete cracking, I_e is taken as the gross moment of inertia (I_g) that accounts also for reinforcement stiffness. The moment of inertia corresponding to a fully-cracked section (I_{cr}) is calculated using an elastic analysis for the beam section in which the concrete in tension is neglected [181]. During the service-load stage, I_e is calculated to represent the transition between I_g and I_{cr}. The ACI 318 [181] adopts Branson's model [188] to calculate I_e as follows:

$$I_e = \left(\frac{M_{cr}}{M_a}\right)^3 I_g + \left(1 - \left(\frac{M_{cr}}{M_a}\right)^3\right) I_{cr} \tag{5.5}$$

where M_a is the applied moment and M_{cr} is the cracking moment.

An alternative formula was suggested by Bischoff [189] to calculate I_e as follows:

$$I_e = \frac{I_{cr}}{1 - (1 - \frac{I_{cr}}{I_g}) \left(\frac{M_{cr}}{M_a}\right)^2} \tag{5.6}$$

Figure 5.13-a presents the predicted load-deflection response for steel-reinforced specimens (up until $P_{ser} = 30.0\ kN$), obtained using both Branson and Bischoff formulas. The latter appears to have a better match with the experimental $P - \delta$ diagrams, for which an acceptable agreement was obtained, particularly in Specimens C-S-1 and B-S-1 (Column 10 of Table 5.4). A high discrepancy was observed, though, between the predicted and experimental deflections for the other steel-RC beams, likely attributed to deviations in the uncracked stiffness.

For FRP-RC beams, ACI-440.1R-06 [184] had recommended the use of an adjusted form of Branson's formula to calculate I_e as follows:

$$I_e = \left(\frac{M_{cr}}{M_a}\right)^3 \beta_d I_g + \left(1 - \left(\frac{M_{cr}}{M_a}\right)^3\right) * I_{cr} \tag{5.7}$$

where $\beta_d = 0.2\rho_f/\rho_{fb}$ is a reduction coefficient related to the reduced tension stiffening of FRP-RC beams. Lately, the ACI-440.1R-15 [86] design guide replaced Eq. (5.7) with an updated form of Bischoff's formula to calculate I_e as follows:

$$I_e = \frac{I_{cr}}{1 - \gamma(1 - \frac{I_{cr}}{I_g}) \left(\frac{M_{cr}}{M_a}\right)^2} \tag{5.8}$$

where γ (function of a/L and M_{cr}/M_a [86]) is a factor that accounts for the variation

in stiffness along the beam span, calculated here as $\gamma = 1.85 - 0.85\frac{M_{cr}}{M_a}$.

The design manual ISIS-2007 [186] recommends using Eq. (5.9) to calculate I_e as follows:

$$I_e = \frac{I_{cr} I_g}{I_{cr} + \left(1 - 0.5\left(\frac{M_{cr}}{M_a}\right)^2\right)\left(I_g - I_{cr}\right)} \tag{5.9}$$

The CSA S806-12 [87] design code recommends using Eq. (5.10) to calculate the deflection of a simply supported beam subject to 4-point loading, as follows:

$$\delta = \frac{PL^3}{48E_c I_{cr}}\left(3\frac{a}{L} - 4\left(\frac{a}{L}\right)^3 - 8\left(1 - \frac{I_{cr}}{I_g}\right)\left(\frac{L_g}{L}\right)^3\right) \tag{5.10}$$

where $L_g = aM_{cr}/M_a$ is the length of the uncracked section.

Figure 5.13-b compares the predicted load-deflection responses among the aforementioned design codes for GFRP-reinforced specimens (up until $P_{ser} = 30.2\ kN$). Compared to the experimental $P - \delta$ diagrams, the ACI-440.1R-06 formula [184] appeared to be the most representative to the tested specimens, while the CSA S806-12 [87] formula was the most conservative.

Columns 8–10 of Table 5.4 compare the predicted service deflections (δ_{ser-Th}) with those experimentally measured at P_{ser}. The stipulated δ_{ser-Th} values are those corresponding to Eq. (5.6) (Bischoff formula [189]) for steel-RC beams and to Eq. (5.7) (ACI-440.1R-06 [184]) for GFRP-RC beams. A reasonable agreement was obtained between the experimental and predicted δ_{ser} values for GFRP-RC beams, with an approximate average difference of 13%.

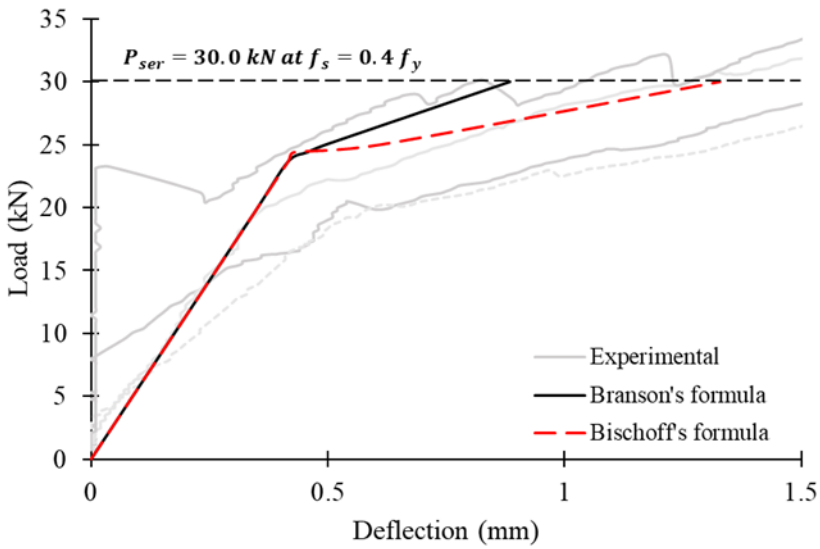

(a)

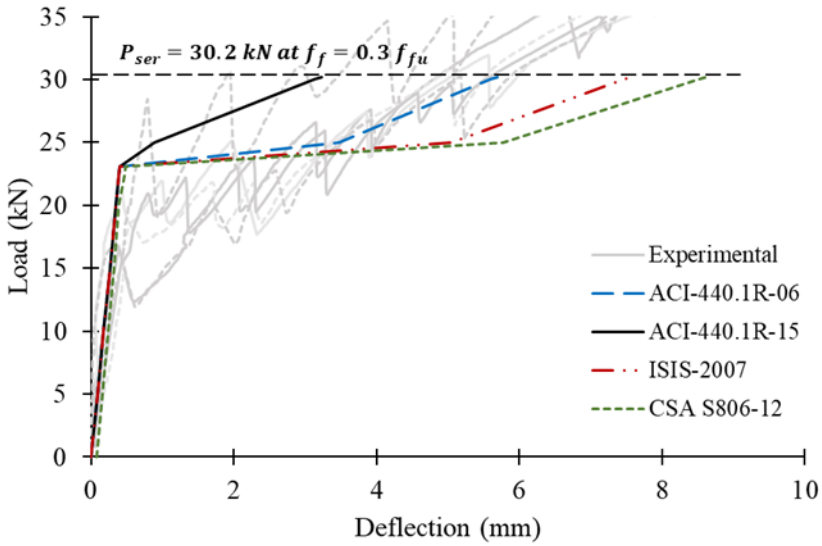

(b)

Figure 5.13. Predicted vs. experimental load-deflection diagrams (taking fc'=60 MPa) for (a) steel-RC and (b) GFRP-RC beams.

5.4 Summary and Conclusion

This effort investigated the flexural performance of seawater-mixed recycled-aggregate GFRP-reinforced concrete beams. Twelve medium-scale RC beams were tested under four-point loading considering three test variables, namely, mixing water (seawater/freshwater), aggregates type (virgin/recycled), and reinforcement material (black steel/GFRP). Based on the study results, the following conclusions have been drawn:

- If reductions in concrete performance are averted (using admixtures and/or changes in concrete mix design), using seawater and recycled coarse aggregate in concrete mixtures has little-to-no effect on the short-term flexural capacity of RC beams. The reinforcement material controls the flexural performance of RC beams.
- Steel-RC beams generally failed due to concrete crushing that follows the steel yielding. The GFRP-RC beams showed a more brittle failure due to rebar tensile rupture. On average, GFRP-RC beams showed an approximately 25% increase in the load-carrying capacity as compared to their steel-reinforced counterparts, but they also showed notable reductions in deformational and cracking performance.
- Theoretical values of flexural capacity, deflection, and crack width were predicted for the tested specimens and compared with the experimental results. A reasonable agreement was obtained between the predicted and experimental values of flexural capacity (7.5% difference on average). The predicted deflections of GFRP-RC beams somewhat conformed with the experimental values (averagely 13% difference). Some deviations were observed, though, in crack-width and deflection predictions for certain specimens, mostly attributed to discrepancies in the uncracked stiffness.

CHAPTER 6: LIFE CYCLE COST ANALYSIS OF STRUCTURAL CONCRETE USING SEAWATER, RECYCLED CONCRETE AGGREGATES, AND GFRP REINFORCEMENT

Chapters 2–5 have detailed experimental studies on the performance of plain concrete mixed with seawater and RCA as well as the flexural performance of this concrete reinforced with GFRP. Chapter 6 aims at verifying the cost effectiveness of the proposed combination (i.e., seawater + RCA + GFRP reinforcement) as compared to that of the traditional RC structure (i.e., freshwater + natural aggregates + black steel reinforcement), using life cycle cost analysis.

6.1 Materials and Methods

6.1.1 Design alternatives

Two design alternatives for reinforced concrete in high-rise buildings are considered, with reference to the concrete mixture and reinforcement material (Table 6.1). RC1 represents the conventional design - with freshwater, natural aggregates (NA), and black steel reinforcement – and is considered as a reference. As opposed to the well-known RC1, the proposed design alternative RC2 combines the seawater-mixed concrete with RCA and GFRP reinforcement.

Table 6.1

Design Alternatives Considered in Study 4.

Design Alternative	Mixing water	Aggregates used	Reinforcement material
RC1	Freshwater	Natural aggregate	Black steel
RC2	Seawater	Recycled concrete aggregate	GFRP

6.1.2 Reinforced concrete design

The relative amounts of concrete and reinforcement are critical in achieving a safe and economic concrete structure. For the conventional reinforced concrete (RC1), the structural design data were obtained from Foraboschi et al. [190] in their work concerning the embodied energy of high-rise buildings. These authors performed structural design on several reinforced concrete tall buildings of different height and gross floor area [190]. The compressive strength of concrete was taken as 40 MPa [190], assumed valid for high-rise reinforced concrete buildings. A uniformly-distributed dead load of 2.5 kN/m², in addition to the self-weight, was assumed for loading over the entire floor area to represent internal non-bearing elements. The external facade was reproduced by a uniform dead load of 4 kN/m applied along the perimeter beams. The vertical live load was assumed as 3 kN/m², uniformly-distributed over the entire floor area. The wind load was applied as per the Eurocode [191]. Seismic actions were not considered since they are generally deemed to have negligible structural effects on tall buildings compared to those induced by the wind load [192–194]. The structural analyses were performed using the finite element method. The buildings were designed to consistently meet the same serviceability margins, by imposing the maximum horizontal and vertical displacements for each building to equal 1/400 of the building height and 1/400 of the longest floor span, respectively [190].

The amounts of concrete and reinforcement are summed up for all structural elements (i.e., slabs, beams, columns, etc.) and divided by the gross floor area [190] (Table 6.2). The reinforced concrete design is thus expressed in terms of the overall concrete volume and reinforcement weight needed per unit floor area. The average concrete volume, reinforcement weight, and reinforcement ratio, ratio (ρ), the latter being the ratio between the volume of reinforcement to the volume of concrete, are

taken as 0.32 m^3/m^2, 50.45 kg/m², and 2%, respectively for the same unit floor area. These are considered as input quantities for the RC1 LCCA calculations.

The GFRP reinforcement, on the other hand, exhibits a brittle failure at the ultimate stress [21,26] but has higher tensile strength and lower elastic modulus [25]. Consequently, the balanced reinforcement ratio (ρ_b) of a typical GFRP-reinforced concrete flexural member is approximately one-fifth that of steel-reinforced counterpart [184]. This lower balanced ratio leads to a lower reinforcement volume needed for the structural design of GFRP-reinforced concrete. However, to ensure meeting the minimum reinforcement requirements as per ACI 440.1 [184], the reinforcement ratio of GFRP-reinforced concrete (i.e. RC2) is assumed to be the same as that of steel-reinforced counterpart (ρ = 2%). This assumption yields an over-reinforced section (i.e. $\rho > \rho_b$), that is recommended due to the corresponding less severe failure mode [184]. The relatively low density of GFRP (1/4–1/5 that of steel [184]), provides a notably lower reinforcement weight per unit area for RC2 compared with the steel-reinforced counterpart.

Table 6.2

Summary of the Design of Conventional Steel-Reinforced Concrete for Tall Buildings with Different Heights and Gross Floor Areas [190].

No. of stories	Gross floor area (m²)	Total concrete volume (m^3)	Total steel weight (kg)	Volume of concrete per unit area (m^3/m^2)	Steel weight per unit area (kg/m²)
20	8,000	2,185	341,547	0.27	42.69
30	17,280	4,883	764,123	0.28	44.22
40	36,000	11,222	1,764,518	0.31	49.01
50	57,800	20,772	3,275,740	0.36	56.67
60	105,840	36,371	5,772,557	0.34	54.54
70	189,280	66,345	10,515,272	0.35	55.55

6.1.3 Concrete mix design

As per BS EN 206 [131], the mix design quantities (per m^3) for concrete with a 40-MPa compressive strength are 530 kg of sand, 1150 kg of gravel, 463 kg of ordinary Portland cement, and 186 kg of water, maintaining a water-to-cement ratio of 0.4. These quantities are assumed for the traditional concrete mix of RC1. For the RC2 concrete mixture, the freshwater and natural coarse aggregates are considered to be fully replaced by seawater and RCA, respectively. However, this reduces the performance of the resulting concrete in RC2 compared to that in RC1 [15,41]. Since the LCCA comparison should be carried out on the same basis regarding the strength performance, remedial measures are considered to eliminate such shortcomings in the RC2 concrete. Due to the high porosity and water absorption of RCA, the workability of RC2 fresh concrete is expected to be lower than that of the traditional mix [15]. Therefore, the addition of the appropriate amount of superplasticizer is considered for RC2 to achieve the desired workability. Whilst the comparatively low density of RCA may reduce the

compressive strength of RC2 concrete [195], experimental results show that a slightly increased cement concentration (5–10%) is sufficient to obtain a compressive strength equivalent to that of conventional concrete [14]. Likewise, using seawater in the concrete mix may also lead to a slight change in concrete characteristics [16,35], which can be resolved with the same strategies applied to address the issues in using RCA [41]. In effect, a strength performance comparable to that in conventional concrete was reported by Khatibmasjedi et al. [17] for the concrete mixed with seawater and RCA.

6.1.4 Life cycle cost model

The LCC model components (*Figure 6.1*) comprise the costs associated with the materials, construction, maintenance, and end-of-life. The LCC is calculated for each design alternative (Table 6.1) to identify the most economical option based on:

a) the financial perspective of the building's owner, and
b) the structural component of the building, rather than other aspects such as operational, electrical, mechanical, etc., which are independent of the construction material. This is valid under the reasonable assumption that the two design alternatives of structural concrete have the same thermal performance.

All costs are allocated for a functional unit of one square meter of floor area, considering an average concrete volume of 0.32 m^3 with 2% reinforcement ratio. Since ISO 15686–5 [196] requires that the study period must be long enough to include all repair or replacement actions of the design alternatives, a life cycle period of 100 years is assumed. This is longer than the commonly selected study period of 40–75 years for conventional reinforced concrete (RC1) buildings [197–199] due to the long-term durability provided by the corrosion-resistant reinforcement of RC2. At the end of the 100-year study period, it is assumed that the building will be demolished regardless of any prospective residual service life.

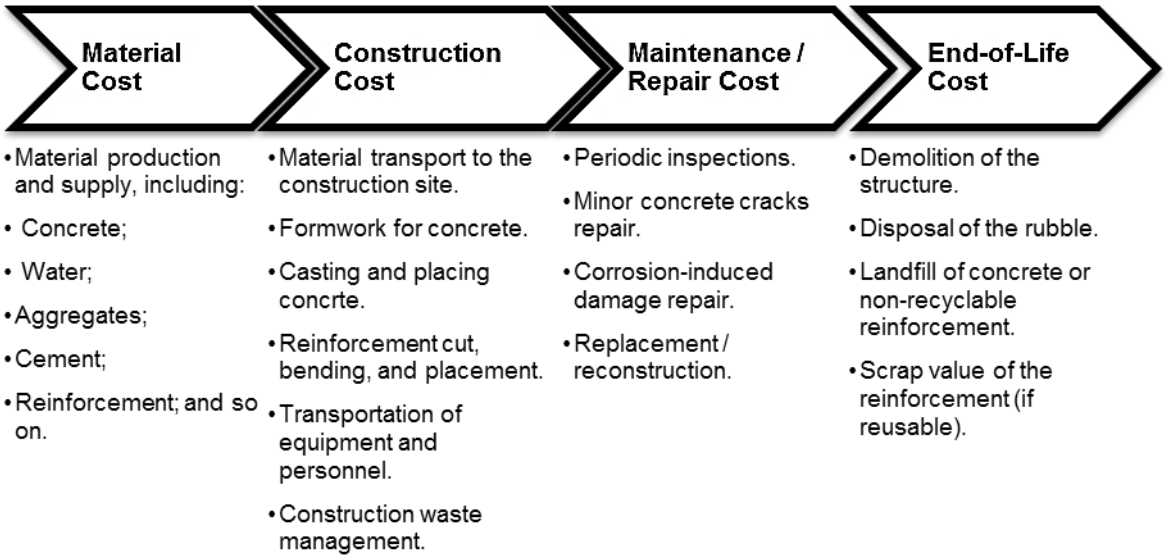

Figure 6.1. Components of the life cycle cost model of Study 4.

Material cost

Material costs are incurred from the production and supply of the basic materials, including concrete, reinforcement bars, water, aggregates, admixtures, etc. obtained primarily from the *RSMeans* online dataset [200] along with previous publications (as shown in Table 6.3). Data were inflation-adjusted to 2017 prices based on US annual general inflation rates [201].

Table 6.3

Unit Costs Considered in the LCCA of Study 4 (as of 2017 Prices).

Cost Item	Unit cost	Source	Notes
Ready mix concrete	177 $/m³	RSMeans [200]	28-day compressive strength of 40 MPa
Black steel bars	0.66 $/kg	RSMeans [200]	ASTM A615 Grade 60, western mill, mill base price, density of 7860 kg/m³
GFRP bars	9.4 $/kg	RSMeans [200]	Average density of 1950 kg/m³
Superplasticizer	4.2 $/m³ of ready mix concrete	RSMeans [200]	-
Natural coarse aggregate	14.73 $/ton	Davis and McGinnis [202]	Averaged for the US, inflation rates applied as per [201] to estimate the current price.
Recycled concrete aggregate	10.88 $/ton	Davis and McGinnis [202]	Averaged for the US, inflation rates applied as per [201] to estimate the current price.
Desalination / Freshwater	1.26 $/m³ of desalted water	Ghaffour et al. [4]	Assuming reverse osmosis desalination technique, inflation rates applied as per [201] to estimate the current price.
Demolition – concrete building	122 $/m³ of concrete	RSMeans [200]	Including 20-mile haul to dump, excluding dumping fees
Landfill rate	0.089 $/kg	RSMeans [200]	Dumping charge for construction materials; typical urban city
black steel bars – scrap value	0.11 $/kg	Capital Scrap Metal LLC [203]	-

The cost of the concrete mix for RC2 was estimated using the market price differences between the traditional and alternative materials with adding the cost of

admixtures required to achieve the same performance of the equivalent traditional concrete. Seawater and freshwater were assumed to have the same transport cost from their source to the concrete plant, and thus their price differs by the desalination cost for freshwater production. This assumption is considered valid if the use of seawater in concrete becomes as well-established as that of freshwater currently, such that the essential infrastructure (i.e., pipelines, tanks, etc.) are correspondingly provided for seawater. Against this, the transport cost of NA and RCA is not actually the same [14,202,204]. Paranhos et al. [204] suggested the cost of truck transport to be linearly proportional to the distance traveled, and thus can be used to estimate the differences between RCA and NA transport costs in relation to the comparative distance of the recycling plants and NA quarries. The same authors estimated a transport cost difference of approximately 10 US$/ton based on a 100-km comparative travel distance [204]. To account for this factor, a range of possible RCA-to-NA price ratios (50% to 200% [202]) were considered as part of sensitivity analysis. Despite having relatively very high cost per unit weight, the low density of GFRP reinforcement (~20% that of steel) makes a reasonable difference in the cost per unit floor area between RC1 and RC2.

Construction cost

Construction cost comprises labor and equipment required for material transport, concrete formwork, concrete casting, reinforcement placement, and construction waste management. Common practice is to define construction cost estimates as a percentage of the material cost [205,206]. The nominal construction cost, denoted C, for RC1 is estimated as 150% of the RC1 material cost, denoted M. For the GFRP-reinforced concrete (RC2), the construction cost is expected to be less due to the low weight and prefabricated profile of GFRP reinforcement [22,207]. In accordance

with [208], the use of GFRP reinforcement was assumed to reduce construction costs by 20% compared to that of classical black-steel reinforced concrete, i.e. 80% of C.

Maintenance cost

Maintenance cost refers to all expenses incurred during the service life of the building to maintain structural performance. This includes periodic inspections, minor and major repairs, rehabilitation, and replacement or reconstruction as needed. Only repair actions from corrosion are considered in this study, with inspection and minor concrete repairs assumed to be the same for all design alternatives and can be disregarded in the LCCA calculations [196,209,210].

The cost of repairing reinforced concrete structures can be considered as a percentage of the material and construction costs [205,206]. This includes the production, transportation, and installation of the new materials as well as the disposal of those replaced. In the current study, the cost of the repair was estimated assuming 10% of the total area to be affected at the time of repair [206], with 50% of the material requiring replacement [206], for which the manpower and equipment costs were assumed to be 200% of C [205].

Life-365 software [211] was used to predict the repair scheduling for RC1. This software is used to estimate the service life of concrete structures whose reinforcing steel is subject to corrosion due to chloride exposure. The service life is calculated as the sum of the corrosion initiation and propagation periods, after which the structure undergoes sufficient damage to demand repair [211]. The structure was considered to lie within 800 m of the ocean, a default exposure category defined in *Life-365* database [211] corresponding to a maximum surface chloride concentration of 0.6% reached within a 15-year period. The clear cover to reinforcement was taken as 40 mm, with no corrosion inhibitors or protection membranes in place.

The *Life-365* results indicated required structure repair every 10 years for RC1. It was assumed that the structure repair to be conducted with the same material quality and specifications as per the initial construction, i.e. with no change in the original durability performance. Since damage would then re-occur, with multiple repairs required during the service life of the structure, a total service life of 50 years was assumed for RC1 due to irreparable corrosion damage, demanding complete reconstruction.

Since the GFRP reinforcement is completely non-corrosive, RC2 may be assumed to be maintenance-free on the basis of the glass fibers being permanently protected from the direct contact with concrete by the resin of GFRP. Whilst the long-term durability of GFRP-reinforced concrete can only be postulated, it has been suggested [212] that GFRP bars in concrete retain ~70% of their ultimate tensile strength after 100 years of service life at a temperature of 50°C. This retained strength is still sufficient to fulfill the minimum design tensile strength required by ACI 440.1 [184] for GFRP bars in concrete**.**

End-of-life cost

The end-of-life cost includes the demolition of the structure and disposal of the rubble to landfill (Table 6.3). The value earned from the reusable/recyclable reinforcement scrap is also considered. Steel is considered completely recyclable metal, with the scrap recovered and converted to the same or even higher grade following processing [213–215]. At the end of the service life of RC1 structure, 90% of the original steel weight was assumed to be resold, the remaining 10% of the material being landfilled. Against this, the complex, heterogeneous, and anisotropic characteristics of GFRP make it difficult to be reused or recycled [216], with research still underway to address this challenge [217–219]. The RC2 reinforcement was thus considered to be

disposed of to landfill at the end of the study period.

Determination of life cycle cost (LCC)

LCC is the sum of all costs incurred over the study period, discounted to present value, according to [196]:

$$LCC = \sum_{t=0}^{T} \frac{C_t}{(1+r)^t} \tag{6.1}$$

where t is the time (in years) at which the cost is incurred, T the study period, C_t the cost incurred at year t, and r the discount rate, with emphasizing that the term 'discount rate' throughout Chapter 6 refers to the 'real' discount rate. At a certain life stage (t), the total cost incurred (C_t) can be expressed as the sum of LCC model components (*Figure 6.1*):

$$C_t = C_M(t) + C_C(t) + C_R(t) + C_E(t) \tag{6.2}$$

where C_M is the material cost, C_c the construction cost, C_R the repair and/or reconstruction cost, and C_E the end-of-life cost; each component is included only where applicable at the life stage (t).

The discount rate reflects the time value of money; it is used to evaluate the future costs in terms of present value, accounting for the nominal rates of interest and inflation [220]. The inflation rate represents the average annual increase in the consumer price index (i.e. the decrease in the purchasing power of money), while the 'nominal' interest rate refers to the interest rate before considering inflation [220]. The discount rate varies across time, place, and investment period [221]. In this study, r was considered as 0.7% as suggested by White House Office of Management and Budget [222] in the US for long-term investments (as of Year 2017) by the federal government (30-year or longer). Since private sector investments typically consider higher values of r [223], and given that the LCC is highly sensitive to this parameter [210,220], a

range of its common values (0%–10%) were considered as part of the sensitivity analysis. This range is consistent with previous LCCA studies on buildings [209,224].

6.2 Results and Discussion

6.2.1 Influence of concrete mixture cost

The change in concrete mix from the traditional (RC1) to the proposed (RC2) materials appears to have negligible impact on the ultimate unit cost of concrete. The cost difference between the design alternatives is influenced primarily by the reinforcement selected. Though less expensive, the use of alternative materials (i.e. seawater and RCA vs. freshwater and natural virgin aggregates) leads to some reduction in concrete performance compared to that of the traditional mix. Remedial measures to address this shortfall eliminate or even exceed the direct savings, resulting in comparable unit prices for both concrete mixtures. However, these findings are solely from a cost perspective on the part of the building's owner: a life cycle assessment and/or a consideration of the general public perspective reflect additional environmental benefits of the alternative approach [5,14,105,106].

6.2.2 LCCA results

Figure 6.2 shows the cash flow diagrams throughout the study period for the design alternatives. The costs incurred at each life stage (C_t) are expressed in US$ per square meter of the building floor area, and are calculated based on Eq. (6.2).

The incurred LCCA costs for the base conditions of $r = 0.7\%$ indicate the LCC of RC2 to be 50% lower than that of RC1 (Table 6.4). Despite the relatively low initial cost associated with the conventional design (RC1), the design alternative RC2 outperforms RC1 in the long term. The use of corrosion-resistant reinforcement in RC2 results in longer service lives as well as reduced repair costs over the entire life cycle. This also reflects on the insignificant contribution of the recovered reinforcement material value to the overall LCC. Similar observations have been reported in previous

research concerning the economic viability of using FRP reinforcement in structural concrete. Eamon et al. [24] reported that the LCC obtained for different design cases of a conventional steel-reinforced concrete bridge was 50–200% more than that of the FRP-reinforced material based on a discount rate of 3%.

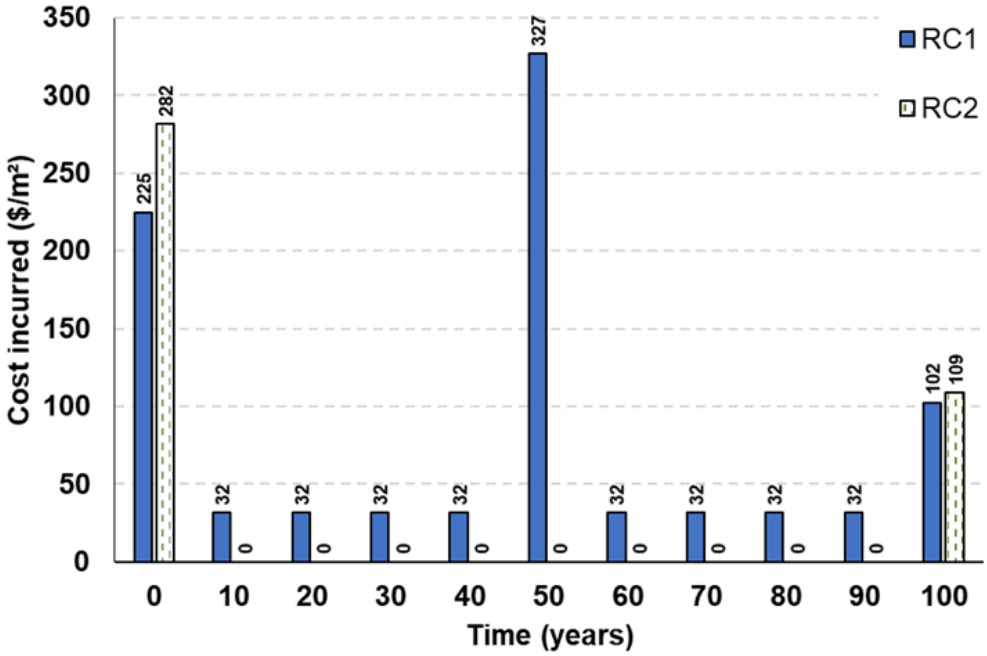

Figure 6.2. Cash flow diagrams for the design alternatives (future costs are not discounted).

Table 6.4

Summary of LCCA Results.

Design alternative	Present Costs ($/m²)					LCC ($/m²)
	Material	Construction	Repair	Reconstruction	End-of-life	
RC1	90	135	183.9	230.7	50.8	690.4
RC2	174	108	-	-	54.3	336.3

Figure 6.3 presents the cumulative LCC for each year until the end of the study period. The design alternative RC2 attains the same cumulative LCC as the conventional design alternative RC1 at t = 20–30 years; this representing the payback period for the initial investment in GFRP bars. Previous research contributions have generally corroborated these results. Eamon et al. [24] reported a 95% probability that using FRP to reinforce concrete bridges results in an overall cost reduction compared with traditional steel after a service life of 23–77 years.

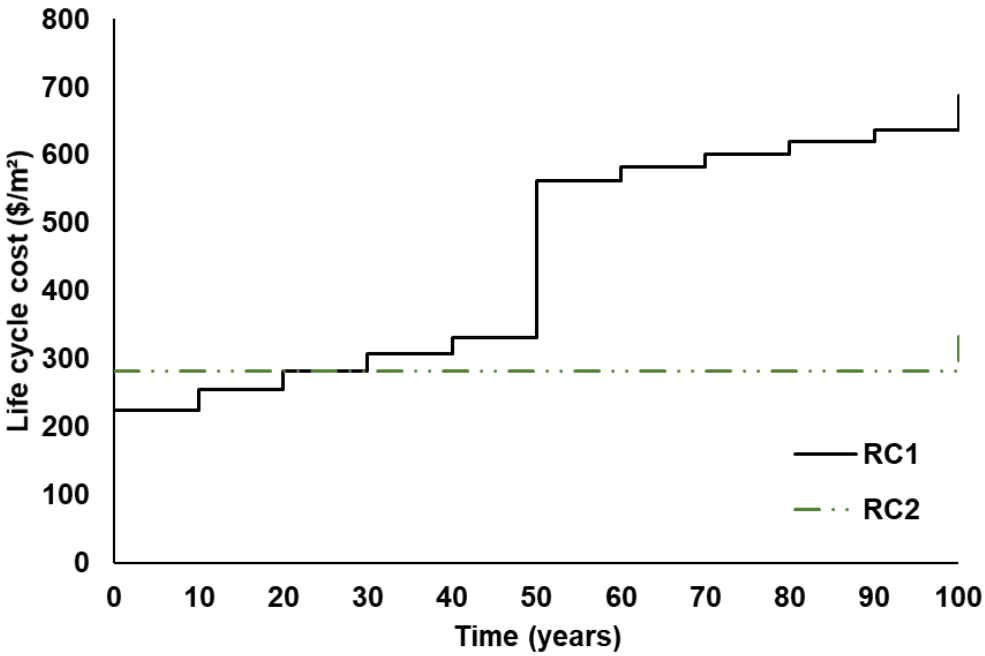

Figure 6.3. Life cycle cost results (considering the baseline scenario where r= 0.7%).

6.2.3 Sensitivity analysis

A sensitivity analysis was conducted for the discount rate (r), assumed to be 0.7% under base conditions, this being the most influential parameter. Since there is an exponential relationship between the time elapsed and the LCC as shown in Eq. (6.1), the discounting of future costs is highly influenced by r. For a discount rate of 5.9% or

more, the LCC of the design alternative RC2 becomes higher than that of RC1 (*Figure 6.4*) because the present values of the repair and reconstruction costs of the conventional design RC1 are decreased such that the initial investment in GFRP bars of RC2 is not recovered. Accordingly, the design alternative RC2 is no longer economically viable from an LCC perspective.

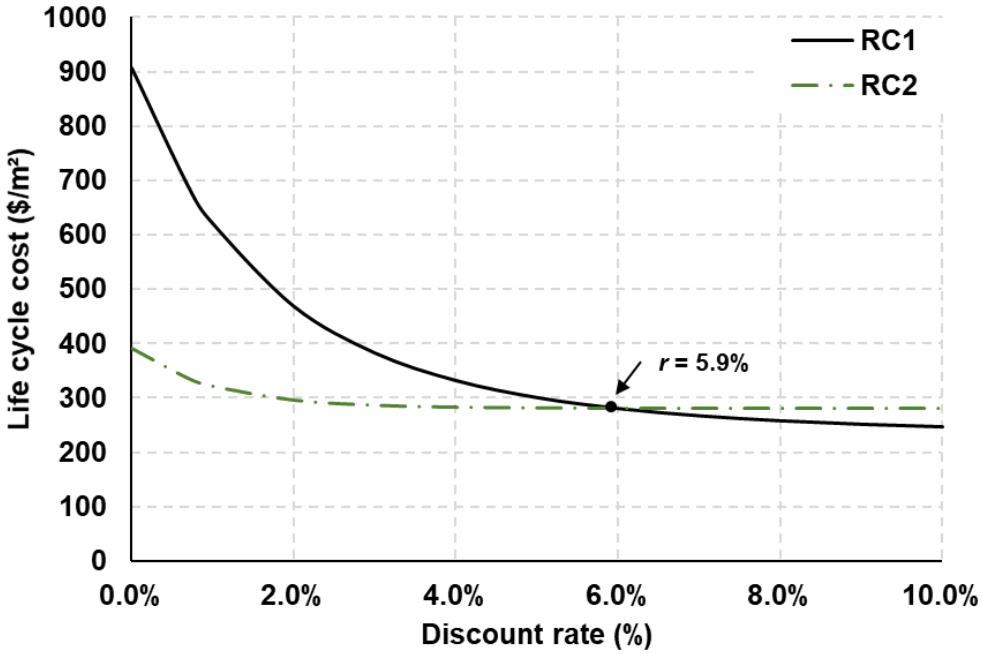

Figure 6.4. Sensitivity of LCC results to the discount rate.

Despite it being influential on the concrete unit cost (*Figure 6.5*), the effect of the aggregates transport cost, represented by varying RCA-to-NA price ratio, was found to have negligible impact on the ultimate LCCA results (*Figure 6.6*). This confirms the negligible effect of concrete direct cost on the LCCA outcomes when compared to that obtained from altering reinforcement material.

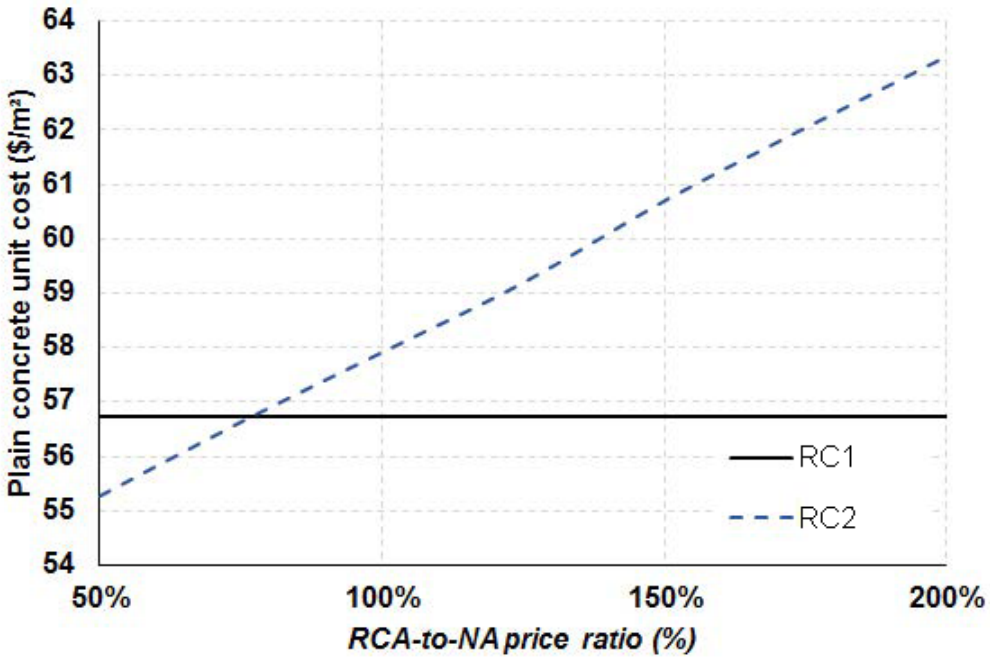

Figure 6.5. Variation of the concrete cost with different RCA-to-NA price ratios.

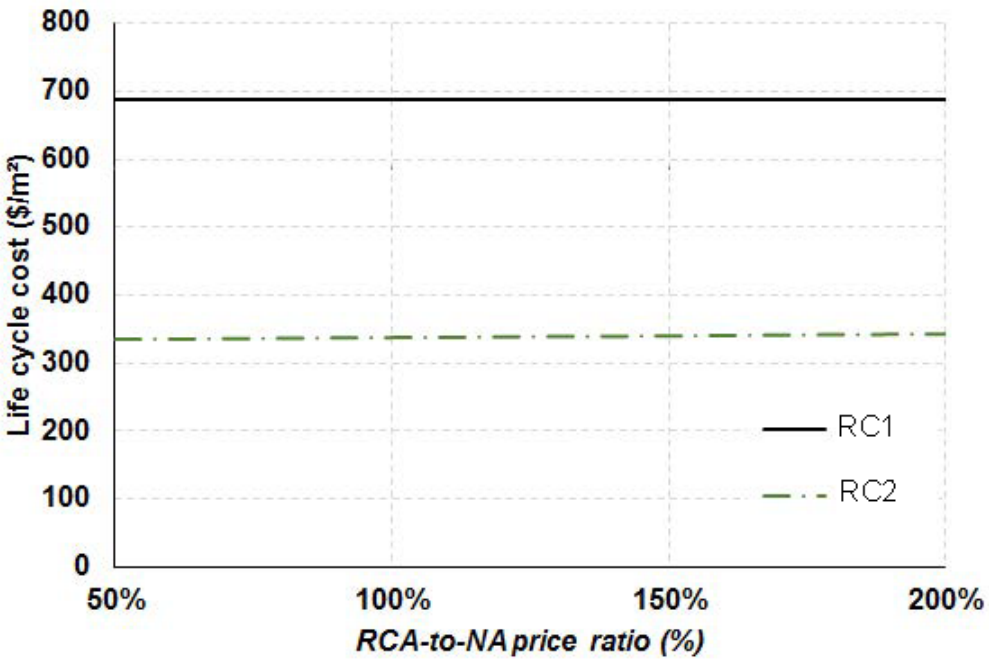

Figure 6.6. Variation of LCCA results with respect to different RCA-to-NA price ratios.

6.3 Summary and Conclusions

The economic impact of combining seawater, recycled concrete aggregate, and glass fiber reinforced polymer (GFRP) reinforcement in structural concrete has been investigated through life cycle cost analysis (LCCA) of two design alternatives for the same structure. The two approaches considered were: (a) RC1, traditional concrete mix with black-steel reinforcement, and (b) RC2, concrete with seawater, RCA, and GFRP reinforcement. Based on the assumptions, data, and approach implemented, the following can be concluded:

- The use of alternative materials for the concrete mix has no significant impact on the cost of concrete and thus the LCC performance. Cost savings are instead influenced by the selection of reinforcement material. This is further evidenced by the negligible change in the ultimate LCC results while including the effects of aggregate transport costs.
- The use of GFRP reinforcement improves the long-term economic performance of the structural concrete. Based on a 100-year study period and a 0.7% discount rate, the LCC of the proposed design alternative RC2 is approximately 50% less than that of the traditional reinforced concrete (RC1). The payback period (break-even point) for the initial investment in GFRP reinforcement ranges from 20–30 years according to the base conditions applied.
- The LCCA outputs are highly sensitive to the choice of the discount rate (r). At a discount rate of 5.9% or higher, the LCC of RC1 over the 100-year study period considered is lower than RC2.

The findings are limited to the assumptions made regarding the equivalence of the water transport costs, the nature of the high-rise buildings, 100% replacement of NA by RCA, and other factors. More LCCA studies are required to validate the cost effectiveness of

the proposed combination (i.e. concrete with seawater, RCA, GFRP reinforcement), accounting for different cases and assumptions. However, based on the reasonable assumptions made, a long-term cost benefit is evident from the use of corrosion-resistant reinforcement.

CHAPTER 7: COST EFFECTIVENESS OF REINFORCEMENT ALTERNATIVES FOR A CONCRETE WATER CHLORINATION TANK

In Chapter 6, we investigated the cost benefits associated with combining seawater, recycled coarse aggregates, and GFRP reinforcement in structural concrete for high-rise buildings. It was concluded that the long-term cost of structural concrete ultimately depends on the selection of the reinforcement material rather than the concrete mixture design. Chapter 7 extends the previous work with a greater focus on the cost benefits of using non-corrosive reinforcement, considering a different type of structure (RC water chlorination tank).

7.1 Introduction

The World Commission on Environment and Development has defined "Sustainable Development" as [225]: "a process of change in which the exploitation of resources, the direction of investments, the orientation of technological development, and institutional change are all in harmony and enhance both current and future potential to meet human needs and aspirations". Currently, there is a growing industrial and academic interest to produce sustainable reinforced concrete (RC) structures, mostly by using alternative "greener" materials in building new structures [18,41,106,207,226] or strengthening existing structures [227,228]. Concrete structures are traditionally steel-reinforced; as such, corrosion is a significant factor causing deterioration of RC structures and leading to reductions in service life, thereby hindering sustainable development. Classically, design codes, standards, and guidelines provide stringent limits on chlorides in concrete mixtures to mitigate corrosion (Table 7.1). However, for structures exposed to chlorides, such as those in the proximity to the sea [229] or those exposed to deicing salts [230], these limits can often be reached over long-term exposure period, especially if the concrete is cracked, either because of poor

construction practices, shrinkage, or other durability issues. Recently, the global cost of corrosion damage has been estimated at $2.5 trillion; out of which around 35% is directly attributed to damages in infrastructure and services [231].

Table 7.1

Maximum Limits of Water-Soluble Chloride Content in Concrete Mixture According to Different Standards.

RC Type	Maximum chloride content				
	Kg/m^3 of concrete	% of the cement mass			
	IS 456 [232]	BS 8110 [233]	ACI 201 [234]	ACI 318 [181]	ACI 222 [235]
Pre-stressed concrete	0.4	0.1	0.06	0.06	0.06
Reinforced concrete exposed to moisture/chloride sources	0.6	0.2	0.1	0.15	0.08
Reinforced concrete which is in dry service or protected from moisture	-	0.4	0.2	1	0.15

Several strengthening techniques have been proposed to mitigate corrosion-induced damage and to extend the service life of RC structures. In these techniques, different strengthening materials such as fiber-reinforced polymers (FRPs) [236,237], ferrocement [238], and fabric-reinforced cementitious matrix [182,227,239] are typically used. However, strengthening/rehabilitation of an existing RC structure can be expensive, time and labor-intensive, and occasionally impractical. Therefore, it is often more feasible (or practical) to prevent reinforcement corrosion in concrete structures by using non-corrosive reinforcement such as stainless steel [240,241] or

FRP [93,242]. The latter shows more potential given its high strength-to-weight ratio [21] and excellent durability performance [19]. Among the different FRP reinforcement types, glass-FRP (GFRP) is the most popular, having relatively lower cost [23] and acceptable mechanical properties and durability performance [25,26,38]. Several research studies have conclusively demonstrated the effectiveness of FRPs in various applications such as bridges, parking garages, tunnels, and marine structures [88–91,243]. A recent survey conducted in North America [244] showed that the most accepted standard practices for the use of FRPs in civil infrastructure are (i) CFRP-strengthening for retrofitting bridge piers and (ii) GFRP-reinforced bridge decks. Nevertheless, the higher initial cost of non-corrosive reinforcing materials (with respect to conventional black steel) necessitates long-term economic investigations to quantify their cost effectiveness throughout the service life of RC structures.

7.2 Research Significance

Existing literature highlights the potential cost savings with the use of FRP [22,24,31,245–248] or stainless steel [205,206,248,249] reinforcement in structural concrete. However, the majority of these LCCA studies have been in the context of RC bridges. Whilst numerous studies have been conducted to explore the financial viability of using alternative construction materials and methods in the building sector [250–255], those concerning the cost implications of using corrosion-resistant reinforcement are relatively scarce (mainly because such reinforcement types are less often used in structures other than bridges). When considering non-bridge applications of corrosion-resistant reinforcement, Ahmed et al. [90] performed a comparative cost analysis between steel- and GFRP-reinforced designs for RC flat slabs of a parking garage in Québec, Canada and concluded that the initial higher cost of GFRP bars can be recompensed at the construction stage by replacing the asphalt flooring layer with a

polyurethane one. However, this analysis considered only direct/initial costs. More recently, Younis et al. [256] investigated the cost benefits associated with combining seawater, recycled coarse aggregates, and GFRP reinforcement in structural concrete for high-rise buildings and concluded that the long-term cost of structural concrete ultimately depended on the selection of the reinforcement material rather than on the concrete mixture design. The current study builds on the previous work [256] with a greater focus on the cost benefits of using non-corrosive reinforcement, considering a different type of structure (RC water chlorination tank) on which little life-cycle work with GFRP has been performed. The effect of several sensitivity parameters on the long-term cost performance is evaluated.

In general, concrete water tanks (especially those for water treatment purposes) are likely to experience severe corrosion because of the direct and prolonged exposure to aggressive chemical environments [257]. In principle, using chlorine to disinfect/treat water has a strong negative effect on the reinforcing steel [257]. Classically, corrosion issues in such structures are addressed by optimizing concrete mixture design (e.g., reducing water-to-cement ratio, using supplementary cementitious materials, corrosion inhibitors, etc.) and/or waterproofing techniques; unfortunately, these have had somewhat limited success [258]. The American Water Works Association has estimated the corrosion-related cost in the water sector (drinking and sewer) at approximately $36 billion per year [259]. Consequently, using non-corrosive reinforcement appears to be a viable solution to mitigate corrosion-induced damages for RC water tanks. In order to validate the preceding statement from an economic standpoint, the current study provides a detailed comparison among black steel, epoxy-coated steel, stainless steel, and GFRP as reinforcement materials for an existing concrete water chlorination tank in terms of their cost effectiveness, using life-cycle

cost analysis.

7.3 Materials and Design

This study considers an existing GFRP-RC water chlorination tank as part of a new water treatment plant located in Quebec, Canada [258]. The tank is 24 m in length, 23 m in width, 4.65 m in height, and has a 2500 m^3 volume capacity. It is composed of two identical cells, each of which is divided by a discontinuous internal RC wall to create two interconnected zones (*Figure 7.1*). The RC structure is underground, resting on the rock, and buried with compacted soil surrounding the walls. The cover slab of the tank is supported by vertical RC walls that, in turn, rest on an RC raft. The dimensions of the concrete elements (walls, slab, and raft) as well as reinforcement details are presented in *Figure 7.1*. Further details about the project and the structural system of the tank can be found elsewhere [258].

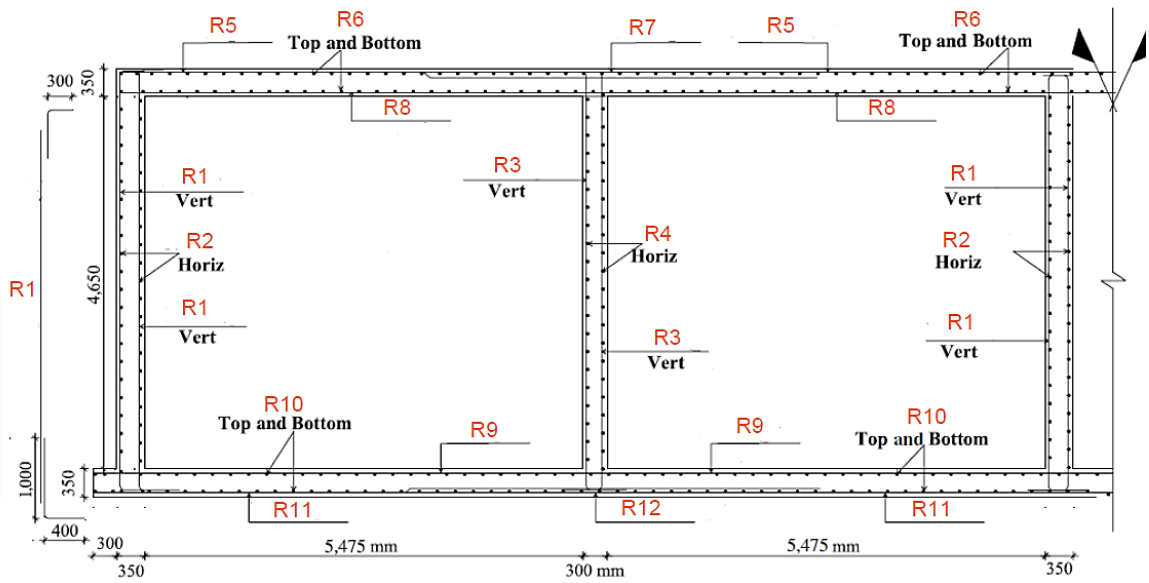

Figure 7.1. Reinforcement details for the main vertical cross-section of the water tank (adapted, with modifications, from [258]).

Four reinforcing materials proposed for RC structures were compared, namely, black steel (the reference material), epoxy-coated steel, stainless steel, and GFRP; the latter three are studied for their corrosion resistance compared to the reference material. For the GFRP reinforced concrete, the actual reinforcement details were obtained from [258] and are presented in Table 7.2. Assumptions concerning the material properties, loads applied, and the analysis routine used in the GFRP-RC structural design can be found in [258]. According to Mohamed and Benmokrane [258], using noncorrosive GFRP enables reducing the clear concrete cover to 50 mm, as opposed to the 60 mm required by ACI 350 [260] for the black steel reinforced water tanks.

Table 7.2

Reinforcement Design for the RC Water Tank.

Reinforcement form (Figure 7.1)	Actual GFRP reinforcement [258]
R1	$\emptyset 16@120\ mm$
R2	$\emptyset 16@250\ mm$
R3	$\emptyset 16@250\ mm$
R4	$\emptyset 16@300\ mm$
R5	$\emptyset 16@180\ mm$
R6	$\emptyset 16@250\ mm$
R7	$\emptyset 16@180\ mm + \emptyset 16@180\ mm\ (extra)$
R8	$\emptyset 16@140\ mm$
R9	$\emptyset 20@130\ mm$
R10	$\emptyset 16@250\ mm$
R11	$\emptyset 16@130\ mm$
R12	$\emptyset 20@130\ mm + \emptyset 16@130\ mm$

The GFRP reinforcement has distinct material characteristics: unlike the steels, the GFRP reinforcement exhibits a brittle failure associated with relatively high tensile strength and low elastic modulus [25]. Typically, the GFRP-RC flexural member has a balanced reinforcement ratio (ρ_b), which is approximately one-fifth that of the steel-RC counterpart [184]. This, in theory, leads to a relatively lower reinforcement ratio in the structural design of GFRP-RC structures. However, in practice, the design of FRP structures accounts for equal or slightly more reinforcement compared to black steel because of the lower stiffness of FRP (i.e., lower elastic modulus) which in turn affects the long-term performance of the structure (in terms of crack width and deflection) [31,96]. According to Mohamed and Benmokrane [258], the design ratio for the black steel reinforcement of the RC water tank, obtained in accordance with ACI 318 [181] and ACI 350 [260] and considering the same concrete properties and thicknesses, was very close to that needed for GFRP bars. This is attributed to the use of high-strength, low-spaced, and small-diameter GFRP bars with less concrete cover to control the crack width [258]. Therefore, the reinforcement ratio of GFRP- and steel-reinforced concrete was considered here to be the same (~1.7% in total). This assumption also guaranteed minimum reinforcement requirements for GFRP-reinforced concrete, and increased the likelihood of an over-reinforced section (i.e., $\rho > \rho_b$) that is theoretically preferred as it is associated with less acute compression-controlled failure [184].

The total amounts of concrete and reinforcement of the structural members (i.e., walls, slabs, raft, and so on) were obtained with respect to the volume capacity of the water tank. On average, the concrete volume and the black steel reinforcement weight per cubic meter of the water capacity are 0.23 m^3 and 30.5 kg, respectively. These were considered to be input quantities for the LCCA calculations of the black, epoxy coated, and stainless steel reinforced concretes (assuming comparable mechanical

characteristics among the different reinforcing steel types). Because of the significantly lower density of GFRP (~1870 kg/m^3) compared to black steel bars (~7860 kg/m^3), the GFRP reinforcement weight per cubic meter of the water capacity (~7.6 kg/m^3) was considerably lower than that of the steel reinforcement (~30.5 kg/m^3).

The baseline scenario considers the actual design compressive strength of concrete — i.e., 35 MPa [258]. This was complemented by considering another case with higher concrete strength (60 MPa) in order to investigate the effect of this parameter on steel corrosion and, thus, on the life-cycle cost of the structure. It is emphasized that the effect of concrete strength was insignificant on the design quantities of the reinforcing steel (because the failure is tension-controlled in steel-RC design) or GFRP (although the flexural failure in GFRP-reinforced concrete is compression-controlled, crack width and deflection are the governing design parameters). Nevertheless, increasing concrete strength intuitively offers some advantages in regard to crack-width control by means of increasing the concrete rupture stress [181].

7.4 Cost Modeling

The cost model was divided into four main components, namely, material, construction, repairs, and end-of-life costs. All costs were allocated for a functional unit of 1 m^3 of the volume capacity of the water tank. As suggested in the literature [196], the analysis period should be long enough to account for all repair/replacement actions during the service life of the structure. To satisfy this, a 100-year life-cycle period was assumed. Although it has been occasionally considered for life-cycle studies on buildings [261] or on bridges [24,247], this analysis period is longer than that typically assumed for life-cycle studies on water services, which is 25–50 years [262–264]. This longer analysis period is justified because of the high performance and durability

anticipated with non-corrosive reinforcement. Indeed, Mohamed and Benmokrane [258] suggested that using GFRP reinforcement in RC water tanks can extend their service life up to 100 years or more as compared to black steel counterparts. Nevertheless, a cumulative LCCA was performed (i.e., from initial construction up to 100 years following that) so the effects of the analysis period can be quantified. The LCCA was performed considering the structural components and neglecting other aspects (e.g., electrical supply, plumbing, operations, etc.).

7.4.1 Material cost

Material cost refers to the expenses required for the fabrication and procurement of the raw materials (i.e., concrete ingredients and uncut reinforcement bars). Table 7.3 lists the material unit costs adopted in the current study, obtained from RSMeans [200] and/or other publications as listed (as of 2019 prices). Stainless steel had the highest price (around 7–8 times that of the black steel). Despite the higher cost (per unit weight) of GFRP compared to stainless steel bars, the former ultimately has lower cost per unit water capacity of the tank because of its lower density (1870 kg/m^3 versus 7860 kg/m^3 for steel reinforcement).

Table 7.3

Unit Costs Considered in Study 5 (as of 2019 Prices).

Cost Item	Unit cost	Source
Ready mix concrete (28-day compressive strength = 35 MPa, density = 2400 kg/m^3)	180 \$/m^3	[200]
Ready mix concrete (28-day compressive strength = 60 MPa, density = 2400 kg/m^3)	210 \$/m^3	[200]
Black steel reinforcement (ASTM A615 Grade 60; yield tensile stress = 420 MPa; density = 7860 kg/m^3)	0.7 \$/kg (mill-based)	[200]
Epoxy coated steel reinforcement (physical/mechanical properties are similar to black steel)	1.2 \$/kg (mill-based, inflation-adjusted)	[249]
Stainless steel reinforcement (ASTM A955-316L; physical/mechanical properties are same as black steel)	5.5 \$/kg (mill-based, inflation-adjusted)	[249]
GFRP reinforcement (made with resin and E-CR Glass; tensile strength is assumed as 1000–1100 MPa, and elastic modulus as 60–65 GPa)	Ø16 bar (0.375 kg/m): 4.33 \$/m → 11.4 \$/kg Ø20 bar (0.590 kg/m): 6.84 \$/m → 11.6 \$/kg	[200]
Elastomeric sheet waterproofing, EPDM, plain, nylon-reinforced sheets, 60 mils thick	22.5 \$/m^2	[200]
Black steel scrap	0.15 \$/kg	[203]
Stainless steel scrap	0.75 \$/kg	[203]
Demolition of RC structure (per cubic meter of concrete; covering 20-mile haul to dump)	125 \$/m^3	[200]
Landfill (for construction materials; assuming urban city)	0.092 \$/kg	[200]

7.4.2 Construction cost

Construction cost refers to the expenses associated with the manpower and/or equipment needed to transport materials, cast concrete, place reinforcement, and dispose the construction waste. In accordance with [205,206], construction cost can be considered as a ratio of the material cost. In the current study, the reference construction cost (C) was considered as that corresponding to the black steel reinforced concrete. In the baseline scenario, C was assumed to be 1.5 times the reference material cost (M). The construction methods and technology are likely to be the same for black, epoxy coated, and stainless steel reinforced concretes; therefore, the construction cost of the RC tanks utilizing epoxy coated or stainless steel reinforcements was also taken as C. This was complemented by sensitivity analysis which was performed on a range of possible C/M ratios from 0 (i.e. negligible construction cost) to 2.5 (not typically exceeded in building construction [200,265]).

Construction costs are thought to be relatively lower for GFRP-reinforced concrete, since the GFRP bars have lower density and prefabricated profiles (although GFRP reinforcement needs to be tied more considering the risk of floating during concrete casting activities given the lower density [31,245]). Brown and Tce [208] suggested that using GFRP reinforcement results in around 20% reduction in the labor time and costs compared to black steel. Berg et al. [22] reported approximately 60% savings in the construction costs of concrete bridge decks with the use of GFRP in lieu of black steel reinforcement. Here, the construction cost of GFRP-reinforced concrete, C_{GFRP}, was assumed as $0.8C$ in the baseline scenario. A range of possible C_{GFRP}/C ratios from 0.6 to 1 were considered as part of sensitivity analysis.

7.4.3 Repair/maintenance cost

Repair/maintenance cost represents the expenses incurred to maintain the performance of the structure: this includes inspections, routine maintenance, major/minor repairs, and/or replacement. Two inspection strategies were considered, namely, general (periodic) inspection and detailed inspection. The general (periodic) inspection is conducted at 5-year intervals for detecting obvious defects that lead to safety problems or restrictions on the use of the structure. Detailed inspections are carried out before repair actions to analyze the deterioration of the structure and therefore, they are scheduled together with repair/rehabilitation activities. Routine maintenance is conducted on a regular basis (every 5 years) and includes cleansing, repainting and drainage clearing works, as well as repairing visual concrete cracks. In the current study, periodic inspection and routine maintenance activities were considered to be the same among the design alternatives.

Common practices assume the repair/maintenance cost as a ratio of the material and/or construction costs [205,206]. Based on the unit costs provided by Cheung et al. [249], the costs of general inspection, detailed inspection, and routine maintenance were taken as 0.5% $(M + C)$, 2.5% $(M + C)$, and 1.5% $(M + C)$, respectively. Only repair of corrosion-induced damages was considered, as the focus of the study is on the differences among the reinforcement materials with respect to corrosion resistance. Following a detailed inspection, the repair cost involves procuring and installing new materials, in addition to the disposal of the materials replaced. The repair cost was estimated based on the following:

(a) 10% of the total exposed area to be damaged at the repair time [206];

(b) 50% of the materials in the damaged area to be replaced [206]; for which the replacement cost was taken as $2C$ [205].

Life-365 [211] was used to predict the repair schedules for the black, epoxy coated, and stainless steel reinforced concretes. This tool predicts the service life of RC structures considering the corrosion induced as a result of chloride exposures. In theory, the predicted service life is the summation of the corrosion initiation and corrosion propagation periods, after which the structure encounters sufficient damage and requires repair [211]. The built-in yearly temperature profile of *Life-365* for Sherbrooke, Quebec was used to simulate the ambient exposure. A default 'severe' exposure category in *Life-365* was considered, in which a 0.8% chloride concentration (Cl_s, as % of the cement weight) is reached at the concrete surface after a 1-year period [211]. The concrete compressive strength and clear cover to reinforcement were taken as 35 MPa (baseline scenario) and 60 mm, respectively. In the baseline scenario, the w/c ratio was correspondingly calculated to be 0.47 (as per BS EN 206 [131] for 35-MPa concrete), and neither supplementary cementitious materials (i.e., fly ash, silica fume, slag, etc.) nor corrosion inhibitors were considered in the concrete mixture. Protection membranes (with 20-year time to failure) were considered on both sides of the water tank. The use of stainless steel and GFRP reinforcement, however, substitutes the need for waterproofing membrane (on the external side only) to mitigate corrosion. A default chloride-threshold (Cl_t) value (0.05% wt. of concrete) in *Life-365* was considered, associated with a diffusion decay index (m) of 0.2 and a reference diffusion coefficient (D_{ref}, at time $t_{ref} = 28\ days$) of $1.17 \times 10^{-11}\ m^2/sec$.

Life-365 results showed that the RC tank requires repair after approximately 16–17 years in the case of black steel reinforcement and 30 years when using epoxy-coated steel. This extension in the service life of the epoxy-coated steel (compared to black steel) is due to the additional corrosion-inhibitor effect provided by the protective coating on the bar's surface. Stainless steel, on the other hand, requires no repair (due

to corrosion damages) up until 130 years following construction. This is in line with findings from García-Alonso et al. [241] who reported that the corrosion resistance of stainless steel bars embedded in concrete is approximately 10 times that of the black steel counterparts. In case of higher concrete strength (with $f_c = 60\ MPa, w/c = 0.33$, and $D_{28} = 5.4 \times 10^{-12}\ m^2/sec$), the required repair periods become 25 and 40 years for black and epoxy coated steel reinforcements, respectively. The effect of concrete strength on the embedded steel rebar corrosion was experimentally demonstrated by Abosrra et al. [266] - the rate of corrosion was reduced by approximately 40% with an increase in the concrete strength from 20 to 46 MPa.

The structural damage repair was assumed to restore the original structural and durability performance (i.e., no improvements compared to as-built specifications). Accordingly, damage is likely to re-occur and multiple repairs might be needed during the service life of the structure. In the case of black steel, the total cumulative damage from corrosion was assumed to be too severe in 50 years after multiple rounds of repair; therefore, a complete reconstruction would be required. The event of reconstruction, however, occurs at Year 75 in the case of high-strength concrete (60 MPa) (presuming the same rounds of repair prior to reconstruction). For the epoxy-coated steel, it can be fairly assumed that the protective coating on the bar does not remain intact after the first round of repair and, accordingly, the repair schedule becomes the same as that of the black steel. Consequently, epoxy-coated steel RC tank requires reconstruction, at Year 65 and Year 90 in the case of normal (35 MPa) and high-strength (60 MPa) concretes, respectively.

Given that GFRP and stainless steel reinforcements are non-corrosive (at least during the 100-year analysis period), the corresponding RC tank was considered to be repair-free (again, considering solely corrosion-induced damages, as the focus in this

comparison among reinforcements is on the differences with respect to corrosion resistance). For the GFRP reinforcement, it was presumed that the glass fibers inside the bar are perfectly protected by the resin from any direct contact with concrete. This assumption is supported by existing literature, which generally postulates an acceptable long-term durability performance of GFRP-reinforced concrete. For instance, Robert and Benmokrane [212] suggested that the GFRP reinforcement in concrete can maintain up to 70% of its ultimate tensile strength after a 100-year exposure period at 50 °C temperature (based on specimens subject to exposure up to a one-year period and using Arrhenius approach for long-term prediction): this retained tensile strength meets the minimum requirements as per ACI 440.1 [184] for the design strength of GFRP reinforcement in concrete. In addition, Masmoudi et al. [267] reported no significant reduction in the bond strength between GFRP bars and concrete after 8-month exposure at high temperatures (up to 60 °C). Also, Gooranorimi and Nanni [268] investigated the performance of GFRP bars exposed to concrete alkalinity and ambient conditions after 15 years of service. Results from scanning electron microscopy and energy dispersive X-ray did not show any sign of GFRP microstructural deterioration or change of chemical composition, and the glass transition temperature and the fiber content of the GFRP bars were comparable to pristine values.

7.4.4 End-of-life cost

The end-of-life cost refers to the cost of demolition, disposal, and landfill activities, as opposed to the (earned) residual value of the reinforcement scrap (Table 7.3). Steel is a perfectly recyclable metal whose scrap can be reconverted to comparable or even higher grades with suitable processing [214,215]. In this study, 90% of the original steel was considered for resale at the end life of the steel-RC structure. On the other hand, GFRP has complex and heterogeneous characteristics that make it

challenging to be reused/recycled [216]; research is in progress to address this issue [217,219].

As previously indicated, stainless steel and GFRP reinforced concretes are expected to have service lives longer than the 100-year analysis period. However, due to the lack of reported evidence on the actual service life of stainless steel/GFRP reinforced concretes, Year 100 (i.e., the end of the analysis period) was considered here as the end of their service life to achieve a valid cradle-to-grave comparison among the design alternatives. Also, the earned value from the prospective remaining service life at Year 100 was disregarded from the comparative analysis.

7.4.5 Net present cost

The net present cost (NPC) is the sum of all partial costs incurred over the entire life cycle, considering the time value of money, calculated as follows [196]:

$$NPC = \sum_{n=0}^{N} \frac{C_n}{(1+r)^n} \tag{7.1}$$

where C_n is the total cost at Year n; N is the analysis period (100 years); and r the real discount rate (referred to as "discount rate" in the rest of the chapter). At a certain year (n), the cost incurred (C_n) was calculated as the summation of the cost elements as follows:

$$C_n = C_M(n) + C_C(n) + C_R(n) + C_i(n) + C_E(n) \tag{7.2}$$

where C_M is the material cost, C_c the construction cost, C_R the repair, maintenance and/or replacement cost, C_i the inspection cost, and C_E the end-of-life cost, wherever applicable.

The discount rate is a key parameter in the calculation of the NPC since it reflects the opportunity value of time: the higher the discount rate, the more effect it has on the NPC by decreasing the present cost of future activities such as repair or

reconstruction. The discount rate is used to evaluate the present dollar value of future costs taking into account the nominal interest rate and the inflation rate [220]. In this study, a discount rate of 0.6% was assumed as recommended by the Office of Management and Budget [222] (as of 2019) for long-term federal investments (≥30 years). Sensitivity analysis was performed on a range of common *r* values (0–10%) that conform with previous cost studies on buildings and infrastructure [209,224].

7.5 Results and Discussion

7.5.1 LCCA results

Figure 7.2 presents a summary of the NPC results for the baseline scenario ($r = 0.6\%$, $C = 1.5M$, and $C_{GFRP} = 0.8C$). The NPC of epoxy-coated steel reinforced concrete was approximately 11% lower than that with black steel reinforcement; this indicates a higher cost performance of the former in the long term. Likewise, stainless steel reinforcement had approximately a 25% lower NPC compared to the conventional design. The GFRP-reinforced concrete showed the highest cost effectiveness as the NPC was approximately 43% lower than that of the black steel counterpart. Despite the lower preliminary costs associated with the black steel, corrosion-resistant reinforcements revealed long-term cost savings as they resulted in longer service lives and lower repair costs throughout the analysis period; allowing them to make up for the upfront investment. For instance, the use of epoxy-coated steel (in lieu of black steel) extended the service life of the water tank by 14 years, reduced the overall repair/maintenance cost by 20%, and reduced the end-of-life cost by 48% (*Figure 7.2*). Also, non-corrosive reinforcements (i.e., stainless steel and GFRP) outperformed epoxy coated or black steel mainly because of the significant savings obtained from averting corrosion-induced repairs or replacement. The better performance of GFRP over stainless steel reinforcement is attributed to the lower initial cost of the former (by 40%)

compared to the latter.

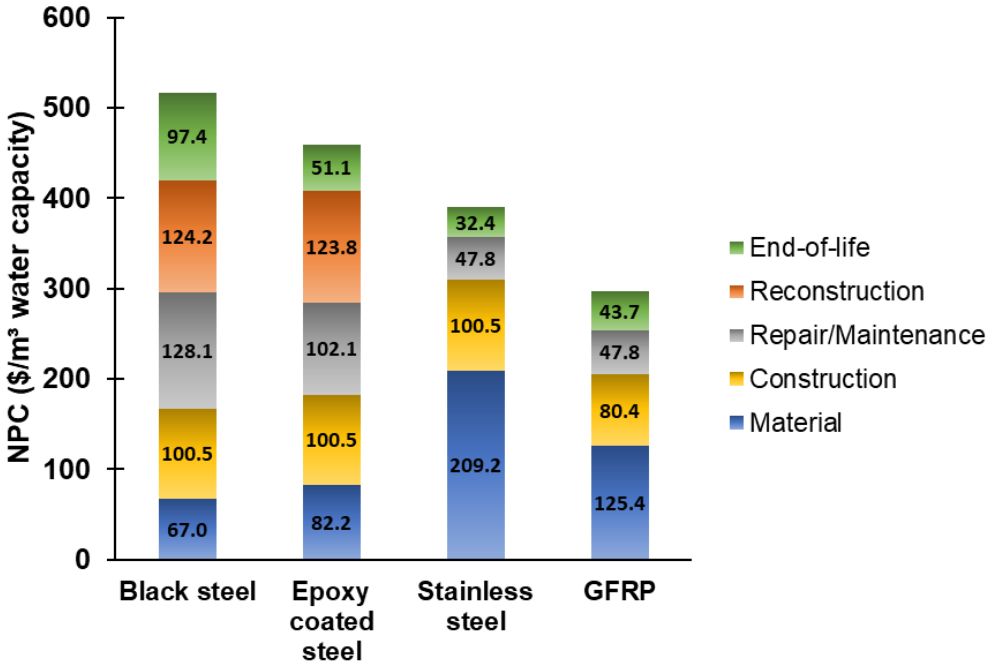

Figure 7.2. Summary of LCCA results (100-year study period).

The end-of-life cost associated with black steel was the highest among the design alternatives as a result of the two demolition activities during the 100-year analysis period. On the other hand, stainless steel showed the lowest end-of-life cost (approximately one-third that of the black steel) because of only one demolition activity occurring during the life-cycle (at Year 100) and the high resale prices of stainless steel (Table 7.3). Considering resale prices of black and stainless steel reinforcements resulted in approximately 5% and 25% reductions in the end-of-life cost of the RC tank, respectively. However, reinforcement resale prices, while considered, are quite small when compared to other items in the cost model.

Previous studies have also demonstrated the economic viability of corrosion-resistant reinforcement [24,205,206] for other structures. For instance, Cheung et al.

[249] reported approximately 10% saving in the life-cycle cost accompanied by a 20-year extension in the service life of bridge decks when using epoxy-coated steel in lieu of conventional steel (assuming 4% discount rate, 50 MPa concrete, and 70-mm concrete cover). Mistry et al. [206] reported that the use of stainless steel in reinforced concrete piers resulted in 44% lower NPC compared to the black steel reinforced counterpart (with $r = 0.01\%$). Thompson et al. [269] reported approximately 50% savings in the cost of corrosion (and 20% in the overall NPC) associated with the use of epoxy-coated steel in RC bridges. Grace et al. [247] and Eamon et al. [24] estimated the NPC of FRP-reinforced concrete bridges to be 30–50% lower than that of their steel-reinforced counterparts (assuming $r = 3\%$). Cadenazzi et al. [31] estimated the NPC of a conventional steel-RC bridge in Florida to be 25% higher than that reinforced with GFRP (assuming a 1% discount rate and a 100-year analysis period).

Figure 7.3 depicts the cumulative NPC values through the analysis period. As shown in the figure, reconstruction was the key activity resulting in cost differences between conventional and stainless steel reinforced concretes. The crossover point between these two alternatives was at Year 50, after which the initial investment in stainless steel was realized. Likewise, stainless steel outperformed epoxy coated steel reinforced concrete at the reconstruction Year 65. However, GFRP-reinforced concrete outperformed the conventional design at Year 35 (particularly due to the second round of corrosion repair). These results generally agree with previous research [24,205,206,247]. Mistry et al. [206] estimated the payback period of stainless steel reinforcement as the reconstruction year of the black steel RC structure. Eamon et al. [24] reported that the initial high cost associated with using FRP in lieu of black steel in RC bridges can be recouped in 23–77 years (depending on the structural design conditions). Grace et al. [247] suggested that FRP-RC bridges become more cost-

effective than their black steel RC counterparts after 20 years following construction (with a probability higher than 90%); this period (20 years) was the time of the first major repair event in their assumed maintenance schedule.

The LCCA outcomes are sensitive to the assumption of the analysis period. For instance, as shown in *Figure 7.3*, considering a 65-year or shorter analysis period makes epoxy coated steel more cost-effective than stainless steel as a reinforcement material. Similarly, if a service life of 50 years (or lower) is considered, the cost benefits of using corrosion-resistant reinforcement generally become less obvious, and the black steel alternative becomes more viable (*Figure 7.3*).

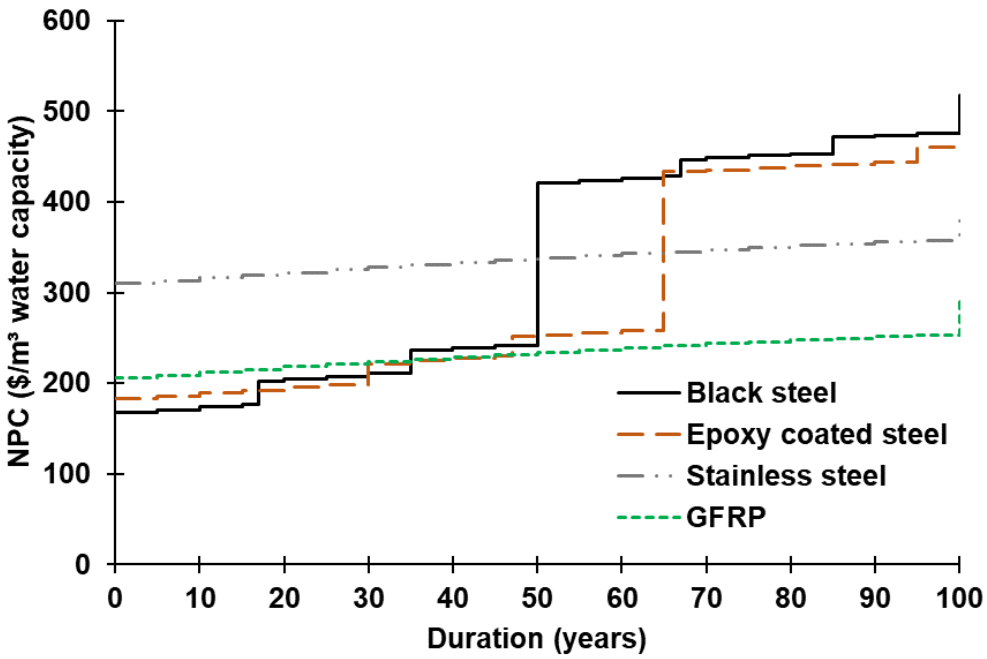

Figure 7.3. Cumulative NPC results for the reinforcement design alternatives.

7.5.2 Sensitivity analysis

Sensitivity analysis was performed on the discount rate and the construction costs, as they are the most influential parameters affecting the NPC. The significance of r is clearly noticed on major long-term future costs such as reconstruction. *Figure 7.4* demonstrates the sensitivity of the NPC to the selection of r (considering $C = 1.5M$, and $C_{GFRP} = 0.8C$). With $r \geq 1.95\%$, the NPC of stainless steel reinforced concrete becomes higher than that of the black steel reinforced counterpart. This means that the repair and/or reconstruction costs of black steel reinforced concrete were decreased so that the initial investment in stainless steel was not recompensed. Likewise, the crossover point between stainless steel and epoxy coated steel was at a 1.40% discount rate. However, the crossover point between GFRP and black or epoxy coated steel reinforcements occurred at much higher r values (5.15% and 4.50%, respectively, as shown in *Figure 7.4*).

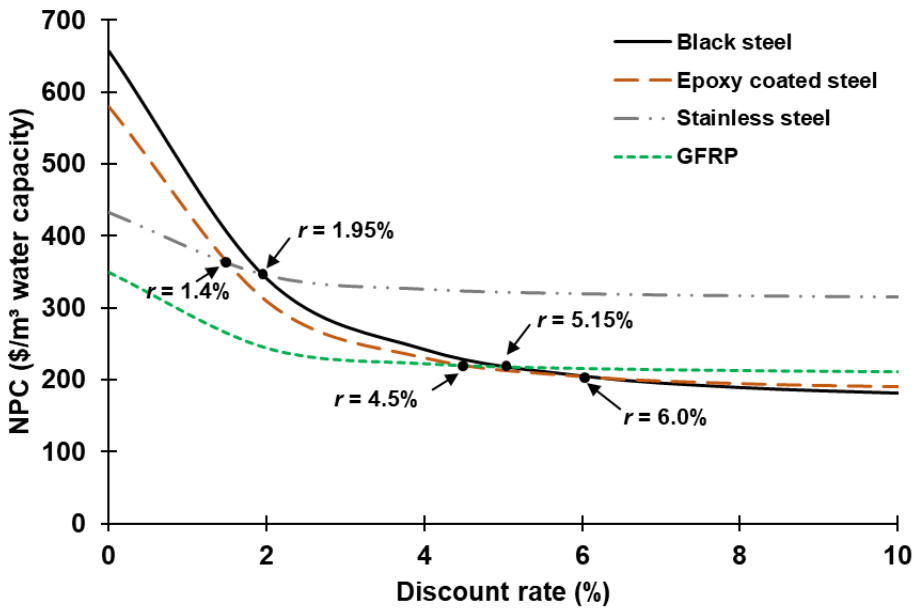

Figure 7.4. Sensitivity of NPC to the assumed discount rate (C is fixed at 1.5M and $C_{GFRP} = 0.8C$).

The significance of the parameter C is attributed to its high contribution to the initial, repair, and replacement costs. *Figure 7.5* shows the sensitivity of the NPC to the assumption of C/M ratio (considering $r = 0.6\%$ and $C_{GFRP} = 0.8C$). As shown in the figure, GFRP reinforcement outperformed the black/epoxy coated/stainless steels at all C/M values, with the cost gap widening with an increase in the C/M ratio. Stainless steel, however, showed higher cost effectiveness than epoxy coated steel only when considering $C \geq 0.55M$ (*Figure 7.5*). Similarly, the crossover point between black and stainless steel reinforced concretes was at $C/M = 0.15$.

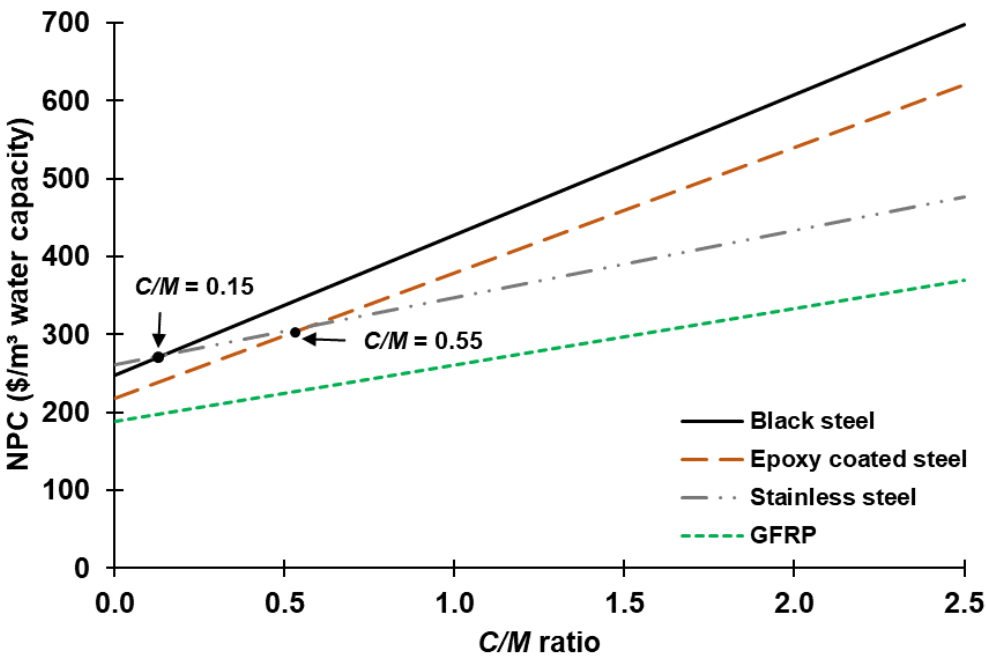

Figure 7.5. Sensitivity of NPC to the assumed construction cost (r is fixed at 0.6% and $C_{GFRP} = 0.8C$).

Another sensitivity analysis was performed by altering both the discount rate and the construction cost (C). *Figure 7.6*-a, *Figure 7.6*-b, and *Figure 7.6*-c present the NPC plot (as a function of discount rate and C/M ratio) for the conventional RC tank as opposed to that of the epoxy coated steel, stainless steel, and GFRP reinforced counterparts, respectively. As shown in *Figure 7.6*-a, epoxy-coated steel predominantly outperforms black steel except in the region of high discount rates ($4\% \leq r_{crossover} \leq 8\%$ depending on C/M ratio). However, the area where stainless steel becomes more cost-effective than black steel is limited to low discount rates and high C/M ratios (*Figure 7.6*-b). On the other hand, GFRP outperforms black steel at a wider range of assumptions for r and C/M (*Figure 7.6*-c). This demonstrates the superior economic performance of GFRP compared to stainless steel as an alternative non-corrosive reinforcement. Moreover, it was observed that as C increases, the discount rates at the crossover points also increase. For instance, when assuming $C = 2M$, the crossover points occurred at $r = 7\%$ for epoxy coated steel, $r = 2.3\%$ for stainless steel, and $r = 6.2\%$ for GFRP reinforcement, as opposed to those obtained for C/M ratio of 1.0 (5.8%, 1.5%, and 4.1% for epoxy coated steel, stainless steel, and GFRP, respectively).

Increasing C_{GFRP}/C ratio intuitively leads to an increase in the NPC of GFRP-reinforced concrete (*Figure 7.7*-a), that is associated with a delay in the breakeven year between GFRP and black/epoxy coated steel (*Figure 7.7*-b). For instance, while fixing r at 0.6% and C at $1.5M$, increasing C_{GFRP}/C ratio from 0.6 to 1.0 yields a change in the crossover point from Year 17 to Year 50 between GFRP and black steel (i.e., a delay in the payback period of the high initial cost of GFRP), and also from Year 30 to Year 65 for that between GFRP and epoxy coated steel (*Figure 7.7*-b).

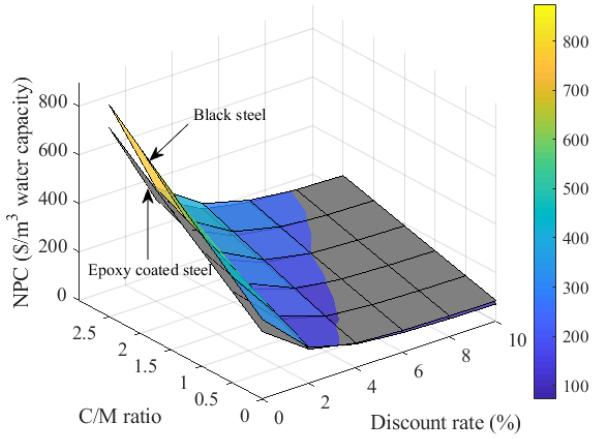

(a)

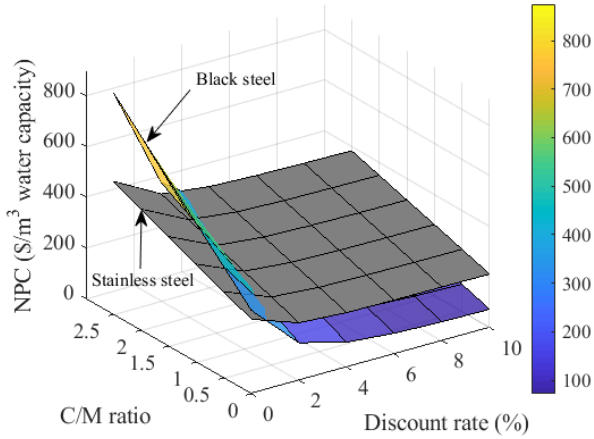

(b)

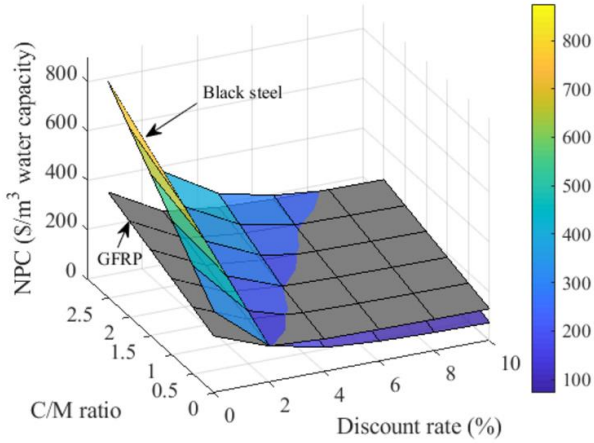

(c)

Figure 7.6. NPC plots of (a) black vs. epoxy coated steel (b) black vs. stainless steel and (c) black steel vs. GFRP reinforced concrete as a function of discount rate and C/M ratio.

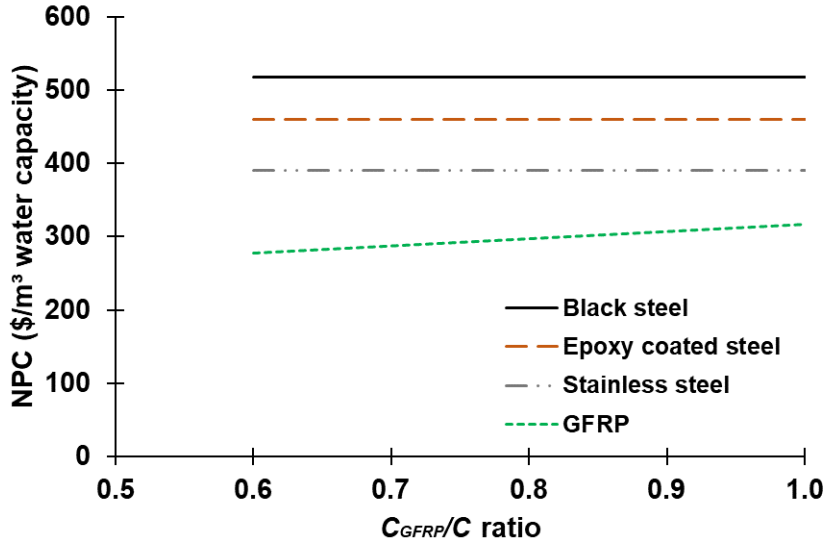

(a)

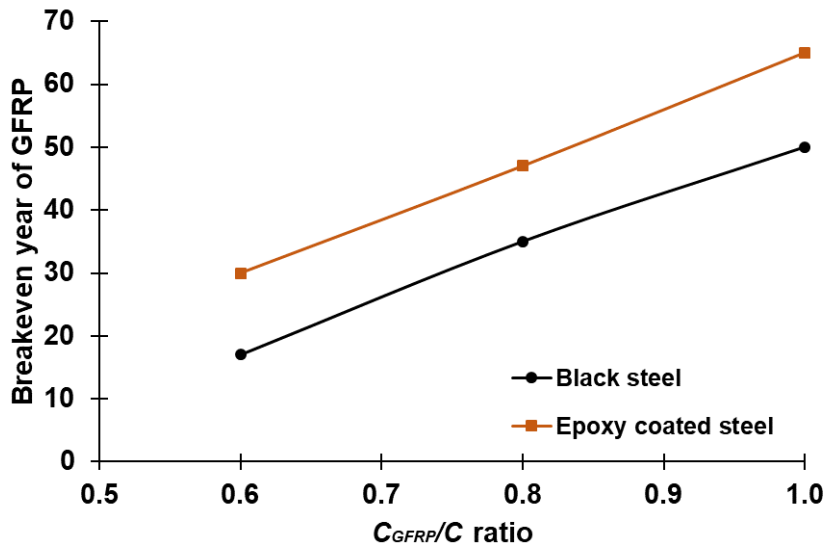

(b)

Figure 7.7. Sensitivity of (a) NPC and (b) breakeven year of GFRP reinforced concrete to the assumption of C_{GFRP} (r is fixed at 0.6% and C=1.5M).

As shown in *Figure 7.8*, increasing concrete strength (from 35 MPa to 60 MPa) led to a slightly higher initial/direct cost (~4%) in black or epoxy-coated steel reinforced concrete. However, this increase was reimbursed with an improvement in the overall life-cycle performance of the structure, by means of postponing corrosion-induced damages and thus extending the service life of the RC tank (by 25 years in both black steel and epoxy-coated steel reinforced concretes). In case of corrosion-free reinforcement (GFRP or stainless steel), it is suggested that the additional cost of high-concrete strength may be recompensed by the superior durability performance gained from the use of high-strength concrete.

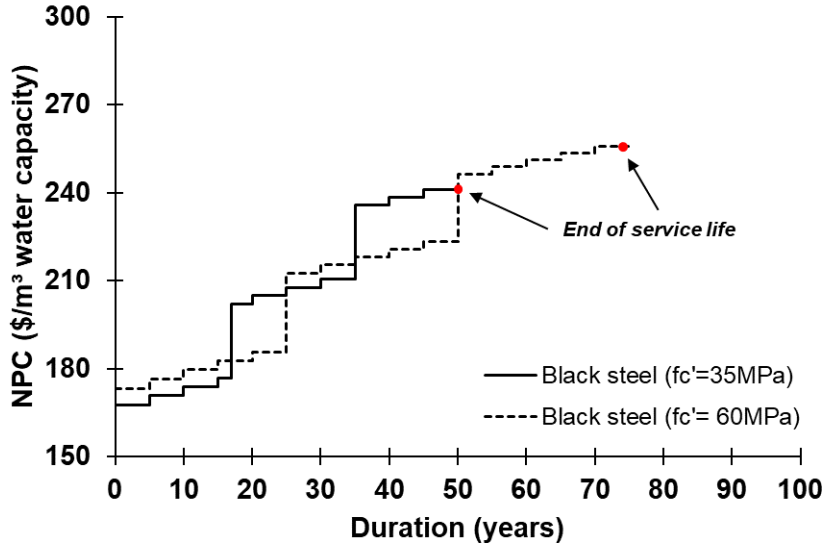

(a)

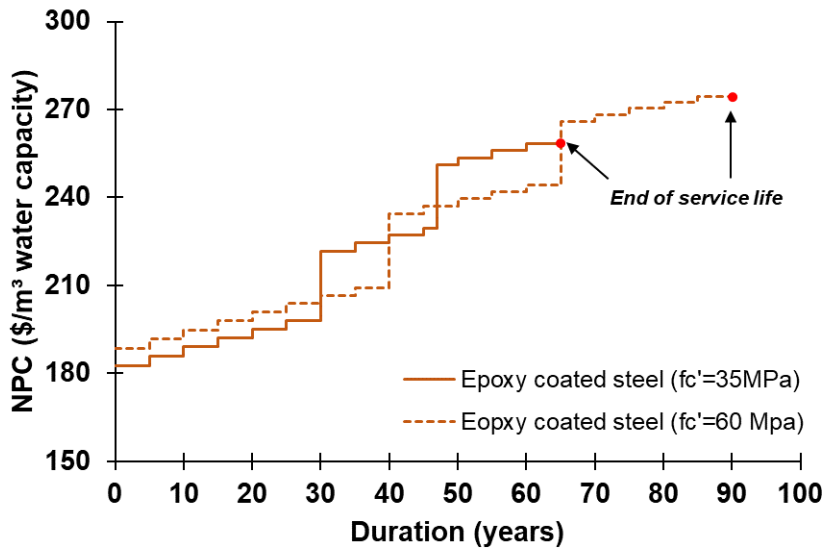

(b)

Figure 7.8. Effect of concrete strength on life cycle performance of (a) black steel and (b) epoxy coated steel reinforced concrete (considering the baseline scenario where $r = 0.6\%$, $C = 1.5M$, and $C_{GFRP} = 0.8C$).

It is emphasized that the cost benefits associated with the use of corrosion-resistant reinforcement are most pronounced in the case of traditional concrete mixtures (i.e., using 100% ordinary Portland cement as binder). Here, the LCCA results were obtained without considering supplementary cementitious materials (SCMs) in the concrete mixture (baseline scenario); these showed a significant life-cycle cost gap between black steel and the corrosion-resistant reinforcements. *Figure 7.9* demonstrates the effect of using some common SCMs on the life-cycle performance of the black steel RC structure. Using Class F fly ash at 20% OPC replacement level (common replacement range is 15–25% [270]) increased the diffusion decay index (m) from 0.2 to 0.36 [211], and thus extended the major-repair milestones by ~8 years as well as the ultimate service life by 25 years. Likewise, using ground granulated blast furnace slag (or 'slag') in the concrete mix at 35% OPC replacement level (common replacement range is 20–50% [270]) resulted in an m value of 0.4 [211] as well as a major repair event every 30 years (compared to $m = 0.2$ and scheduled major repairs every 16–17 years in the baseline scenario). Using silica fume at 5% OPC replacement level (common replacement range is 5–10% [270]) resulted in a higher degree of concrete chloride impermeability (with $D_{28} = 5.13 \times 10^{-12}$ compared to 1.17×10^{-11} in the traditional mix [211]), leading to an approximately 10-year extension in the scheduled major repairs. These results are in line with previous studies showing the effects of SCMs in improving the durability performance of structural concrete [271,272]. On average, the concrete mixtures incorporating SCMs (shown in *Figure 7.9*) resulted in an approximate 100-year life-cycle cost saving of 25% for the black steel-RC structure (compared to the traditional 100% OPC concrete mix).

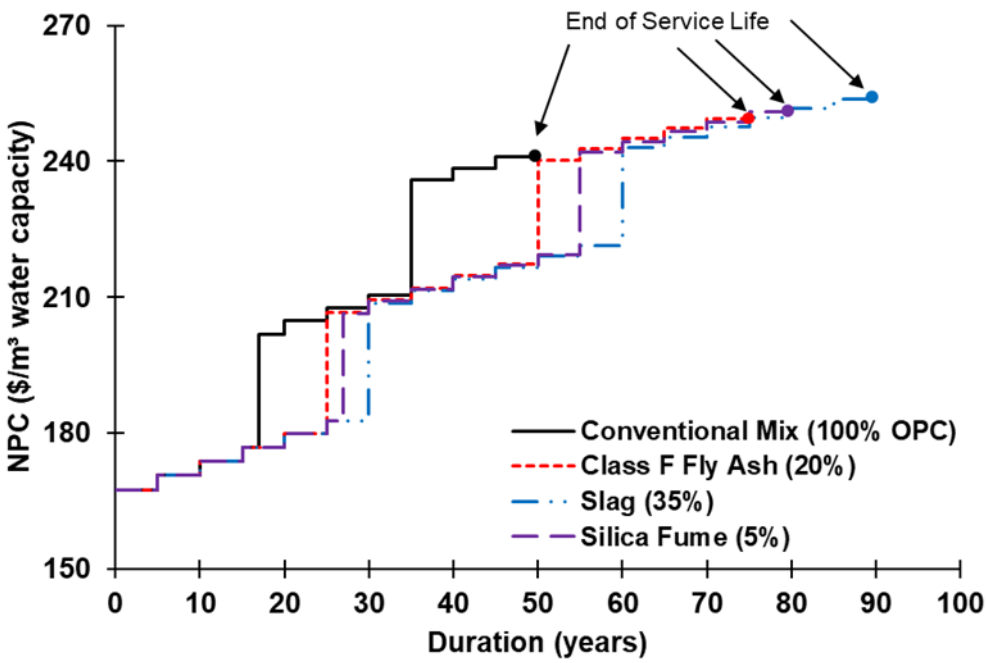

Figure 7.9. Effect of using SCMs on the life cycle performance of black steel RC structure (considering the baseline scenario where r=0.6%, C=1.5M, and w/cm ratio is fixed at 0.47).

7.6 Conclusions

This effort investigated the cost benefit of using non-corrosive reinforcement in structural concrete. Life-cycle cost analysis (LCCA) was performed on an RC water chlorination tank with different reinforcement materials (black steel, epoxy-coated steel, stainless steel, and GFRP). Based on the study results, the following conclusions are drawn:

- Using corrosion-resistant reinforcement improves the long-term cost performance of the structural concrete. The NPC values obtained for epoxy coated and stainless steel reinforced concrete were 11% and 25% lower than that of the black steel reinforced counterpart, respectively. The GFRP-reinforced concrete achieved the best cost performance with an NPC 43% lower than that of the conventional design.
- Stainless steel outperformed the conventional steel after 50 years following initial construction, particularly due to reconstruction of the black steel alternative. Reconstruction at Year 65 was also the breakeven point between stainless and epoxy coated steel reinforcements. However, GFRP reinforcement achieved a lower NPC (compared to black steel) at Year 35 following construction, particularly due to corrosion repairs.
- Results were sensitive to the assumption of the discount rate (r). Considering $r \geq 5.15\%$ made the GFRP reinforcement not economically viable in the long term (i.e., with NPC higher than that of the black steel). The crossover point between the black and stainless steel reinforcements occurred at $r = 1.95\%$. Epoxy coated steel was less economic than black steel at relatively higher r values ($\geq 6.0\%$).
- Results were sensitive to the assumption of construction costs. Stainless steel became more economic than epoxy coated and black steel reinforcements only by assuming a reference construction cost of $C \geq 0.55M$ and $C \geq 0.15M$,

respectively. Moreover, increasing C led to higher values of r at the crossover points between black steel and corrosion-resistant reinforcements.

- Despite it resulting in higher initial costs, increasing the concrete strength extends the service life and reduces the future repair demands for steel reinforced concrete; and thereby improves the overall life-cycle performance of RC structures.
- The cost benefits of non-corrosive reinforcement are most pronounced when supplementary cementitious materials are not used in the concrete mixture. Using fly ash, slag, or silica fume significantly improves the durability performance of black steel-RC structure, and thus reduces the life-cycle cost gap between black steel and corrosion-resistant reinforcements.

The above findings and specifically the numbers here are solely based on the assumptions, the data, and the methods implemented herein. Future studies are required to justify the cost benefit of alternate reinforcement materials for concrete considering other cases and assumptions. Finally, it is emphasized that the current study solely assesses the cost savings of non-corrosive reinforcements from an economic standpoint: future studies to investigate the environmental/ecological savings that can be achieved with the use of corrosion-resistant reinforcements in various concrete structures are critical.

CHAPTER 8: SUMMARY AND FUTURE OUTLOOK

8.1 Summary

This thesis aimed at verifying the safe and economic utilization of seawater, recycled concrete aggregate, and GFRP-reinforcement to produce sustainable and efficient concrete structures. The research program includes five core studies conducted to investigate the effectiveness of the proposed combination (i.e., seawater + RCA + GFRP) in structural concrete. Based on the results of these studies, the following conclusions have been drawn:

- In the first study (Chapter 3), two concrete mixtures were compared; namely, freshwater and seawater-mixed concretes. It was concluded that the use of seawater had a notable effect on the fresh concrete properties. Mechanical performance of seawater concrete was slightly lower than that of the freshwater-mixed concrete. The permeability performance of hardened concrete in the two mixtures was similar. Accordingly, remedial measures were proposed based on lab trials to improve the properties of seawater concrete.
- Likewise, the second study (Chapter 4) investigated the performance of plain concrete mixed with seawater and recycled coarse aggregates at 100% replacement level. The results suggest that the use of seawater and RCA together has negative effects on concrete performance. As compared to the reference/conventional mixture, the seawater-mixed recycled-aggregate concrete showed approximately 5% lower density, 25% lower slump flow, 50% lower setting time, 35% lower strength gain, 10% higher drying shrinkage, 60% higher water absorption, and 100% higher charge passed (in rapid chloride permeability test). Consequently, strategies to improve the performance of such concrete, such as a reduction in the water-to-cementitious materials ratio and the use of chemical admixtures, are

suggested. These strategies, however, may somewhat reduce the “green” aspect of the proposed seawater-mixed concrete with RCA.

- The third study (Chapter 5) reports the results of an experimental study on the flexural performance of seawater-mixed recycled-aggregate concrete beams reinforced with GFRP bars. Twelve medium-scale reinforced concrete (RC) beams ($150 \times 260 \times 2200$ mm) were tested under four-point loading. The test variables included the mixing water (seawater/freshwater), aggregate type (conventional/recycled), and reinforcement material (black steel/GFRP). A wide range of flexural properties, including failure mode, cracking behavior, load-carrying capacity, deformation, energy absorption, and ductility were characterized and compared among the beam specimens. The results suggest that the use of seawater and RCA in concrete has insignificant effects on the flexural capacity of RC beams, especially if concrete strength is preserved by adjusting the mixture design. Indeed, altering reinforcement material had a strong influence on the flexural capacity and performance of the tested specimens: the GFRP-RC beams exhibited higher load-carrying capacities (on average 25%) but inferior deformational characteristics as compared to their steel-reinforced counterparts. Theoretical predictions were obtained for the flexural capacity, crack width, and deflection of steel- and GFRP-RC beams based on their corresponding design guides, and compared with the experimental results.
- In the fourth study (Chapter 6), a life cycle cost analysis (LCCA) has been performed to establish the relative cost savings of structural concrete combining seawater, RCA, and GFRP reinforcement in high-rise buildings compared with the traditional RC concrete. The proposed combination of seawater, RCA, and

GFRP in structural concrete was found to achieve cost savings over a 20 to 30-year period following initial construction. The life cycle cost (LCC) obtained for the proposed combination was approximately 50% less than that of the conventional counterpart (i.e., concrete with freshwater, natural aggregates, and black steel) based on a 100-year study period. Results were found to be highly sensitive to the assumed discount rate: the proposed combination achieved cost savings only with a real discount rate (r) of 5.9% or higher. The differences in concrete mixture cost, however, appeared to have insignificant influence on the ultimate LCCA results compared to those obtained from altering the reinforcement material.

- The fifth study (Chapter 7) carried out a life-cycle cost analysis on structural concrete with more focus on the reinforcement material and considering a special type of RC structure (water chlorination tank). A comparison was established between four concrete reinforcing materials, namely, black steel, epoxy-coated steel, stainless steel, and GFRP through a 100-year analysis period. The results of this study suggest that the use of non-corrosive reinforcement helps achieve a considerable long-term cost saving. LCCA showed that GFRP becomes more economical than black steel in 35 years following construction. The net present cost (NPC) obtained for the GFRP-reinforced concrete was approximately 43% lower than that of the black steel reinforced concrete. The use of stainless steel also had a potential advantage but was less cost-effective than GFRP, with a 50-year payback period and an NPC 25% lower than that of the conventional design. Epoxy coated steel also shows a long-term cost benefit when compared to black steel, with approximately 11% reduction in NPC and 15-year extension in the service life. Sensitivity analyses

were performed to assess the effects of the analysis period, discount rate, construction costs, concrete strength, and the use of supplementary cementitious materials on the LCCA outcomes.

8.2 Future Outlook

If future building codes and standards were to permit seawater for mixing and curing concrete, and if recycled aggregates could be used without pre-washing with freshwater, we could save critical resources, especially in coastal areas where the impact of rapid infrastructure growth and climate change are most pronounced. Indeed, the technology developed over the last two decades has facilitated the use of FRPs to replace steel in RC structures especially when durability is of concern. Accordingly, this research promotes the use of a more sustainable concrete that utilizes non-corrosive reinforcement to save critical resources.

Nonetheless, the current thesis merely represents a step forward towards completely verifying the proposed combination (seawater + RCA + GFRP) in RC structures from technical, economic, and environmental standpoints. Based on the limitations of this research, the following topics are encouraged for future studies:

(i) Investigate the structural performance of seawater-mixed recycled-aggregate concrete but with the use of other composite materials (e.g., Basalt-FRP).

(ii) Shear, torsional, and fatigue behaviors of seawater-mixed recycled-aggregate concrete beams with FRP reinforcement.

(iii) Long-term behavior of seawater concrete elements (decks, girders, pile caps, etc.) reinforced with FRP composite materials.

(iv) Life cycle assessment of structural concrete of the proposed combination (seawater + RCA + GFRP).

REFERENCES

[1] M.M. Mekonnen, A.Y. Hoekstra, Four billion people facing severe water scarcity, Science Advances. 2 (2016) e1500323. doi:10.1126/sciadv.1500323.

[2] S. Miller, H. Shemer, R. Semiat, Energy and environmental issues in desalination, Desalination. 366 (2015) 2–8. doi:10.1016/j.desal.2014.11.034.

[3] M. Elimelech, W.A. Phillip, The future of seawater desalination: Energy, technology, and the environment, Science. 333 (2011) 712–717. doi:10.1126/science.1200488.

[4] N. Ghaffour, T.M. Missimer, G.L. Amy, Technical review and evaluation of the economics of water desalination: Current and future challenges for better water supply sustainability, Desalination. 309 (2013) 197–207. doi:10.1016/j.desal.2012.10.015.

[5] D.R. Vieira, J.L. Calmon, F.Z. Coelho, Life cycle assessment (LCA) applied to the manufacturing of common and ecological concrete: A review, Construction and Building Materials. 124 (2016) 656–666. doi:10.1016/j.conbuildmat.2016.07.125.

[6] S.A. Miller, A. Horvath, P.J.M. Monteiro, Readily implementable techniques can cut annual CO2 emissions from the production of concrete by over 20%, Environmental Research Letters. 11 (2016) 74029. doi:10.1088/1748-9326/11/7/074029.

[7] S.A. Miller, A. Horvath, P.J.M. Monteiro, Impacts of booming concrete production on water resources worldwide, Nature Sustainability. 1 (2018) 69–76. doi:10.1038/s41893-017-0009-5.

[8] I. Fernandez, M.F. Herrador, A.R. Marí, J.M. Bairán, Structural effects of steel reinforcement corrosion on statically indeterminate reinforced concrete

members, Materials and Structures. 49 (2016) 4959–4973. doi:10.1617/s11527-016-0836-2.

[9] J.I. Antonov, D. Seidov, T.P. Boyer, R.A. Locarnini, A. V Mishonov, H.E. Garcia, O.K. Baranova, M.M. Zweng, D.R. Johnson, World Ocean Atlas 2009, Volume 2: Salinity. S. Levitus, Ed, U.S. Gov. Printing Office, Washington, D.C., 2010.

[10] V.W.Y. Tam, M. Soomro, A.C.J. Evangelista, A review of recycled aggregate in concrete applications (2000–2017), Construction and Building Materials. 172 (2018) 272–292. doi:10.1016/j.conbuildmat.2018.03.240.

[11] T. Townsend, C. Wilson, B. Beck, The benefits of construction and demolition materials recycling in the United States, 2014. http://www.cdrecycling.org/assets/docs/exec summary_cd recycling impact white paper.pdf.

[12] S. Butera, T.H. Christensen, T.F. Astrup, Life cycle assessment of construction and demolition waste management, Waste Management. 44 (2015) 196–205. doi:10.1016/j.wasman.2015.07.011.

[13] M. Malešev, V. Radonjanin, S. Marinković, Recycled concrete as aggregate for structural concrete production, Sustainability. 2 (2010) 1204–1225. doi:10.3390/su2051204.

[14] S. Marinković, V. Radonjanin, M. Malešev, I. Ignjatović, Comparative environmental assessment of natural and recycled aggregate concrete, Waste Management. 30 (2010) 2255–2264. doi:10.1016/j.wasman.2010.04.012.

[15] M. Behera, S.K. Bhattacharyya, A.K. Minocha, R. Deoliya, S. Maiti, Recycled aggregate from C&D waste & its use in concrete - A breakthrough towards sustainability in construction sector: A review, Construction and Building

Materials. 68 (2014) 501–516. doi:10.1016/j.conbuildmat.2014.07.003.

[16] T. Nishida, N. Otsuki, H. Ohara, Z.M. Garba-Say, T. Nagata, Some considerations for applicability of seawater as mixing water in concrete, Journal of Materials in Civil Engineering. 27 (2013) B4014004.

[17] S. Khatibmasjedi, F. De Caso, A. Nanni, SEACON : Redefining sustainable concrete, in: The 4th International Conference on Sustainability Construction Materials and Technologies., 2016.

[18] A. Younis, U.A. Ebead, A. Nanni, A perspective on seawater/FRP reinforcement in concrete structures, in: Proceedings of the Ninth International Structural Engineering and Construction Conference, Resilient Structures and Sustainable Construction, ISEC Press, Valencia, Spain, 2017: p. St-38.

[19] B. Benmokrane, A.H. Ali, H.M. Mohamed, A. ElSafty, A. Manalo, Laboratory assessment and durability performance of vinyl-ester, polyester, and epoxy glass-FRP bars for concrete structures, Composites Part B: Engineering. 114 (2017) 163–174. doi:10.1016/j.compositesb.2017.02.002.

[20] D.J. Cleland, G. Tharmarajah, D. Robinson, S.E. Taylor, Corrosion-resistant FRP reinforcement for bridge deck slabs., in: Bridge Engineering, Thomas Telford Ltd, 2015: pp. 208–217. doi:10.1680/bren.13.00001.

[21] D.A. Hensher, Fiber-reinforced-plastic (FRP) reinforcement for concrete structures: properties and applications, Elsevier, 2016.

[22] A.C. Berg, L.C. Bank, M.G. Oliva, J.S. Russell, Construction and cost analysis of an FRP reinforced concrete bridge deck, Construction and Building Materials. 20 (2006) 515–526.

[23] P. Ilg, C. Hoehne, E. Guenther, High-performance materials in infrastructure: A review of applied life cycle costing and its drivers - The case of fiber-reinforced

composites, Journal of Cleaner Production. 112 (2016) 926–945. doi:10.1016/j.jclepro.2015.07.051.

[24] C.D. Eamon, E.A. Jensen, N.F. Grace, X. Shi, Life-cycle cost analysis of alternative reinforcement materials for bridge superstructures considering cost and maintenance uncertainties, Journal of Materials in Civil Engineering. 24 (2012) 373–380. doi:10.1061/(asce)mt.1943-5533.0000398.

[25] S. Kocaoz, V.A. Samaranayake, A. Nanni, Tensile characterization of glass FRP bars, Composites Part B: Engineering. 36 (2005) 127–134. doi:10.1016/j.compositesb.2004.05.004.

[26] Z. Wu, X. Wang, X. Zhao, M. Noori, State-of-the-art review of FRP composites for major construction with high performance and longevity, International Journal of Sustainable Materials and Structural Systems. 1 (2014) 201. doi:10.1504/IJSMSS.2014.062757.

[27] V. Arosio, A. Arrigoni, G. Dotelli, Reducing water footprint of building sector: concrete with seawater and marine aggregates, IOP Conference Series: Earth and Environmental Science. 323 (2019) 12127. doi:10.1088/1755-1315/323/1/012127.

[28] M.U. Hossain, C.S. Poon, I.M.C. Lo, J.C.P. Cheng, Comparative environmental evaluation of aggregate production from recycled waste materials and virgin sources by LCA, Resources, Conservation and Recycling. 109 (2016) 67–77. doi:10.1016/j.resconrec.2016.02.009.

[29] X. Shan, J. Zhou, V.W.C. Chang, E.H. Yang, Life cycle assessment of adoption of local recycled aggregates and green concrete in Singapore perspective, Journal of Cleaner Production. 164 (2017) 918–926. doi:10.1016/j.jclepro.2017.07.015.

[30] Z. Chao, L. Wenxiu, A. Muhammad, C. Lee, Environmental evaluation of FRP in UK highway bridge deck replacement applications based on a comparative LCA study, Advanced Materials Research. 374–377 (2012) 43–48. doi:10.4028/www.scientific.net/AMR.374-377.43.

[31] T. Cadenazzi, G. Dotelli, M. Rossini, S. Nolan, A. Nanni, Life-cycle cost and life-cycle assessment analysis at the design stage of a fiber-reinforced polymer-reinforced concrete bridge in Florida, Advances in Civil Engineering Materials. 8 (2019) 20180113. doi:10.1520/ACEM20180113.

[32] C. Zhang, Life cycle assessment (LCA) of fibre reinforced polymer (FRP) composites in civil applications, in: Eco-Efficient Construction and Building Materials: Life Cycle Assessment (LCA), Eco-Labelling and Case Studies, Woodhead Publishing Limited, 2014: pp. 565–591. doi:10.1533/9780857097729.3.565.

[33] L. Chen, W. Qu, P. Zhu, Life cycle analysis for concrete beams designed with cross-sections of equal durability, Structural Concrete. 17 (2016) 274–286. doi:10.1002/suco.201400117.

[34] K. Amnon, Environmental impact of steel and fiber–reinforced polymer reinforced pavements, Journal of Composites for Construction. 8 (2004) 481–488. doi:10.1061/(ASCE)1090-0268(2004)8:6(481).

[35] S.K. Kaushik, S. Islam, Suitability of sea water for mixing structural concrete exposed to a marine environment, Cement and Concrete Composites. 17 (1995) 177–185. doi:10.1016/0958-9465(95)00015-5.

[36] A. Witze, Seawater is the secret to long-lasting Roman concrete, Nature. (2017). https://www.nature.com/news/seawater-is-the-secret-to-long-lasting-roman-concrete-1.22231.

[37] M.D. Jackson, J. Moon, E. Gotti, R. Taylor, S.R. Chae, M. Kunz, A.H. Emwas, C. Meral, P. Guttmann, P. Levitz, H.R. Wenk, P.J.M. Monteiro, Material and elastic properties of Al-tobermorite in ancient roman seawater concrete, Journal of the American Ceramic Society. 96 (2013) 2598–2606. doi:10.1111/jace.12407.

[38] H. El-Hassan, T. El-Maaddawy, A. Al-Sallamin, A. Al-Saidy, Durability of glass fiber-reinforced polymer bars conditioned in moist seawater-contaminated concrete under sustained load, Construction and Building Materials. 175 (2018) 1–13.

[39] H. El-Hassan, T. El-Maaddawy, A. Al-Sallamin, A. Al-Saidy, Performance evaluation and microstructural characterization of GFRP bars in seawater-contaminated concrete, Construction and Building Materials. 147 (2017) 66–78. doi:10.1016/j.conbuildmat.2017.04.135.

[40] M. Khatibmasjedi, Sustainable concrete using seawater and glass fiber reinforced polymer bars, Ph.D. Thesis, University of Miami, 2018.

[41] J. Xiao, C. Qiang, A. Nanni, K. Zhang, Use of sea-sand and seawater in concrete construction: Current status and future opportunities, Construction and Building Materials. 155 (2017) 1101–1111. doi:10.1016/j.conbuildmat.2017.08.130.

[42] D.L. Narver, Good concrete made with coral and water, Civil Engineering. 24 (1964) 654–658.

[43] H.H. Steinour, Concrete mix water — How impure can it be?, J. Res. Development Labs. 2 (1960) 32–50.

[44] F.M. Wegian, Effect of seawater for mixing and curing on structural concrete, The IES Journal Part A: Civil & Structural Engineering. 3 (2010) 235–243.

[45] T.U. Mohammed, H. Hamada, T. Yamaji, Performance of seawater-mixed

concrete in the tidal environment, Cement and Concrete Research. 34 (2004) 593–601. doi:10.1016/j.cemconres.2003.09.020.

[46] Q. Guo, L. Chen, H. Zhao, J. Admilson, W. Zhang, The effect of mixing and curing sea water on concrete strength at different ages, in: MATEC Web of Conferences, EDP Sciences, 2018: p. 02004.

[47] D.F. Griffin, R.L. Henry, The effect of salt in concrete on compressive strength, water vapor transmission, and corrosion of reinforcing steel, Port Hueneme, California, 1964.

[48] J.D. Dewar, The workability and compressive strength of concrete made with sea water, Cement and Concrete Association, London, 1963.

[49] Z. Shi, Z. Shui, Q. Li, H. Geng, Combined effect of metakaolin and sea water on performance and microstructures of concrete, Construction and Building Materials. 74 (2015) 57–64. doi:10.1016/j.conbuildmat.2014.10.023.

[50] S.S. Park, S.J. Kwon, H.W. Song, Analysis technique for restrained shrinkage of concrete containing chlorides, Materials and Structures. 44 (2011) 475–486. doi:10.1617/s11527-010-9642-4.

[51] M. Etxeberria, A. Gonzalez-Corominas, P. Pardo, Influence of seawater and blast furnace cement employment on recycled aggregate concretes' properties, Construction and Building Materials. 115 (2016) 496–505. doi:10.1016/j.conbuildmat.2016.04.064.

[52] N. Otsuki, T. Saito, Y. Tadokoro, Possibility of seawater as mixing water in concrete, Journal of Civil Engineering and Architecture. 6 (2012) 1273–1279.

[53] H. Li, N. Farzadnia, C. Shi, The role of seawater in interaction of slag and silica fume with cement in low water-to-binder ratio pastes at the early age of hydration, Construction and Building Materials. 185 (2018) 508–518.

doi:https://doi.org/10.1016/j.conbuildmat.2018.07.091.

[54] H.-U. Jensen, P.L. Pratt, The effect of fly ash on the hydration of cements at low temperature mixed and cured in sea-water, MRS Online Proceedings Library Archive. 113 (1987) 279–289.

[55] M. Yan, Y.T. Li, Y. Zhang, Research on influence of mixtures on strength of seawater and sea sand concrete, Shanxi Arch. 38 (2012) 135–136.

[56] Q. Li, H. Geng, Y. Huang, Z. Shui, Chloride resistance of concrete with metakaolin addition and seawater mixing: A comparative study, Construction and Building Materials. 101 (2015) 184–192. doi:10.1016/j.conbuildmat.2015.10.076.

[57] Q. Li, H. Geng, Z. Shui, Y. Huang, Effect of metakaolin addition and seawater mixing on the properties and hydration of concrete, Applied Clay Science. 115 (2015) 51–60. doi:10.1016/j.clay.2015.06.043.

[58] H.Y. Ghorab, M.S. Hilal, A. Antar, Effect of mixing and curing waters on the behaviour of cement pastes and concrete Part 2: Properties of cement paste and concrete, Cement and Concrete Research. 20 (1990) 69–72.

[59] H.Y. Ghorab, M.S. Hilal, E.A. Kishar, Effect of mixing and curing waters on the behaviour of cement pastes and concrete part 1: microstructure of cement pastes, Cement and Concrete Research. 19 (1989) 868–878.

[60] K. Katano, N. Takeda, Y. Ishizeki, K. Iriya, Properties and application of concrete made with sea water and un-washed sea sand, in: Third International Conference on Sustainable Construction Materials and Technologies, 2012. doi:10.3151/coj.49.12_17.

[61] F.M. Khalaf, A.S. DeVenny, Recycling of demolished masonry rubble as coarse aggregate in concrete: Review, Journal of Materials in Civil Engineering. 16

(2004) 331–340. doi:10.1061/(ASCE)0899-1561(2004)16:4(331).

[62] R. V. Silva, J. De Brito, R.K. Dhir, Fresh-state performance of recycled aggregate concrete: A review, Construction and Building Materials. 178 (2018) 19–31. doi:10.1016/j.conbuildmat.2018.05.149.

[63] H. Guo, C. Shi, X. Guan, J. Zhu, Y. Ding, T.C. Ling, H. Zhang, Y. Wang, Durability of recycled aggregate concrete – A review, Cement and Concrete Composites. 89 (2018) 251–259. doi:10.1016/j.cemconcomp.2018.03.008.

[64] N. Kisku, H. Joshi, M. Ansari, S.K. Panda, S. Nayak, S.C. Dutta, A critical review and assessment for usage of recycled aggregate as sustainable construction material, Construction and Building Materials. 131 (2017) 721–740. doi:10.1016/j.conbuildmat.2016.11.029.

[65] R. V. Silva, J. De Brito, R.K. Dhir, The influence of the use of recycled aggregates on the compressive strength of concrete: A review, European Journal of Environmental and Civil Engineering. 19 (2015) 825–849. doi:10.1080/19648189.2014.974831.

[66] R. V. Silva, J. De Brito, R.K. Dhir, Prediction of the shrinkage behavior of recycled aggregate concrete: A review, Construction and Building Materials. 77 (2015) 327–339. doi:10.1016/j.conbuildmat.2014.12.102.

[67] R. V. Silva, J. De Brito, R.K. Dhir, Tensile strength behaviour of recycled aggregate concrete, Construction and Building Materials. 83 (2015) 108–118. doi:10.1016/j.conbuildmat.2015.03.034.

[68] R. Neves, A. Silva, J. De Brito, R. V. Silva, Statistical modelling of the resistance to chloride penetration in concrete with recycled aggregates, Construction and Building Materials. 182 (2018) 550–560. doi:10.1016/j.conbuildmat.2018.06.125.

[69] C. Shi, Y. Li, J. Zhang, W. Li, L. Chong, Z. Xie, Performance enhancement of recycled concrete aggregate - A review, Journal of Cleaner Production. 112 (2016) 466–472. doi:10.1016/j.jclepro.2015.08.057.

[70] G. Wardeh, E. Ghorbel, H. Gomart, Mix design and properties of recycled aggregate concretes: Applicability of Eurocode 2, International Journal of Concrete Structures and Materials. 9 (2015) 1–20. doi:10.1007/s40069-014-0087-y.

[71] M. Amario, C.S. Rangel, M. Pepe, R.D.T. Filho, Optimization of normal and high strength recycled aggregate concrete mixtures by using packing model, Cement and Concrete Composites. 84 (2017) 83–92. doi:10.1016/j.cemconcomp.2017.08.016.

[72] S.C. Kou, C.S. Poon, F. Agrela, Comparisons of natural and recycled aggregate concretes prepared with the addition of different mineral admixtures, Cement and Concrete Composites. 33 (2011) 788–795. doi:10.1016/j.cemconcomp.2011.05.009.

[73] G. Dimitriou, P. Savva, M.F. Petrou, Enhancing mechanical and durability properties of recycled aggregate concrete, Construction and Building Materials. 158 (2018) 228–235. doi:10.1016/j.conbuildmat.2017.09.137.

[74] D. Matias, J. De Brito, A. Rosa, D. Pedro, Mechanical properties of concrete produced with recycled coarse aggregates - Influence of the use of superplasticizers, Construction and Building Materials. 44 (2013) 101–109. doi:10.1016/j.conbuildmat.2013.03.011.

[75] Z. Dong, G. Wu, X.L. Zhao, H. Zhu, J.L. Lian, Durability test on the flexural performance of seawater sea-sand concrete beams completely reinforced with FRP bars, Construction and Building Materials. 192 (2018) 671–682.

doi:10.1016/j.conbuildmat.2018.10.166.

[76] W. Alnahhal, O. Aljidda, Flexural behavior of basalt fiber reinforced concrete beams with recycled concrete coarse aggregates, Construction and Building Materials. 169 (2018) 165–178. doi:10.1016/j.conbuildmat.2018.02.135.

[77] S. Sunayana, S. V. Barai, Flexural performance and tension-stiffening evaluation of reinforced concrete beam incorporating recycled aggregate and fly ash, Construction and Building Materials. 174 (2018) 210–223. doi:10.1016/j.conbuildmat.2018.04.072.

[78] M. Arezoumandi, A. Smith, J.S. Volz, K.H. Khayat, An experimental study on flexural strength of reinforced concrete beams with 100% recycled concrete aggregate, Engineering Structures. 88 (2015) 154–162. doi:10.1016/j.engstruct.2015.01.043.

[79] I.S. Ignjatović, S.B. Marinković, Z.M. Mišković, A.R. Savić, Flexural behavior of reinforced recycled aggregate concrete beams under short-term loading, Materials and Structures/Materiaux et Constructions. 46 (2013) 1045–1059. doi:10.1617/s11527-012-9952-9.

[80] A.M. Knaack, Y.C. Kurama, Behavior of reinforced concrete beams with recycled concrete coarse aggregates, Journal of Structural Engineering (United States). 141 (2015) B4014009. doi:10.1061/(ASCE)ST.1943-541X.0001118.

[81] T.H.K. Kang, W. Kim, Y.K. Kwak, S.G. Hong, Flexural testing of reinforced concrete beams with recycled concrete aggregates, ACI Structural Journal. 111 (2014) 607–616. doi:10.14359/51686622.

[82] G. Fathifazl, A.G. Razaqpur, O.B. Isgor, A. Abbas, B. Fournier, S. Foo, Flexural performance of steel-reinforced recycled concrete beams, ACI Structural Journal. 106 (2009) 858–867.

[83] R. Sato, I. Maruyama, T. Sogabe, M. Sogo, Flexural behavior of reinforced recycled concrete beams, Journal of Advanced Concrete Technology. 5 (2007) 43–61. doi:10.3151/jact.5.43.

[84] A.B. Ajdukiewicz, A.T. Kliszczewicz, Comparative tests of beams and columns made of recycled aggregate concrete and natural aggregate concrete, Journal of Advanced Concrete Technology. 5 (2007) 259–273. doi:10.3151/jact.5.259.

[85] T. D'Antino, M.A. Pisani, Long-term behavior of GFRP reinforcing bars, Composite Structures. (2019) 111283. doi:10.1016/j.compstruct.2019.111283.

[86] ACI Committee 440, Guide for the design and construction of structural concrete reinforced with FRP bars (ACI 440.1 R-15), American Concrete Institute, 2015.

[87] Canadian Standards Association, Design and construction of building components with fiber reinforced polymers (CAN/CSA-S806-12), Ontario, Canada, 2012.

[88] B. Benmokrane, E. El-salakawy, A. El-ragaby, T. Lackey, Designing and testing of concrete bridge decks reinforced with glass FRP bars, Journal of Bridge Engineering. 11 (2006) 217–229. doi:10.1061/(ASCE)1084-0702(2006)11:2(217).

[89] V. Mara, R. Haghani, P. Harryson, Bridge decks of fibre reinforced polymer (FRP): A sustainable solution, Construction and Building Materials. 50 (2014) 190–199. doi:10.1016/j.conbuildmat.2013.09.036.

[90] E.A. Ahmed, B. Benmokrane, M. Sansfaçon, Case study: design, construction, and performance of the La Chancelière parking garage's concrete flat slabs reinforced with GFRP bars., Journal of Composites for Construction. 21 (2017) 05016001. doi:10.1061/(ASCE)CC.1943-5614.0000656.

[91] H.M. Mohamed, B. Benmokrane, Recent field applications of FRP composite

reinforcing bars in civil engineering infrastructures, in: Proc., Int. Conf. ACUN6–Composites and Nanocomposites in Civil, Offshore and Mining Infrastructure, Melbourne, Australia, 2012: pp. 14–16.

[92] I. Fatih, A.F. Ashour, Flexural performance of FRP reinforced concrete beams, Composite Structures. 94 (2012) 1616–1625. doi:10.1016/j.compstruct.2011.12.012.

[93] C. Barris, L. Torres, A. Turon, M. Baena, A. Catalan, An experimental study of the flexural behaviour of GFRP RC beams and comparison with prediction models, Composite Structures. 91 (2009) 286–295. doi:10.1016/j.compstruct.2009.05.005.

[94] R.J. Gravina, S.T. Smith, Flexural behaviour of indeterminate concrete beams reinforced with FRP bars, Engineering Structures. 30 (2008) 2370–2380. doi:10.1016/j.engstruct.2007.12.019.

[95] L. Ascione, G. Mancusi, S. Spadea, Flexural behaviour of concrete beams reinforced with GFRP bars, Strain. 46 (2010) 460–469. doi:10.1111/j.1475-1305.2009.00662.x.

[96] C. Kassem, A.S. Farghaly, B. Benmokrane, Evaluation of flexural behavior and serviceability performance of concrete beams reinforced with FRP bars, Journal of Composites for Construction. 15 (2011) 682–695. doi:10.1061/(ASCE)CC.1943-5614.0000216.

[97] I.F. Kara, A.F. Ashour, C. Dundar, Deflection of concrete structures reinforced with FRP bars, Composites Part B: Engineering. 44 (2013) 375–384. doi:10.1016/j.compositesb.2012.04.061.

[98] P.H. Bischoff, S.P. Gross, Design approach for calculating deflection of FRP-reinforced concrete, Journal of Composites for Construction. 15 (2011) 490–499.

doi:10.1061/(ASCE)CC.1943-5614.0000195.

[99] R. Al-Sunna, K. Pilakoutas, I. Hajirasouliha, M. Guadagnini, Deflection behaviour of FRP reinforced concrete beams and slabs: An experimental investigation, Composites Part B: Engineering. 43 (2012) 2125–2134. doi:10.1016/j.compositesb.2012.03.007.

[100] C. Barris, L. Torres, J. Comas, C. Miàs, Cracking and deflections in GFRP RC beams: An experimental study, Composites Part B: Engineering. 55 (2013) 580–590. doi:10.1016/j.compositesb.2013.07.019.

[101] A. El-Nemr, E.A. Ahmed, B. Benmokrane, Flexural behavior and serviceability of normal- And high-strength concrete beams reinforced with glass fiber-reinforced polymer bars, ACI Structural Journal. 110 (2013) 1077–1087.

[102] R. Anex, R. Lifset, Life cycle assessment, Journal of Industrial Ecology. 18 (2014) 321–323. doi:10.1111/jiec.12157.

[103] E. Sterner, R.J. Cole, Reconciling theory and practice of life-cycle costing, Building Research and Information. 28 (2000) 368–375.

[104] D. Elmakis, A. Lisnianski, Life cycle cost analysis: Actual problem in industrial management, Journal of Business Economics and Management. 7 (2006) 5–8. doi:10.1080/16111699.2006.9636115.

[105] V.W.Y. Tam, Economic comparison of concrete recycling: A case study approach, Resources, Conservation and Recycling. 52 (2008) 821–828. doi:10.1016/j.resconrec.2007.12.001.

[106] S. Senaratne, D. Gerace, O. Mirza, V.W.Y. Tam, W.H. Kang, The costs and benefits of combining recycled aggregate with steel fibres as a sustainable, structural material, Journal of Cleaner Production. 112 (2016) 2318–2327. doi:10.1016/j.jclepro.2015.10.041.

[107] QCS, Qatar Construction Specifications, Qatar General Organization for Standards and Metrology, Qatar, 2014.

[108] BS 1377-3: Methods of test for soils for civil engineering purposes. Chemical and electro-chemical tests, BSI, 1990.

[109] BS 6068-2.51: Water quality. Determination of alkalinity. Determination of total and composite alkalinity, BSI, 1996.

[110] BS 1377-2: Methods of test for soils for civil engineering purposes. Classification tests, BSI, 1990.

[111] BS 6068-2.50: Water quality. Physical, chemical and biochemical methods. Determination of pH, BSI, 1995.

[112] M. Al-Ansary, S.R. Iyengar, Physiochemical characterization of coarse aggregates in Qatar for construction industry, International Journal of Sustainable Built Environment. 2 (2013) 27–40. doi:10.1016/j.ijsbe.2013.07.003.

[113] BS EN 933-1: Tests for geometrical properties of aggregates. Determination of particle size distribution. Sieving method, BSI, 2012.

[114] BS EN 1097-6: Tests for mechanical and physical properties of aggregates. Determination of particle density and water absorption, BSI, 2013.

[115] ASTM C142 / C142M-17: Standard test method for clay lumps and friable particles in aggregates, ASTM International, 2017.

[116] BS EN 933-3: Tests for geometrical properties of aggregates. Determination of particle shape. Flakiness index, BSI, 2012.

[117] BS EN 933-4: Tests for geometrical properties of aggregates. Determination of particle shape. Shape index, BSI, 2008.

[118] ASTM C123/C123M - 14: Standard test method for lightweight particles in

aggregate, ASTM International, 2014.

[119] BS 812-111: Testing aggregates. Methods for determination of ten per cent fines value (TFV), BSI, 1990.

[120] BS EN 1097-2: Tests for mechanical and physical properties of aggregates. Methods for the determination of resistance to fragmentation, BSI, 2010.

[121] BS EN 1367-2: Tests for thermal and weathering properties of aggregates. Magnesium sulfate test, BSI, 2009.

[122] ASTM C40/C40M - 16: Standard test method for organic impurities in fine aggregates for concrete, ASTM International, 2016.

[123] BS EN 1744-5: Tests for chemical properties of aggregates. Determination of acid soluble chloride salts, BSI, 2006.

[124] BS EN 1744-1: Tests for chemical properties of aggregates. Chemical analysis, BSI, 2012.

[125] BS EN 196-2:2013. Method of testing cement. Chemical analysis of cement, BSI, 2013.

[126] S. Cheng, Z. Shui, T. Sun, Y. Huang, K. Liu, Effects of seawater and supplementary cementitious materials on the durability and microstructure of lightweight aggregate concrete, Construction and Building Materials. 190 (2018) 1081–1090. doi:https://doi.org/10.1016/j.conbuildmat.2018.09.178.

[127] BS EN 15167-1:2006. Ground granulated blast furnace slag for use in concrete, mortar and grout. Definitions, specifications and conformity criteria, BSI, 2006. http://shop.bsigroup.com/ProductDetail/?pid=000000000030157392.

[128] Y.L. Li, X.L. Zhao, R.K. Singh Raman, S. Al-Saadi, Thermal and mechanical properties of alkali-activated slag paste, mortar and concrete utilising seawater and sea sand, Construction and Building Materials. 159 (2018) 704–724.

doi:10.1016/j.conbuildmat.2017.10.104.

[129] N. Chousidis, I. Ioannou, E. Rakanta, C. Koutsodontis, G. Batis, Effect of fly ash chemical composition on the reinforcement corrosion, thermal diffusion and strength of blended cement concretes, Construction and Building Materials. 126 (2016) 86–97. doi:10.1016/j.conbuildmat.2016.09.024.

[130] BS EN 196-6: 2010 - Methods of testing cement. Determination of fineness, 2010.

[131] BS EN 206: Concrete specification, performance, production and conformity, BSI, 2013.

[132] ASTM C143/C143M-15a: Standard test method for slump of hydraulic-cement concrete, ASTM International, 2015.

[133] ASTM C138/C138M-17: Standard test method for density (Unit Weight), yield, and air content (gravimetric) of concrete, ASTM International, 2017.

[134] ASTM C403/C403M-16: Standard test method for time of setting of concrete mixtures by penetration resistance, ASTM International, 2016.

[135] ASTM C39/C39M-16b: Standard test method for compressive strength of cylindrical concrete specimens, ASTM International, West Conshohocken, PA, 2016.

[136] ASTM C496/C496M-11: Standard test method for splitting tensile strength of cylindrical concrete specimens, ASTM International, West Conshohocken, PA, 2011.

[137] ASTM C157/C157M-08: Standard test method for length change of hardened hydraulic-cement mortar and concrete, ASTM International, West Conshohocken, PA, 2014.

[138] G. De Schutter, K. Audenaert, Evaluation of water absorption of concrete as a

measure for resistance against carbonation and chloride migration, Materials and Structures. 37 (2004) 591. doi:10.1007/BF02483288.

[139] L. Wang, T. Ueda, Mesoscale modeling of water penetration into concrete by capillary absorption, Ocean Engineering. 38 (2011) 519–528. doi:https://doi.org/10.1016/j.oceaneng.2010.12.019.

[140] ASTM C1202-17a: Standard test method for electrical indication of concrete's ability to resist chloride ion penetration, ASTM International, 2017. doi:10.1520/C1202-12.2.

[141] NT Build 492, Concrete, mortar and cement-based repair materials: chloride migration coefficient from non-steady-state migration experiments, Nordtest method, Finland, 1999.

[142] BS 1881-122: Testing concrete. Method for determination of water absorption, BSI, 2011.

[143] ASTM C1679-17: Measuring hydration kinetics of hydraulic cementitious mixtures using isothermal calorimetry, ASTM International, 2017.

[144] N.T. Todd, P. Suraneni, W.J. Weiss, Hydration of cement pastes containing accelerator at various temperatures: application to high early strength pavement patching, Advances in Civil Engineering Materials. 6 (2017) 20160079. doi:10.1520/acem20160079.

[145] N.T. Todd, Assessing risk reduction of high early strength concrete mixtures, Theses and Dissertations Available from ProQuest. (2015) 142.

[146] ASTM C1723-16: Standard guide for examination of hardened concrete using scanning electron microscopy, ASTM International, 2016.

[147] N.B. Winter, Scanning electron microscopy for cement and concrete, WHD Microanalysis, 2012.

[148] M.C.G. Juenger, P.J.M. Monteiro, E.M. Gartner, G.P. Denbeaux, A soft X-ray microscope investigation into the effects of calcium chloride on tricalcium silicate hydration, Cement and Concrete Research. 35 (2005) 19–25. doi:https://doi.org/10.1016/j.cemconres.2004.05.016.

[149] J. Cheung, A. Jeknavorian, L. Roberts, D. Silva, Impact of admixtures on the hydration kinetics of Portland cement, Cement and Concrete Research. 41 (2011) 1289–1309. doi:https://doi.org/10.1016/j.cemconres.2011.03.005.

[150] J. Geng, L. Li, D. Easterbrook, Q. Liu, Effect of carbonation on release of bound chlorides in chloride- contaminated concrete, Magazine of Concrete Research. 68 (2016) 353–363.

[151] E.A. Bortoluzzi, N.J. Broon, C.M. Bramante, W.T. Felippe, M. Tanomaru Filho, R.M. Esberard, The influence of calcium chloride on the setting time, solubility, disintegration, and pH of mineral trioxide aggregate and white portland cement with a radiopacifier, Journal of Endodontics. 35 (2009) 550–554. doi:10.1016/j.joen.2008.12.018.

[152] E.A. Kishar, D.A. Ahmed, M.R. Mohammed, R. Noury, Effect of calcium chloride on the hydration characteristics of ground clay bricks cement pastes, Beni-Suef University Journal of Basic and Applied Sciences. 2 (2013) 20–30. doi:10.1016/j.bjbas.2013.09.003.

[153] E.D. Lim, C.L. Roxas, R. Gallardo, T. Nishida, N. Otsuki, Strength and corrosion behavior of mortar mixed and/or cured with seawater with various fly ash replacement ratios, Asian Journal of Civil Engineering. 16 (2015) 835–849.

[154] M. Cui, J.-Z. Mao, D.-G. Jia, B. Li, Experimental study on mechanical properties of marine sand and seawater concrete., in: Proceedings of the 2014 International Conference on Mechanics and Civil Engineering, 2014: pp. 106–111.

[155] S. Diamond, The microstructure of cement paste and concrete—a visual primer, Cement and Concrete Composites. 26 (2004) 919–933. doi:10.1016/j.cemconcomp.2004.02.028.

[156] W. Franus, R. Panek, M. Wdowin, SEM investigation of microstructures in hydration products of portland cement, Springer Proceedings in Physics. 164 (2015) 105–112. doi:10.1007/978-3-319-16919-4_14.

[157] K. De Weerdt, H. Justnes, The effect of sea water on the phase assemblage of hydrated cement paste, Cement & Concrete Composites. 55 (2015) 215–222.

[158] P. Pereira, L. Evangelista, J. De Brito, The effect of superplasticisers on the workability and compressive strength of concrete made with fine recycled concrete aggregates, Construction and Building Materials. 28 (2012) 722–729. doi:10.1016/j.conbuildmat.2011.10.050.

[159] R. Dubey, P. Kumar, Effect of superplasticizer dosages on compressive strength of self compacting concrete, International Journal of Civil and Structural Engineering. 3 (2012) 360–366. doi:10.6088/ijcser.201203013034.

[160] M. Bravo, J. De Brito, J. Pontes, L. Evangelista, Mechanical performance of concrete made with aggregates from construction and demolition waste recycling plants, Journal of Cleaner Production. 99 (2015) 59–74. doi:10.1016/j.jclepro.2015.03.012.

[161] J.C. Souche, P. Devillers, M. Salgues, E.G. Diaz, Influence of recycled coarse aggregates on permeability of fresh concrete, Cement and Concrete Composites. 83 (2017) 394–404. doi:10.1016/j.cemconcomp.2017.08.002.

[162] J. Wang, E. Liu, L. Li, Multiscale investigations on hydration mechanisms in seawater OPC paste, Construction and Building Materials. 191 (2018) 891–903. doi:10.1016/j.conbuildmat.2018.10.010.

[163] C.S. Poon, S.C. Kou, L. Lam, Influence of recycled aggregate on slump and bleeding of fresh concrete, Materials and Structures/Materiaux et Constructions. 40 (2007) 981–988. doi:10.1617/s11527-006-9192-y.

[164] L. Montanari, P. Suraneni, M. Tsui-Chang, M. Khatibmasjedi, U. Ebead, J. Weiss, A. Nanni, Hydration, pore Solution, and porosity of cementitious pastes made with seawater, Journal of Materials in Civil Engineering. 31 (2019) 04019154. doi:10.1061/(ASCE)MT.1943-5533.0002818.

[165] M. Etxeberria, E. Vázquez-Ramonich, A.R. Marí, M.B. Oliveira, Influence of amount of recycled coarse aggregates and production process on properties of recycled aggregate concrete, Cement and Concrete Research. 37 (2007) 735–742. doi:10.1016/j.cemconres.2007.02.002.

[166] C.S. Poon, Z.H. Shui, L. Lam, H. Fok, S.C. Kou, Influence of moisture states of natural and recycled aggregates on the slump and compressive strength of concrete, Cement and Concrete Research. 34 (2004) 31–36. doi:10.1016/S0008-8846(03)00186-8.

[167] L. Ferreira, J. De Brito, M. Barra, Influence of the pre-saturation of recycled coarse concrete aggregates on concrete properties, Magazine of Concrete Research. 63 (2011) 617–627. doi:10.1680/macr.2011.63.8.617.

[168] E.A.B. Koenders, M. Pepe, E. Martinelli, Compressive strength and hydration processes of concrete with recycled aggregates, Cement and Concrete Research. 56 (2014) 203–212. doi:10.1016/j.cemconres.2013.11.012.

[169] J. Xiao, H. Xie, Z. Yang, Shear transfer across a crack in recycled aggregate concrete, Cement and Concrete Research. 42 (2012) 700–709. doi:10.1016/j.cemconres.2012.02.006.

[170] I.F.S. Bosque, W. Zhu, T. Howind, A. Matías, M.I.S. Rojas, C. Medina,

Properties of interfacial transition zones (ITZs) in concrete containing recycled mixed aggregate, Cement and Concrete Composites. 81 (2017) 25–34. doi:10.1016/j.cemconcomp.2017.04.011.

[171] M.B. Leite, P.J.M. Monteiro, Microstructural analysis of recycled concrete using X-ray microtomography, Cement and Concrete Research. 81 (2016) 38–48. doi:10.1016/j.cemconres.2015.11.010.

[172] Q. Liu, J. Xiao, Z. Sun, Experimental study on the failure mechanism of recycled concrete, Cement and Concrete Research. 41 (2011) 1050–1057. doi:10.1016/j.cemconres.2011.06.007.

[173] Y. Kim, A. Hanif, M. Usman, W. Park, Influence of bonded mortar of recycled concrete aggregates on interfacial characteristics – Porosity assessment based on pore segmentation from backscattered electron image analysis, Construction and Building Materials. 212 (2019) 149–163. doi:10.1016/j.conbuildmat.2019.03.265.

[174] L. Jianyong, Y. Yan, A study on creep and drying shrinkage of high performance concrete, Cement and Concrete Research. 31 (2001) 1203–1206.

[175] G. Fathifazl, A.G. Razaqpur, O.B. Isgor, A. Abbas, B. Fournier, S. Foo, Creep and drying shrinkage characteristics of concrete produced with coarse recycled concrete aggregate, Cement and Concrete Composites. 33 (2011) 1026–1037. doi:10.1016/j.cemconcomp.2011.08.004.

[176] J. Zhang, C. Shi, Y. Li, X. Pan, C.S. Poon, Z. Xie, Performance enhancement of recycled concrete aggregates through carbonation, Journal of Materials in Civil Engineering. 27 (2015). doi:10.1061/(ASCE)MT.1943-5533.0001296.

[177] N. Singh, S.P. Singh, Carbonation resistance of self-compacting recycled aggregate concretes with silica fume, Journal of Sustainable Cement-Based

Materials. 7 (2018) 214–238. doi:10.1080/21650373.2018.1471425.

[178] ISE/104 Committee, BS 4449:2005: Steel for the reinforcement of concrete. Weldable reinforcing steel. Bar, coil and decoiled product, BSI, 2005.

[179] U. Ebead, H.E. El-Sherif, Near surface embedded-FRCM for flexural strengthening of reinforced concrete beams, Construction and Building Materials. 204 (2019) 166–176. doi:10.1016/j.conbuildmat.2019.01.145.

[180] ATP Construction Composites, Data sheet for GFRP rebars, (2019). http://www.atp-frp.com/html/products_tds.html#rwb-v.

[181] ACI Committee 318, Building code requirements for structural concrete (ACI 318-14), American Concrete Institute, Farmington Hills, USA, 2014.

[182] A. Younis, U. Ebead, K.C. Shrestha, Different FRCM systems for shear-strengthening of reinforced concrete beams, Construction and Building Materials. 153 (2017) 514–526. doi:10.1016/j.conbuildmat.2017.07.132.

[183] A.E. Naaman, S.-M. Jeong, Structural ductility of concrete beams prestressed with FRP tendons, in: The 2nd International Symposium on Fiber Reinforced Polymer Reinforcement for Reinforced Concrete Structures (FRPRCS-2), Spon, Ghent; Belgium, 1995: pp. 379–386.

[184] ACI Committee 440, Guide for the design and construction of concrete reinforced with FRP Bars (ACI 440.1 R-06), American Concrete Institute, Farmington Hills, USA, 2006.

[185] B. Benmokrane, V.L. Brown, K. Mohamed, A. Nanni, M. Rossini, C. Shield, Creep-rupture limit for GFRP Bars subjected to sustained loads, Journal of Composites for Construction. 23 (2019) 06019001. doi:10.1061/(asce)cc.1943-5614.0000971.

[186] ISIS Canada Corporation, ISIS Design Manual: Reinforcing concrete structures

with fiber reinforced polymers-Design manual No. 3, Manitoba, Canada, 2007.

[187] J.K. Wight, J.G. Macgregor, Reinforced concrete: Mechanics and design, Sixth edit, Pearson, Upper Saddle River, New Jersey, 2012.

[188] D. Branson, Deformation of concrete structures, McGraw-Hill, New York, 1977.

[189] P.H. Bischoff, Reevaluation of deflection prediction for concrete beams reinforced with steel and fiber reinforced polymer bars, Journal of Structural Engineering. 131 (2005) 752–762. doi:10.1061/(ASCE)0733-9445(2005)131:5(752).

[190] P. Foraboschi, M. Mercanzin, D. Trabucco, Sustainable structural design of tall buildings based on embodied energy, Energy and Buildings. 68 (2014) 254–269. doi:10.1016/j.enbuild.2013.09.003.

[191] Eurocode 1, Actions on structures -Part 1-4: General actions -Wind actions, 2005. doi:ICS 91.010.30; 93.040.

[192] A.E. Abdelnaby, A.S. Elnashai, Integrity assessment of the Pharos of Alexandria during the AD 1303 earthquake, Engineering Failure Analysis. 33 (2013) 119–138. doi:https://doi.org/10.1016/j.engfailanal.2013.04.013.

[193] J. Ji, A.S. Elnashai, D.A. Kuchma, An analytical framework for seismic fragility analysis of RC high-rise buildings, Engineering Structures. 29 (2007) 3197–3209. doi:https://doi.org/10.1016/j.engstruct.2007.08.026.

[194] M.M. Ali, K.S. Moon, Structural developments in tall buildings: Current trends and future prospects, Architectural Science Review. 50 (2007) 205–223. doi:10.3763/asre.2007.5027.

[195] K. Rahal, Mechanical properties of concrete with recycled coarse aggregate, Building and Environment. 42 (2007) 407–415. doi:10.1016/j.buildenv.2005.07.033.

[196] ISO 15686-5, Buildings and constructed assets–Service-life planning–Part 5: Life-cycle costing, International Organization for Standardization, 2008.

[197] I. Zabalza Bribián, A. Aranda Usón, S. Scarpellini, Life cycle assessment in buildings: State-of-the-art and simplified LCA methodology as a complement for building certification, Building and Environment. 44 (2009) 2510–2520. doi:10.1016/j.buildenv.2009.05.001.

[198] A. Sharma, A. Saxena, M. Sethi, V. Shree, Varun, Life cycle assessment of buildings: A review, Renew Sustain Energy Rev. 15 (2011) 871–875.

[199] J. Kneifel, Life-cycle carbon and cost analysis of energy efficiency measures in new commercial buildings, Energy and Buildings. 42 (2010) 333–340. doi:10.1016/j.enbuild.2009.09.011.

[200] RSMeans, Construction and Cost Estimating Data, (2019). https://www.rsmeans.com/.

[201] Coinnews Media Group LLC, US Inflation Calculator: Current Inflation Rates from 2006 to 2017, (2018). http://www.usinflationcalculator.com/inflation/current-inflation-rates/.

[202] M. Davis, M. McGinnis, Use of recycled concrete aggregates for improved sustainability of reinforced concrete building structures – Economic considerations, in: Proceedings of the 2015 ASEE Gulf-Southwest Annual Conference, University of Texas at San Antonio, American Society for Engineering Education, 2015.

[203] Capital Scrap Metal LLC, Price of scrap metal, (2019). https://www.capitalscrapmetal.com/prices/.

[204] R.S. Paranhos, B.G. Cazacliu, C.H. Sampaio, C.O. Petter, R.O. Neto, F. Huchet, A sorting method to value recycled concrete, Journal of Cleaner Production. 112

(2016) 2249–2258. doi:10.1016/j.jclepro.2015.10.021.

[205] D. V. Val, M.G. Stewart, Life-cycle cost analysis of reinforced concrete structures in marine environments, Structural Safety. 25 (2003) 343–362. doi:10.1016/S0167-4730(03)00014-6.

[206] M. Mistry, C. Koffler, S. Wong, LCA and LCC of the world's longest pier: a case study on nickel-containing stainless steel rebar, International Journal of Life Cycle Assessment. 21 (2016) 1637–1644. doi:10.1007/s11367-016-1080-2.

[207] L.S. Lee, R. Jain, The role of FRP composites in a sustainable world, Clean Technologies and Environmental Policy. 11 (2009) 247–249.

[208] J. Brown, H. Tce, Glass fibre reinforced polymer bars in concrete compression members, in: International Conference on Performance-Based and Life-Cycle Structural Engineering, School of Civil Engineering, The University of Queensland, 2015: pp. 1590–1599.

[209] H. Islam, M. Jollands, S. Setunge, Life cycle assessment and life cycle cost implication of residential buildings - A review, Renewable and Sustainable Energy Reviews. 42 (2015) 129–140. http://dx.doi.org/10.1016/j.rser.2014.10.006.

[210] G.N. Tiwari, A. Tiwari, Shyam, Life-cycle cost analysis, in: G.N. Tiwari, A. Tiwari, Shyam (Eds.), Handbook of Solar Energy: Theory, Analysis and Applications, Springer, Singapore, 2016: pp. 671–690. doi:10.1007/978-981-10-0807-8_20.

[211] M.A. Ehlen, M.D.A. Thomas, E.C. Bentz, Life-365 service life prediction model TM Version 2.0, Concrete International. 31 (2009) 41–46.

[212] M. Robert, B. Benmokrane, Combined effects of saline solution and moist concrete on long-term durability of GFRP reinforcing bars, Construction and

Building Materials. 38 (2013) 274–284. doi:10.1016/j.conbuildmat.2012.08.021.

[213] Y. Xuan, Q. Yue, Forecast of steel demand and the availability of depreciated steel scrap in China, Resources, Conservation and Recycling. 109 (2016) 1–12. doi:10.1016/j.resconrec.2016.02.003.

[214] A. Omura, N. Todorova, B. Li, R. Chung, Steel scrap and equity market in Japan, Resources Policy. 47 (2016) 115–124. doi:10.1016/j.resourpol.2016.01.001.

[215] C. Broadbent, Steel's recyclability: demonstrating the benefits of recycling steel to achieve a circular economy, International Journal of Life Cycle Assessment. 21 (2016) 1658–1665. doi:10.1007/s11367-016-1081-1.

[216] A. Yazdanbakhsh, L.C. Bank, A critical review of research on reuse of mechanically recycled FRP production and end-of-life waste for construction, Polymers. 6 (2014) 1810–1826. doi:10.3390/polym6061810.

[217] A. Dehghan, K. Peterson, A. Shvarzman, Recycled glass fiber reinforced polymer additions to Portland cement concrete, Construction and Building Materials. 146 (2017) 238–250. doi:https://doi.org/10.1016/j.conbuildmat.2017.04.011.

[218] A. Yazdanbakhsh, L. C. Bank, C. Chen, Use of recycled FRP reinforcing bar in concrete as coarse aggregate and its impact on the mechanical properties of concrete, Construction and Building Materials. 121 (2016) 278–284. doi:https://doi.org/10.1016/j.conbuildmat.2016.05.165.

[219] J.R. Correia, N.M. Almeida, J.R. Figueira, Recycling of FRP composites: Reusing fine GFRP waste in concrete mixtures, Journal of Cleaner Production. 19 (2011) 1745–1753. doi:10.1016/j.jclepro.2011.05.018.

[220] C. Lee, E.-B. Lee, Prediction method of real discount rate to improve accuracy

of life-cycle cost analysis, Energy and Buildings. 135 (2017) 225–232. doi:https://doi.org/10.1016/j.enbuild.2016.11.020.

[221] P. Fernandez, V. Pershin, I. Fernnndez Acin, Discount Rate (Risk-Free Rate and Market Risk Premium) Used for 41 Countries in 2017: A Survey, SSRN Electronic Journal. (2017) 1–15. doi:10.2139/ssrn.2598104.

[222] Office of Management and Budget, Circular A-94 Appendix C: Discount rates for cost-effectiveness, lease purchase, and related analyses, Washington, D.C., 2018. https://www.federalregister.gov/documents/2018/02/08/2018-02520/discount-rates-for-cost-effectiveness-analysis-of-federal-programs.

[223] P.A. Grout, Public and private sector discount rates in public-private partnerships, The Economic Journal. 113 (2003) 62–68.

[224] B.H. Goh, Y. Sun, The development of life-cycle costing for buildings, Building Research & Information. 44 (2016) 319–333. doi:10.1080/09613218.2014.993566.

[225] World Commission on Environment and Development, Our common future, Oxford University Press, Oxford, United Kingdom, 1987. doi:10.1080/07488008808408783.

[226] S.C. Bostanci, M. Limbachiya, H. Kew, Use of recycled aggregates for low carbon and cost effective concrete construction, Journal of Cleaner Production. 189 (2018) 176–196. doi:10.1016/j.jclepro.2018.04.090.

[227] L.N. Koutas, Z. Tetta, D.A. Bournas, T.C. Triantafillou, Strengthening of concrete structures with textile reinforced mortars : State-of-the-art review, Journal of Composites for Construction. 23 (2019) 03118001. doi:10.1061/(ASCE)CC.1943-5614.0000882.

[228] A. Parghi, M.S. Alam, A review on the application of sprayed-FRP composites

for strengthening of concrete and masonry structures in the construction sector, Composite Structures. 187 (2018) 518–534. doi:10.1016/j.compstruct.2017.11.085.

[229] A. Belarbi, B. Gencturk, M. Dawood, N.G. Ozerkan, M.G. Sohail, N.A. Alnuaimi, R. Kahraman, Reinforced concrete degradation in the harsh climates of the Arabian Gulf: Field study on 30-to-50-year-old structures, Journal of Performance of Constructed Facilities. 32 (2018) 04018059. doi:10.1061/(asce)cf.1943-5509.0001204.

[230] V. Padilla, P. Ghods, A. Alfantazi, Effect of de-icing salts on the corrosion performance of galvanized steel in sulphate contaminated soil, Construction and Building Materials. 40 (2013) 908–918. doi:10.1016/j.conbuildmat.2012.09.077.

[231] G. Koch, J. Varney, N. Thompson, O. Moghissi, M. Gould, J. Payer, International measures of prevention , application , and economics of corrosion technologies study (IMPACT), 2016. http://impact.nace.org/documents/Nace-International-Report.pdf.

[232] IS 456, Plain and reinforced concrete – code of practice, Indian Concrete Institution, New Delhi, 2000.

[233] British Standard 8110: Part 1, Structural use of concrete – code of practice for design and construction, British Standard Institution, UK, 1997.

[234] ACI Committee 201, ACI 201.2R-08: Guide to durable concrete, American Concrete Institute, Farmington Hills, USA, 2008.

[235] ACI Committee 222, ACI 222.3R-11: Design and construction practices to mitigate corrosion of reinforcement in concrete structures., American Concrete Institute, Farmington Hills, USA, 2011.

[236] C.E. Bakis, L.C. Bank, V.L. Brown, E. Cosenza, J.F. Davalos, J.J. Lesko, A. Machida, S.H. Rizkalla, T.C. Triantafillou, Fiber-reinforced polymer composites for construction—State-of-the-art review, Journal of Composites for Construction. 6 (2002) 73–87. doi:10.1061/(ASCE)1090-0268(2002)6:2(73).

[237] H. Rasheed, Strengthening design of reinforced concrete with FRP, CRC Press-Taylor & Francis Group, Florida, US, 2015.

[238] A.B.M.A. Kaish, M. Jamil, S.N. Raman, M.F.M. Zain, L. Nahar, Ferrocement composites for strengthening of concrete columns: A review, Construction and Building Materials. 160 (2018) 326–340. doi:10.1016/j.conbuildmat.2017.11.054.

[239] O. Awani, T. El-Maaddawy, N. Ismail, Fabric-reinforced cementitious matrix: A promising strengthening technique for concrete structures, Construction and Building Materials. 132 (2017) 94–111. doi:10.1016/j.conbuildmat.2016.11.125.

[240] N.R. Baddoo, Stainless steel in construction: A review of research, applications, challenges and opportunities, Journal of Constructional Steel Research. 64 (2008) 1199–1206. doi:10.1016/j.jcsr.2008.07.011.

[241] M.C. García-Alonso, M.L. Escudero, J.M. Miranda, M.I. Vega, F. Capilla, M.J. Correia, M. Salta, A. Bennani, J.A. González, Corrosion behaviour of new stainless steels reinforcing bars embedded in concrete, Cement and Concrete Research. 37 (2007) 1463–1471. doi:10.1016/j.cemconres.2007.06.003.

[242] Z. Saleh, M.N. Sheikh, A.M. Remennikov, A. Basu, Numerical investigations on the flexural behavior of GFRP-RC beams under monotonic loads, Structures. 20 (2019) 255–267. doi:10.1016/j.istruc.2019.04.004.

[243] Z.Y. Yang, J.Y. Liu, Y.D. Zhang, J.B. Qu, Flexural behavior finite element

analysis of CFRP reinforced concrete bridge deck with corrosion and salt resistance, in: Advanced Materials Research, Trans Tech Publ, 2014: pp. 1474–1477. doi:10.4028/www.scientific.net/AMR.1004-1005.1474.

[244] Y.J. Kim, State of the practice of FRP composites in highway bridges, Engineering Structures. 179 (2019) 1–8. doi:10.1016/j.engstruct.2018.10.067.

[245] T. Cadenazzi, M. Rossini, S. Nolan, G. Dotelli, A. Arrigoni, A. Nanni, Resilience and economical sustainability of a FRP reinforced concrete bridge in Florida : LCC analysis at the design stage, in: Proceedings of the Sixth International Symposium on Life-Cycle Civil Engineering (IALCCE 2018), CRC Press-Taylor & Francis Group, Ghent, Belgium, 2018: pp. 2913–2920. https://www.crcpress.com/Life-Cycle-Analysis-and-Assessment-in-Civil-Engineering-Towards-an-Integrated/Caspeele-Taerwe-Frangopol/p/book/9781138626331.

[246] E.A. Jensen, C. Eamon, X. Shi, V. Matsagar, Life-cycle cost analysis of CFRP reinforced concrete bridges, in: Transportation Research Board 89th Annual Meeting, Washington DC, United States, 2010: p. P. 10/1103.

[247] N.F. Grace, E.A. Jensen, C.D. Eamon, X. Shi, Life-cycle cost analysis of carbon fiber-reinforced polymer reinforced concrete bridges, ACI Structural Journal. 109 (2012) 697–704. doi:10.14359/51684047.

[248] T. Cadenazzi, G. Dotelli, M. Rossini, S. Nolan, A. Nanni, Cost and environmental analyses of reinforcement alternatives for a concrete bridge, Structure and Infrastructure Engineering. (2019) 1–16. doi:10.1080/15732479.2019.1662066.

[249] M.M.S. Cheung, K.K.L. So, X. Zhang, Life cycle cost management of concrete structures relative to chloride-induced reinforcement corrosion, Structure and

Infrastructure Engineering. 8 (2012) 1136–1150. doi:10.1080/15732479.2010.507474.

[250] H. Islam, M. Jollands, S. Setunge, N. Haque, M.A. Bhuiyan, Life cycle assessment and life cycle cost implications for roofing and floor designs in residential buildings, Energy and Buildings. 104 (2015) 250–263. doi:10.1016/j.enbuild.2015.07.017.

[251] I.M. Ahmed, K.D. Tsavdaridis, Life cycle assessment (LCA) and cost (LCC) studies of lightweight composite flooring systems, Journal of Building Engineering. 20 (2018) 624–633. doi:10.1016/j.jobe.2018.09.013.

[252] A. Atmaca, Life-cycle assessment and cost analysis of residential buildings in South East of Turkey: part 2—a case study, The International Journal of Life Cycle Assessment. 21 (2016) 925–942. doi:10.1007/s11367-016-1051-7.

[253] A. Atmaca, Life cycle assessment and cost analysis of residential buildings in south east of Turkey: part 1—review and methodology, The International Journal of Life Cycle Assessment. 21 (2016) 831–846. doi:10.1007/s11367-016-1050-8.

[254] J.S. Chou, K.C. Yeh, Life cycle carbon dioxide emissions simulation and environmental cost analysis for building construction, Journal of Cleaner Production. 101 (2015) 137–147. doi:10.1016/j.jclepro.2015.04.001.

[255] T.C. Marrana, J.D. Silvestre, J. de Brito, R. Gomes, Lifecycle cost analysis of flat roofs of buildings, Journal of Construction Engineering and Management. 143 (2017) 04017014. doi:10.1061/(asce)co.1943-7862.0001290.

[256] A. Younis, U. Ebead, S. Judd, Life cycle cost analysis of structural concrete using seawater, recycled concrete aggregate, and GFRP reinforcement, Construction and Building Materials. 175 (2018) 152–160.

doi:https://doi.org/10.1016/j.conbuildmat.2018.04.183.

[257] H. Takeuchi, S. Taketomi, S. Samukawa, A. Nanni, Renovation of concrete water tank in Chiba Prefecture, Japan, Practice Periodical on Structural Design and Construction. 9 (2004) 237–241.

[258] H.M. Mohamed, B. Benmokrane, Design and performance of reinforced concrete water chlorination tank totally reinforced with GFRP bars: Case study, Journal of Composites for Construction. 18 (2014) 05013001. doi:10.1061/(ASCE)CC.1943-5614.0000429.

[259] G.H. Koch, M.P.H. Brongers, N.G. Thompson, Y.P. Virmani, J.H. Payer, Corrosion cost and preventive strategies in the United States, Houston, TX United States, 2002. https://trid.trb.org/view/707382.

[260] ACI Committee 350, Code requirements for environmental engineering concrete structures and commentary., American Concrete Institute, Farmington Hills, USA, 2006.

[261] F.J. Bromilow, M.R. Pawsey, Life cycle cost of university buildings, Construction Management and Economics. 5 (1987) S3–S22. doi:10.1080/01446193.1987.10462089.

[262] A. Arpke, N. Hutzler, Domestic water use in the United States: A life-cycle approach, Journal of Industrial Ecology. 10 (2006) 169–184. doi:10.1162/108819806775545312.

[263] J.E. Fagan, M.A. Reuter, K.J. Langford, Dynamic performance metrics to assess sustainability and cost effectiveness of integrated urban water systems, Resources, Conservation and Recycling. 54 (2010) 719–736. doi:10.1016/j.resconrec.2009.12.002.

[264] M. Ortiz, R.G. Raluy, L. Serra, Life cycle assessment of water treatment

technologies: wastewater and water-reuse in a small town, Desalination. 204 (2007) 121–131. doi:10.1016/j.desal.2006.04.026.

[265] A. Ashworth, S. Perera, Cost studies of buildings, sixth, Routledge, London, UK, 2015.

[266] L. Abosrra, A.F. Ashour, M. Youseffi, Corrosion of steel reinforcement in concrete of different compressive strengths, Construction and Building Materials. 25 (2011) 3915–3925. doi:10.1016/j.conbuildmat.2011.04.023.

[267] R. Masmoudi, A. Masmoudi, M. Ben Ouezdou, A. Daoud, Long-term bond performance of GFRP bars in concrete under temperature ranging from 20°C to 80°C, Construction and Building Materials. 25 (2011) 486–493. doi:https://doi.org/10.1016/j.conbuildmat.2009.12.040.

[268] O. Gooranorimi, A. Nanni, GFRP reinforcement in concrete after 15 years of service, Journal of Composites for Construction. 21 (2017) 04017024. doi:10.1061/(ASCE)CC.1943-5614.0000806.

[269] N.G. Thompson, M. Yunovich, D. Dunmire, Cost of corrosion and corrosion maintenance strategies, Corrosion Reviews. 25 (2007) 247–261. doi:10.1515/CORRREV.2007.25.3-4.247.

[270] Portland Cement Association (PCA), Design and control of concrete mixtures, 16th ed., Portland Cement Association, 2016.

[271] C. Andrade, R. Buják, Effects of some mineral additions to Portland cement on reinforcement corrosion, Cement and Concrete Research. 53 (2013) 59–67. doi:10.1016/j.cemconres.2013.06.004.

[272] K.A. Riding, M.D.A. Thomas, K.J. Folliard, Apparent diffusivity model for concrete containing supplementary cementitious materials, ACI Materials Journal. 110 (2013) 705–713.

APPENDIX

Appendix A: List of Publications

This thesis was written based on the following journal and conference publications:

Younis, A., Ebead, U. A., and Nanni, A. (2017). "A Perspective on Seawater/FRP Reinforcement in Concrete Structures." Proceedings of the Ninth International Structural Engineering and Construction Conference, Resilient Structures and Sustainable Construction, ISEC Press, Valencia, Spain, ST-38.

Younis, A., Ebead, U., and Judd, S. (2018). "Life cycle cost analysis of structural concrete using seawater, recycled concrete aggregate, and GFRP reinforcement." Construction and Building Materials, 175, 152–160.

Younis, A., Ebead, U., Suraneni, P., and Nanni, A. (2018). "Fresh and Hardened Properties of Seawater-Mixed Concrete." Construction and Building Materials, 190, 276–286.

Younis, A., Ebead, U., Suraneni, P., and Nanni, A. (2019). "Strength, Shrinkage, and Permeability Performance of Seawater Concrete." Proceedings of the Tenth International Structural Engineering and Construction Conference (ISEC-10), Chicago, Illinois, United States, ST-52.

Younis, A., Ebead, U., Suraneni, P., and Nanni, A. (2019). "Microstructure Investigation of Seawater Vs. Freshwater Cement Pastes." Proceedings of the Tenth International Structural Engineering and Construction Conference, Chicago (ISEC-10), Illinois, United States, ST-53.

Younis, A., Ebead, U., Suraneni, P., and Nanni, A (2020). "Performance of Seawater-Mixed Recycled-Aggregate Concrete." *Journal of Materials in Civil Engineering*, 32(1), 04019331.

Younis, A., Ebead, U., Suraneni, P., and Nanni, A (2020). "Cost effectiveness of reinforcement alternatives for a concrete water chlorination tank." *Journal of Building Engineering*, 27, 100992.

Younis, A., Ebead, U., Suraneni, P., and Nanni, A. "Flexural Performance of Seawater-Mixed Recycled-Aggregate GFRP-Reinforced Concrete Beams." *Composite Structures* (Submitted/under review).

Younis, A. and Ebead, U. "Effects of using seawater and recycled coarse aggregate on plain concrete characteristics." Proceedings of the International Conference on Civil Infrastructure and Construction (CIC), February 2nd to 5th 2020, Doha, Qatar (Submitted/under review).

Younis, A. and Ebead, U. "Long-term cost performance of corrosion-resistant reinforcements in structural concrete." Proceedings of the International Conference on Civil Infrastructure and Construction (CIC), February 2nd to 5th 2020, Doha, Qatar (Submitted/under review).